Pattern formation as a neural wiring strategy during development of the *Drosophila* visual system

Inaugural-Dissertation
to obtain the academic degree
Doctor rerum naturalium (Dr. rer. nat.)

submitted to the
Department of Biology, Chemistry, Pharmacy
of
FREIE UNIVERSITÄT BERLIN

by

Charlotte Brigitta Wit

March, 2022

Reviewers

This thesis includes experiments that were performed between September 2015 and September 2021 in the lab of Prof. Dr. Hiesinger at Freie Universität Berlin.

First Reviewer:

Prof. Dr. P. Robin Hiesinger
Division of Neurobiology,
Institute of Biology,
Freie Universität Berlin

Second Reviewer:

Prof. Dr. Mathias F. Wernet
Division of Neurobiology,
Institute of Biology,
Freie Universität Berlin

Date of defense: June 24, 2022

Declaration of Independence

I, Charlotte Brigitta Wit,

declare that this thesis titled "Pattern formation as a neural wiring strategy during development of the *Drosophila* visual system" and the work presented in it are my own. I certify that I have prepared and written this thesis independently and that I have not used any sources or aids other than those indicated by me.

I confirm that:

- All work presented in this thesis was done while in candidature for a research degree at Freie Universität Berlin
- Where the thesis is based on work done by myself jointly with others, I have made clear exactly what was done by others and what I have contributed myself
- No work presented in this thesis has previously been submitted for a degree or any other qualification at this university or any other institution
- Where I have consulted the published work of others, this is always clearly stated.
- I have acknowledged all main sources of help

Signed: _____

Date: _____

If you understand everything,
you must be misinformed.

- Japanese proverb -

Contents

List of Figures

List of Abbreviations

Abbreviation	**Meaning**
ANOVA	Analysis Of Variance
Arm	Armadillo
BDSC	Bloomington Drosophila Stock Center
Brp	Bruchpilot
C. elegans	Caenorhabditis elegans
CNS	Central Nervous System
DAH	Differential Adhesion Hypothesis
Dlg	Disc large
DN	Dominant Negative
DNA	Deoxyribonucleic Acid
Dscam	Down syndrome cell adhesion molecule
Dsh	Dishevelled
DSHB	Developmental Studies Hybridoma Bank
Ecad	E-cadherin
DCSP-2	Drosophila Cysteine String Protein-2
EM	Electron Microscopy
Eve	Even-skipped
Fas2	Fasciclin-2
FRT	Flippase Recognition Target
Flp	Flippase
Fmi	Flamingo
Fz	Frizzled
Fz-2	Frizzled-2
GFP	Green Fluorescent Protein

Abbreviation	**Meaning**
GMR	Glass Multimer Reporter
Gogo	Golden goal
Hh	Hedgehog
HRP	Horse-Radish Peroxidase
Hs	Heat-shock
HsFlp	Heat-shock Flippase
Ig	Immunoglobulin
LNs	Lamina Neurons
LP	Lamina Plexus
LPC	Lamina Precursor Cell
MARCM	Mosaic Analysis with Repressible Cell Marker
MCFO	MultiColor FlpOut
MF	Morphogenetic Furrow
NaAz	Sodium Azide
Ncad	N-cadherin
NDS	Normal Donkey Serum
NGS	Normal Goat Serum
OE	Over-Expression
P	Pupal stage
PBS	Phosphate Buffered Saline
PBST	Phosphase Buffered Saline + Triton-X
PCP	Planar Cell Polarity
PFA	Paraformaldehyde
Pk	Prickle
PR	Photoreceptor
R	Photoreceptor sub type
Repo	Reversed polarity
RGC	Retina Ganglion Cell
RNA	Ribonucleic Acid
RNAi	RNA interference
Robo	Roundabout
ROI	Region Of Interest

Abbreviation	**Meaning**
SD	Standard Deviation
Sdk	Sidekick
Smo	Smoothened
Stan	Starry night
Tub	Tubulin
UAS	Upstream Activation Sequence
Vang	Van Gogh
WT	Wild Type
μl	microliter
μm	micrometer

Summary

Natural patterns are everywhere around us and can greatly support the developmental progress of complex organs. The eye of a fruit fly (*Drosophila melanogaster*) is such a perfectly patterned organ. The 800 small eyes, called ommatidia, contain six motion-vision photoreceptors (PRs) each. Via axons, PRs transfer environmental information to the first optic ganglion in the brain; the lamina. The six photoreceptors from neighboring ommatidia that see one point in the environment are connected to one post-synaptic target in the lamina, to form a retinotopic map of the surroundings. Neural superposition sorting systematically sorts PR axons during a series of distinct developmental steps. Initially, PR axons extend in bundles from the ommatidia to the lamina plexus (LP) and form a scaffold, or pre-pattern. Scaffold formation is an essential step in creating a functional visual map, yet, how it establishes is largely unknown. From this scaffold, all six PRs from one ommatidium extend their axonal growth cones in different angles during a lateral extension phase towards their different post-synaptic targets. How PR growth cones determine this sub type specific angle is largely unknown. Finally, extended growth cones adhere and connect with Lamina Neurons (LNs) at the target location to form synapses and a functional visual circuit. Whether LNs are required for axon extension and/or adherence at the target location is unknown.

The aim of this thesis is to describe underlying mechanisms involved in pattern formation and neural superposition sorting during development of the visual map, as well as to investigate the role of LNs during superposition sorting. The results presented in this thesis show that PR growth cones can form a scaffold in absence of LNs. Furthermore, the extension of photoreceptors is independent of the presence of LNs the presentation of adhesion proteins on their cell membrane. Strikingly, it is possible for extending growth cones to find their target correctly and, in rare cases, form photoreceptor clusters where they would normally form a cartridge with LNs. This suggests that photoreceptor and LN dynamics are largely independent and that neural superposition sorting is remarkably robust. I conclude that LNs are required in late development of the visual map for robust circuit formation, but do not contribute to PR sorting. This is a novel finding for the wiring of the *Drosophila* visual system.

Zusammenfassung

Widerkehrende Strukturen und Muster sind überall in der Natur zu finden und können während der Entwicklung einen wichtigen Einfluss spielen. Ein perfekt strukturiertes Organ ist das Auge der Fruchtfliege, *Drosophila melanogaster*. Es besteht aus etwa 800 repetitiven Untereinheiten, den so genannten Ommatidien, welche jeweils sechs bewegungssensitive Photorezeptoren (PRs) besitzen. Diese leiten Umgebungsinformationen über Axone zum ersten optischen Ganglion, der Lamina, weiter. Die sechs Photorezeptoren von benachbarten Ommatidien, die denselben Raumpunkt wahrnehmen, sind mit dem selben postsynaptischen Zellen in der Lamina verbunden um eine retinotope Karte der Umgebung zu arrangieren. Die Axone von Photorezeptoren werden durch neuronale Superposition-Sortierung in einer Reihe von Entwicklungsschritten geordnet. Zunächst wachsen die Axone der Photorezeptoren in Bündeln von den Ommatidien zum Lamina Plexus (LP) und formen dabei ein eindeutiges Grundgerüst oder 'pre-pattern'. Die Bildung dieses Grundgerüsts stellt einen essenziellen Schritt in der Formierung einer funktionellen visuellen Karte dar. Wie genau das Gerüst etabliert wird, ist jedoch größtenteils unbekannt. Nach Bildung des Grundgerüsts wachsen alle sechs PRs eines Ommatidiums in einer lateralen Wachstums-Phase. In dieser wachsen die Wachstumskegel der PRs in unterschiedlichen, subtyp-spezifischen Winkeln zu deren jeweiligen neuronalen Partnern. Wie hierbei die Wachstumskegel der Photorezeptoren ihre spezifischen Winkel bestimmen ist weitestgehend unbekannt. Letztlich verbinden sich Wachstumskegel der Photorezeptoren mit Lamina Neuronen (LNs) an ihren Zielpositionen, formen Synapsen und so einen funktionellen visuellen Schaltplan. Ob LNs für axonales Wachstum und/oder Adhäsion von Wachstumskegeln an ihrer Zielposition nötig sind, ist nicht bekannt.

Das Ziel dieser Studie ist die grundlegenden Mechanismen, die in der Entwicklung einer funktionellen visuellen Karte notwendig sind, zu untersuchen. Hierbei werden die Mechanismen, die für die Grundgerüstformierung und neuronale Superpositions-Sortierung notwendig sind, sowie die Rolle von LNs während dieser, analysiert. Die hier präsentierten Ergebnisse zeigen, dass Wachstumskegel von Photorezeptoren sogar in Abwesenheit von Lamina Neuronen ein

Grundgerüst bilden können. Zudem ist das laterale Wachstum der Photorezeptoren unabhängig von der Laminar Neuronen Präsenz oder deren Membran-Adhäsionsproteinen. Überraschenderweise ist es ausdehnenden Wachstumskegeln möglich ihr Ziel korrekt zu finden und in seltenen Fällen sogar Photorezeptor-Cluster zu bilden, wo normalerweise "cartridges" mit LNs geformt würden. Diese Ergebnisse legen nahe, dass Photorezeptoren und LN-Dynamiken größtenteils voneinander unabhängig sind und neuronale Superpositions-Sortierung erstaunlich robust ist. Ich schlussfolgere, dass LNs während der späteren Entwicklung einer visuellen Karte für robuste Schaltkreisformierung notwendig sind, jedoch keinen Einfluss auf die Photorezeptor-Sortierung haben. Diese Erkenntnisse stellen neue Forschungsergebnisse bezüglich der neuronalen Verschaltung des visuellen Systems von *Drosophila melanogaster* dar.

Samenvatting

Natuurlijke patronen zijn wijdverspreid en kunnen bijdragen aan de ontwikkeling van complexe organen. Het visuele systeem van een fruitvliegje (*Drosophila melanogaster*) is zo'n orgaan dat ontwikkelt met gebruik van patronen. Eén oog bevat ongeveer 800 individuele minioogjes, zogenaamde ommatidia, die elk zes bewegingssensitieve fotoreceptoren bevatten. Via axonen geven zij informatie door aan de eerste hersenlaag in het visueel systeem; de lamina. Zes fotoreceptoren van naburige ommatidia, die allen één punt in de ruimte zien, worden verbonen met één cluster van post-synaptische partners en vormen een visuele kaart. Het sorteren van axonen via "neuron superpositie sorteren", doorloopt verschillende ontwikkelingsstadia. Eerst sturen fotoreceptoren hun axonen in bundels van het oog naar de lamina plexus (LP) waar ze een pre-patroon vormen. Deze stap is essentieel voor de vorming van de visuele kaart, maar hoe het wordt gevormd is grotendeels onbekend. Vanaf het gevormde pre-patroon groeien zes fotoreceptoren uit één ommatidium in zes verschillende richtingen naar hun verschillende post-synaptische targets. Hoe ze deze groeirichting bepalen is onbekend. Tenslotte komen axon extensies samen bij een Lamina Neuron (LN) target en vormen ze synapsen en daarmee een werkend visueel circuit. Of LNs een rol spelen tijdens extensie, of voor de vorming van connecties, is onbekend.

Het doel van deze thesis is het beschrijven van onderliggende mechanismen in neuron superpositie sorteren tijdens de ontwikkeling van het visuele system van *Drosophila* en te onderzoeken of LNs nodig zijn voor dit proces. De resultaten laten zien dat photoreceptoren een pre-patroon kunnen vormen in afwezigheid van LNs en dat hun extensies onafhankelijk zijn van de aanwezigheid van LNs of van moleculen op het celmembraan. Ook is het voor fotoreceptoren mogelijk om vanuit correcte extensies in sommige gevallen een cluster te vormen met andere fotoreceptoren ipv. met LNs. Dit suggereert dat de dynamieken van fotoreceptoren en LNs voor een groot deel onafhankelijk van elkaar zijn. LNs lijken vereist te zijn gedurende de laatste fase van sorteren voor de robuste vorming van een functioneel visueel veld, maar niet voor het eigenlijke sorteren van fotoreceptoren. Dit is een nieuwe vinding in de ontrafeling van het visuele systeem van *Drosophila melanogaster*.

For the ones I love

Chapter 1

Introduction: Pattern formation and neural development

Nature is capable of producing the most astonishing structures and patterns. Observing your surroundings, you can discover a wild variety of patterns, most often very pleasing to the eye. Throughout the fungal-, plant-, and animal kingdom, species possess beautiful structures and patterns that fulfill a vast variety of tasks. Some examples are presented in Figure 1.1 A-E: closely layered gills underneath mushrooms to hold millions of spores, veins crossing a leave deliver nutrients and water, a sunflower consists of hundreds of smaller flowers organized in an optimal pattern to utilize all of the available space to carry sunflower seeds, curves on coral control water flow that creates more surface to exchange chemicals with the environment, and the pattern of giraffe spots provides camouflage in a dangerous environment.

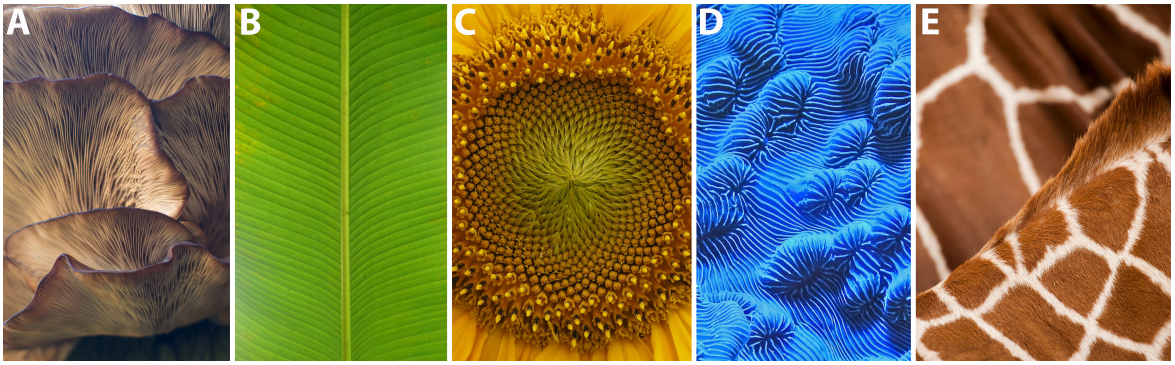

FIGURE 1.1: Patterns can be discovered in all parts of the natural kingdom
From left to right: **A**) Gills underneath mushrooms. Photographed by Damir Omerovic. **B**) Veins on a banana leave. Photographed by Eline Somers. **C**) The heart of a sunflower. Photographed by Lucasz Rawa. **D**) Bio-luminescent blue coral. Photographed by David Clode. **E**) Giraffe spots. Photographed by Louise Pilgaard. Images obtained from `unsplash.com`.

From zebra(-fish) stripes and leopard spots, to rings and lattices; patterns are appealing study material for mathematicians to reproduce visually resembling motifs and for developmental biologists who work to identify the molecular or biophysical factors underlying pattern emergence. How can molecular processes create an intricate design while maintaining reproducibility?

Schweisguth and Corson (2019) show that naturally occurring patterns can be generated even with very basic computer models. Hence, it might be possible that the principles underlying pattern formation in nature are basic too. In fact, many, if not all, naturally occurring patterns have evolutionary roots that tie them back to rudimentary patterning rules. Moreover, many patterns are self-organizing. The brain seems no exception to systematic wiring in patterns. Patterned brain architectures, especially columns and layers, are common in all brains; from the cat's ocular dominance columns, famously described by Hubel and Wiesel (1962), to the columns and layers in the optic lobes of the tiny brain of a fruit fly (*Drosophila melanogaster*) (Braitenberg, 1967; Meinertzhagen and O'Neil, 1991). In the latter, it has been shown that the formation of columnar units in the optic lobe relies on a self-organizing mechanism (Schwabe et al., 2014; Trush et al., 2019).

1.1 *Drosophila* as a model organism to study brain wiring

The brain of a fruit fly (*Drosophila melanogaster*) is roughly the size of a poppy seed, and contains about 100,000 neurons. In a major effort, spanning over a decade of work, scientists are assembling an exhaustive atlas of all cell types and neuronal connections in the *Drosophila* central brain (Scheffer et al., 2020). Humans have a million times more neurons; approximately 100 billion. The reduced size and complexity of the *Drosophila* brain makes it more convenient to study than the vertebrate brain. And despite the reduced complexity, it still makes a good model to extract knowledge about brain development in general. There are many overlapping cellular and molecular mechanisms that fruit flies and humans share. The eyes of insects and vertebrates have a different lay-out, but serve a similar purpose: photoreceptors receive environmental information and neurons transmit this information to the brain. Neurons use the same neurotransmitters and cell-cell communication via chemical synapses to transmit signals, obtain stereotypical morphologies, and express similar proteins on their cell membranes. During development, neurons build neuronal networks and circuits. Fundamental research in fruit flies increases our understanding of brain development in an ethically responsible way. It broadens our understanding of neural wiring dynamics in general and sheds light onto questions concerning molecular mechanism and developmental principles.

Drosophila is commonly used as a model organism for developmental studies. The fruit fly as a model organism has some advantages over other model organisms. It is cost and space efficient to keep and maintain fruit flies in a laboratory environment. They are easy to breed and the generation time is short. Furthermore, both the size and complexity of the brain, makes analyses in the fly nervous system more manageable than in vertebrates. Finally and importantly, there are sophisticated genetic tools and techniques that enable genetic manipulations in distinct populations of cells, and make it possible to label and study individual neurons. The UAS-Gal4 binary system is the most commonly used genetic technique to alter protein expression levels (Brand and Perrimon, 1993; Duffy, 2002). In short: The system consist of two parts; UAS and Gal4. A transcription factor Gal4 (gained from yeast) binds to a DNA binding site known as the Upstream Activation Sequence (UAS) and drives expression of a gene downstream of it. Together, they promote transcription of a gene of interest (connected to the UAS sequence) only in the tissue(s) where the Gal4-promoter is active. In this way, it is possible to artificially express any cloned gene in a wide variety of tissue- and cell-specific patterns.

1.2 Patterns in the *Drosophila* visual system

The *Drosophila* visual system is organized in multiple layers (see Figure 1.2 B) that are connected with each other through neuronal connections. Each layer has a distinct lay-out with a recognizable pattern. On the outside of the adult fly there are two facet eyes that each contain approximately 800 smaller unit eyes, called ommatidia, organized in an iterative pattern (see Figure 1.2 A). Photoreceptor differentiation and development in the eye proceeds in a morphogenic wave. The morphogenetic furrow (MF), that sweeps across the eye imaginal disc, transforms thousands of undifferentiated cells into a precisely patterned eye with 800 ommatidia (see Figure 1.2 A); transforming a previously unpatterned epithelial sheet into a perfectly patterned structure (Wolff and Ready, 1991). The initiation of the MF at the posterior end of the epithelium and its movement across the eye are controlled by the activity of the Hedgehog (Hh) signaling pathway (Huang and Kunes, 1998; Ma et al., 1993).

One ommatidium contains eight photoreceptors (PRs). Six outer (R1-R6) and two centrally located inner photoreceptors (R7 and R8). Following differentiation, PR axons extend and descend into the optic lobes and indirectly induce the differentiation of at least one class of neurons that constitute the optic neuropils (Fernandes et al., 2017); Lamina monopolar cells, or Lamina Neurons (LNs). The six outer photoreceptors have a function in motion-detection and their axons connect to the first optic neuropil; the lamina. R7 and R8 are involved in

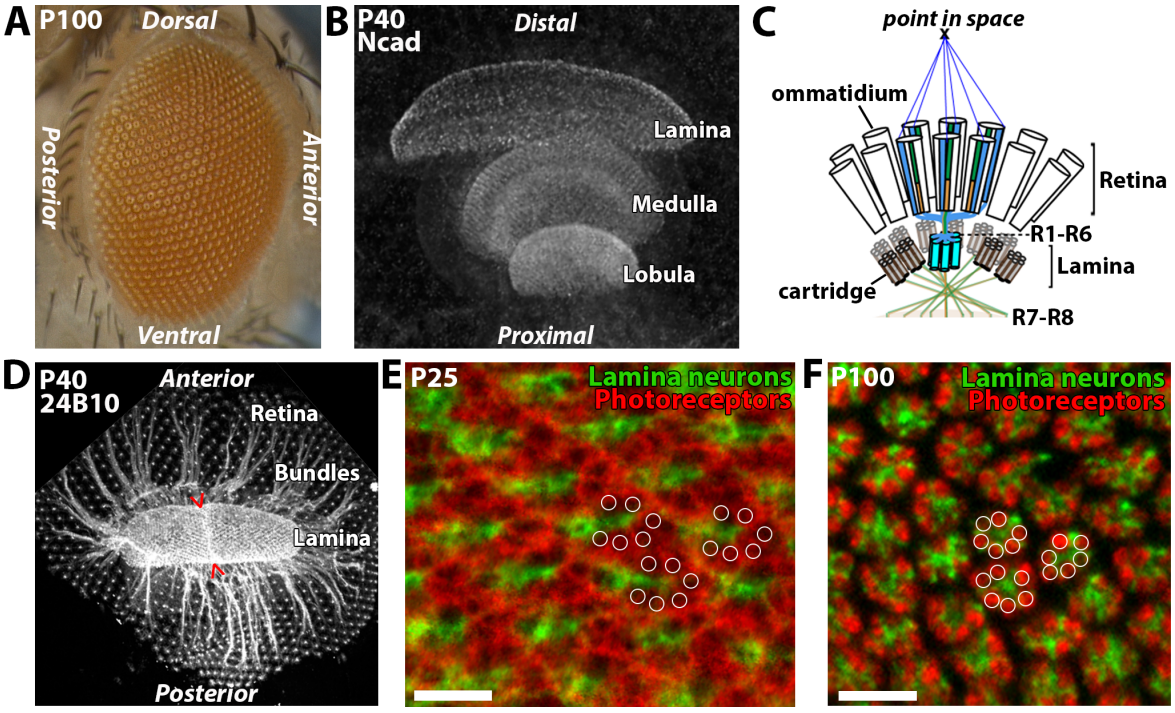

FIGURE 1.2: The patterned organization of the *Drosophila* visual system

A) The *Drosophila* eye consists of approximately 800 tightly packed ommatidia. **B**) Ncad staining of the developing optic lobe at P40 reveals the optic lobe is ordered in layers. Retina (not visible) on the outside (most distal), lamina is the first optic ganglion, followed by the medulla and lobula **C**) Schematic representation of the adult retina and lamina. R1-R6 in six ommatidia see the same point in space (line of sight in blue) and wire to one cartridge in the lamina. R7-R8 wire to the deeper laying medulla. Figure adapted from (Mencarelli and Pichaud, 2015). **D**) anti-chaoptin antibody staining at P40 reveals photoreceptors and their extensions to the lamina, where they create a scaffold, or pre-pattern. Red arrows indicate the equator. Axons are packed into tightly organized bundles in between retina and lamina. **E**) Top view of the scaffold at the lamina plexus (at P25). It consists of photoreceptor heels (photoreceptors in red) and lamina neurons (green). PR axon anchoring points (heels) are organized in a crescent. White circles highlight the six heels of axons originating from one ommatidium/bundle; 3x. **F**) Top view of the adult lamina. It contains approximately 800 cartridges where photoreceptors (red) are organized around lamina neurons (green). White circles highlight six photoreceptors gathered in one cartridge; 3x. Scale bar is 5μm.

color-vision. Their information is transferred to the second layer; the medulla (see Figure 1.2 B). Polarized light is detected with a specialized set of polarization sensitive photoreceptors at the dorsal rim of the fly eye (Labhart, 1988). This polarization information is also relayed to the medulla, but to a distinct part that integrates both color and polarization vision (Sancer et al., 2020).

I focus on photoreceptor 1-6, that convey environmental input to synaptic cartridges in the lamina (see Figure 1.2 C). During development, axons, organized in bundles, arrive to the lamina plexus where they form a scaffold–an organized pre-pattern, or temporary framework– during the scaffolding phase (see Figure 1.2 E). The scaffolding phase lasts between the final larval stage L3 and pupal stage P20; where 20 represents the number of hours of development. At a stable temperature of 25°C, the development of a *Drosophila* pupae until an adult fly

takes 100 hours. Axons arriving at the scaffold in the lamina form stable anchoring points, called heels (Langen et al., 2015), which are organized in an iterative pattern of crescents in the scaffold (see Figure 1.2 E). Every descended bundle forms one crescent of six heels. The curved ends of the crescents point towards the equator, that forms a symmetry break over the lamina plexus (see Figure 1.2 D, red markings). During a approximately 25 hour lasting sorting phase between P20 and P45, photoreceptors are systematically shuffled and finally form columns, called cartridges, in the maturing lamina (see Figure 1.2 F). Inside the forming cartridges, PRs make synapses with their post-synaptic partners (lamina neurons; LNs) starting around P50 (Meinertzhagen and O'Neil, 1991). Note: the axon anchoring points marked in Figure 1.2 E represent heel positions in the scaffold and are not the same axons marked in Figure 1.2 F, which represent the axon terminals in adult cartridges. The sorting mechanism will be further explained in Section 1.3. Thus, depending on the developmental stage, one can observe a scaffold of photoreceptor heels which are organized in a repeated pattern of crescent shapes, alternating like scales on a fish. Or, when observing the adult lamina, a collection of lamina columns comprised of lamina neurons and photoreceptors.

1.3 Neural superposition and its sorting principle

In *Drosophila*, the combination of the curvature of the fly-eye, the position of photoreceptors within one ommatidium, and the lens on top of this ommatidium cause an overlapping visual field (Braitenberg, 1967). In turn, Kirschfeld and Franceschini (1968) found that PRs in several neighboring ommatidia share the same visual axis. Hence, R1-R6 are arranged in an ommatidium so that each one "sees" a different point in space, while one point in space can be seen by different PRs in multiple neighboring ommatidia (see Figure 1.2 C). Overlapping visual fields between ommatidia would harvest the most efficient input for neighboring ommatidia in terms of movement perception and/or pattern recognition (Stavenga, 1975). Kirschfeld and Franceschini (1968) proposed that insects use this redundant sampling of the environment to increase light sensitivity in low light conditions.

Retinotopic mapping describes the idea that neighboring points in space are mapped as neighboring synaptic units in the brain. This ensures a correct spatial representation of the environment in the brain and is found for all vertebrate and invertebrate visual maps. In order to achieve this despite an overlapping visual field, axons from one ommatidium have to wire to six different cartridges in the lamina so that every cartridge receives informational input from one point in space (Horridge and Meinertzhagen, 1970; Kirschfeld and Franceschini,

1968) (see Figure 1.3 C). Sorting occurs in a systematic sorting mechanism called neural superposition sorting.

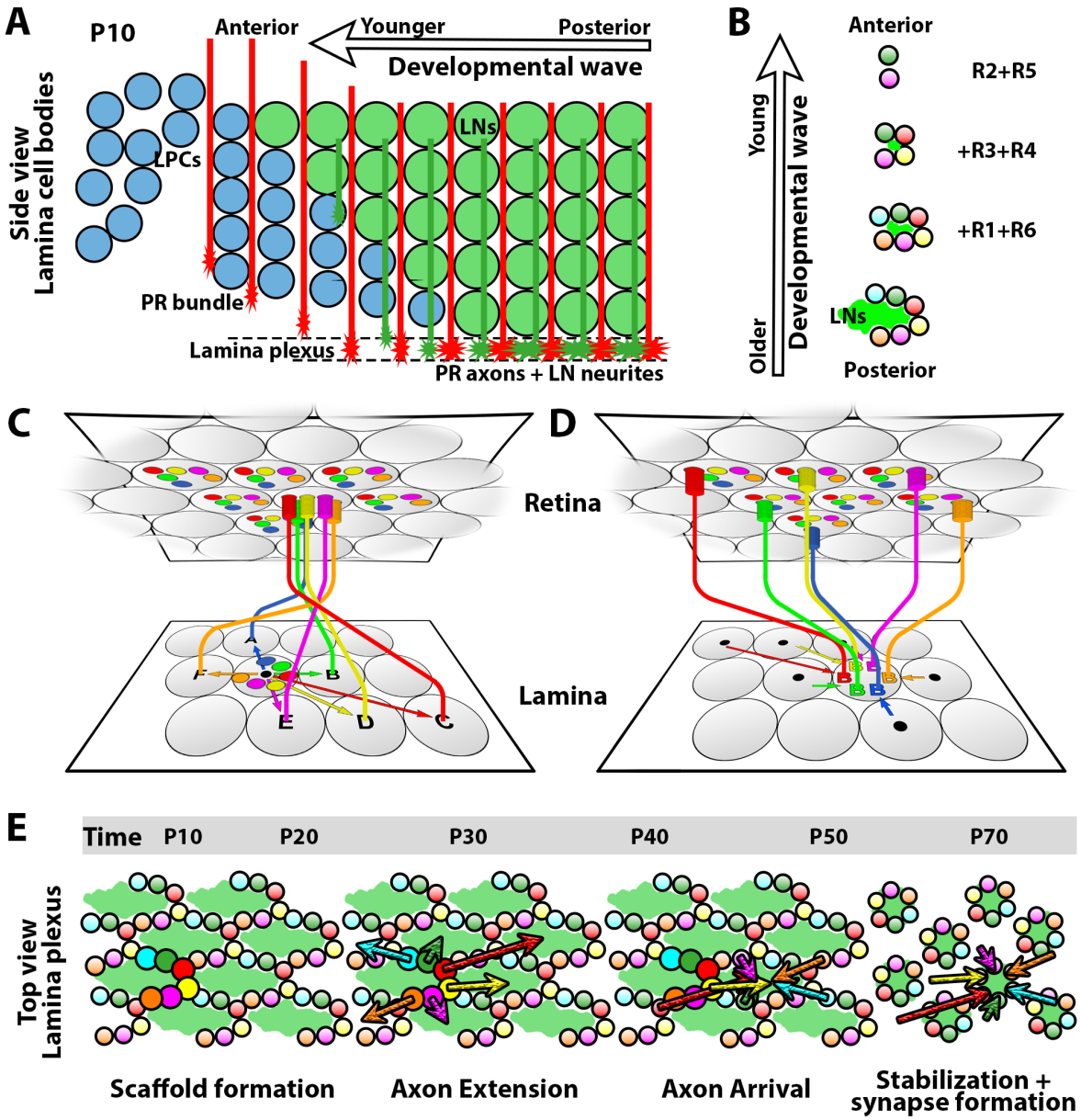

FIGURE 1.3: Development of the lamina plexus and neural superposition sorting

A) In a developmental wave from posterior to anterior, photoreceptor bundles descent from the eye to the lamina. Lamina Precursor Cells (LPCs; blue) migrate between photoreceptor bundles (red) and differentiate into lamina neurons (LNs; green). At the lamina plexus, photoreceptor axons stabilize and neurites of LNs expand. Together they form a scaffold. **B**) Order of photoreceptor arrival at the lamina plexus. Green inside the crescents represents LN neurites. **C**) Neural superposition sorting from the perspective of one bundle. Individual photoreceptors sort to six different cartridges in the lamina. A-F indicate different points in space seen by individual photoreceptors in one ommatidium. **D**) Neural superposition sorting from the perspective of a cartridge. Photoreceptors from six ommatidia that see point B in space wire to the same cartridge. Panel C and D adapted from (Langen et al., 2015). **E**) Neural superposition sorting as a developmental program that progresses over time. Scaffold formation is followed by axon extension, axon arrival, and synapse formation. Brightly colored circles represent axon heels in one crescent (from one ommatidium/bundle). Colored arrows represent individual growth cones of photoreceptor sub types. Different colors indicate photoreceptor sub type (blue R1; green R2; red R3; yellow R4; purple R5; orange R6).

Neural superposition sorting between PR axons happens on a sorting plane in the lamina. PR axons start arriving there during the larval developmental stage. They find their way from the developing eye to the developing lamina by extending their axons into the brain (see Figure 1.3 A). Bundles of photoreceptor axons arrive row by row (developmental wave) to form the lamina plexus by stopping in between layers of glia; their intermediate targets (Poeck et al., 2001). On their way down, PRs encounter lamina precursor cells (LPC) and initiate their differentiation into Lamina Neurons (LNs) through Hedgehog signaling via wrapping glia that enclose PR bundles (Fernandes et al., 2017; Huang and Kunes, 1996). LNs migrate in between PR bundles and descent onto the lamina plexus in stacks of five (L1-L5). At the lamina plexus, PR bundles stabilize their arrival points to become stable heels (Langen et al., 2015) during a phase of scaffold formation that lasts until approximately P20 (see Figure 1.3 E). Together with LN neurites, that extend into the lamina plexus in a similar developmental wave shortly after PR arrival, a highly organized and stereotypic sorting field is formed where synchronized neural superposition sorting takes place.

Neural superposition sorting is an algorithm-like developmental program that progresses over time. Figure 1.3 E shows the developmental steps in the process of neural superposition sorting. Scaffold formation is followed by axon extension, axon arrival, and synapse formation. The actual sorting occurs during the axon extension phase of neural superposition sorting. A bundle defasciculates and each photoreceptor sub type (R1-R6) extends its growth cone at the tip of the axon, while the heel remains stable in the crescent organization. Extension happens in a sub type-specific angle and velocity and it grows a specific length to reach its target cluster of LN neurites (Langen et al., 2015). Recently, these findings have been enforced by the finding that R3 and R4 extension angles and speeds are inherent to their cell identities (Ji et al., 2021). Sorting ensures that each LN cluster receives optical input from six PRs that see one point in space (see Figure 1.3 D). After growth cones have extended and arrived at a target location, axons stabilize and start the process of synapse formation with their partners; the LNs (Braitenberg, 1967; Meinertzhagen and O'Neil, 1991). Thus, PRs target their post-synaptic partners during a sorting phase that ensures synaptic pre-specification; it matches the right PRs and LNs at the right time and at the right location prior to synapse formation.

Synapse formation does not start until P50 (see Figure 1.3 E). If everything goes right, each cluster of LNs receives input from six R-cell sub types from six different photoreceptor bundles. Electron microscopy analysis of lamina cartridges in the fly (*Calliphora*) shows that any mistakes in this respect are rare (Horridge and Meinertzhagen, 1970), although some mistakes are found at the equator (Meinertzhagen, 1972).

1.4 Research questions and scientific aim

One of the big questions in neuroscience is how neurons that originate from different locations extend to the proper location in the brain and create precise neural circuits. The *Drosophila* lamina is a proper model to study precise neural wiring during development of the nervous system. Its patterned scaffold lay-out and neural pre-specification through a sorting process underlie the precision of the wiring program of the visual map, although there are many open questions concerning the underlying mechanisms.

The general aim of this thesis is to describe the molecular and cellular mechanisms underlying neural superposition sorting in *Drosohila*. This thesis can be roughly divided into two parts. Part one focuses on the scaffolding phase, while part two focuses on the sorting and extension phase, although the processes described in the chapters overlap at points.

The first part concentrates on pattern formation at the lamina plexus during the scaffolding phase. While the formation of the scaffold during development is crucial for visual map formation (Clandinin and Zipursky, 2000; Langen et al., 2015), it is largely unknown how it forms the stereotypical pattern of crescents. In Chapter 2, I focus on the arrival of PRs to the lamina plexus and consider the organization of the scaffold in detail. Specifically, I focus on patterned proteins in the lamina plexus. I investigate the role of one of these proteins (Sidekick) during the process of scaffold formation and photoreceptor arrival to the lamina plexus in more detail in Chapter 3.

The second part focuses on extension of PRs in the scaffold. One major question is whether post-synaptic LN clusters, that make up a large portion of the lamina plexus during the sorting phase, contribute to photoreceptor wiring. Their patterned organization in the scaffold raises questions about their role during this early stage of development. Moreover, a study that modelled superposition sorting with a computational model predicted that axon extension and arrival are possibly independent of LNs (Langen et al., 2015). I investigate the necessity of post-synaptic LNs in both the scaffolding and sorting phase of neural superposition sorting (Chapter 4 and Chapter 5). In these chapters, I present different methods to disturb the presence of LNs at the lamina plexus and analyse the contribution of LNs to specific developmental stages. Finally, I investigate how pre-specification could work independently of LNs by mapping other possible contributors in the optic lobe and investigate the role of filopodia during the extension phase of neural superposition sorting in Chapter 6.

In summary, the goal is to understand the foundation of pattern formation at the lamina plexus during scaffolding and investigate the role of post-synaptic LNs to gain more insight

into the wiring principles in the *Drosophila* brain. This will contribute to a better understanding of the requirements for successful neural superposition sorting and thereby to general knowledge of developmental programs and brain wiring.

Chapter 2

Scaffold development: Photoreceptor organization and protein patterning

The lamina plexus is a density of photoreceptor axons that have descended from the eye. Photoreceptor bundles descent into the brain in a wave, following the sweeping developmental wave of the morphogenetic furrow over the eye. In this wave, ommatidia differentiate row by row, and not all PRs within one ommatidium differentiate at the same time. Photoreceptor 8 is the first photoreceptor of an ommatidium to differentiate in the eye. It acts as the pioneer axon and grows down into the brain, passes through the lamina and terminates in the medulla (Wolff and Ready, 1991). Next, the outer photoreceptors differentiate in pairs. First 2 and 5 together, then 3 and 4, and lastly 1 and 6. The inner photoreceptor R7 is last and passes through the lamina and terminates at the medulla, like R8 (Kirschfeld and Franceschini, 1968). It is assumed, but not completely clear, that photoreceptors descent in their order of differentiation so that axons arrive at the LP in pairs (see Figure 1.3 B). In theory, outer photoreceptors could wait for them all to have differentiated before following the R8 pioneer axon to the LP. It seems more likely, however, that PRs descent in the order of their differentiation, as proposed back in 1967 (Braitenberg, 1967).

Once bundles of PRs arrive at the lamina plexus, a scaffold forms out of photoreceptor heels and the neurites of LNs. The heel crescents pattern like fish scales and are mirror symmetric to the other side of the equator. How this pattern establishes itself is largely unknown.

In the broader spectrum of pattern formation, it can be stated that all multi-cellular organisms develop through a sequence of patterning events during which cells adopt distinct cell fates. In these cases, patterns create guidelines for developing systems to organize in a stereotypical fashion and are an essential basis for further development. This often starts in

the embryonic phase, when patterns are established by different forms of cell-cell communication, acting alone or together with morphogen gradients that determine cell fates according to the position of cells within a uniform field (Schweisguth and Corson, 2019). Morphogen-patterned tissues can create precise spatial patterns of different cell types and is based on molecular gradients that originate at opposite poles. This is the case, for instance, in embryonic development of the *Drosophila* embryo. Along the anterior-posterior axis of the embryo, there are two gradients of two proteins: anterior is Bicoid and posterior starts the expression of Caudal. Neuronal precursors in the embryo follow this template for cell fate specification. The combination of these transcription factors is both necessary and sufficient to specify neuronal subtypes (Briscoe and Small, 2015). In the fruit fly, these simple initial patterning rules in the embryo results in the specification of abdomen, thorax, and head (Clyde et al., 2003; Kraut and Levine, 1991). Thus, gradients provide asymmetry to which cells can respond during cell fate specification (Briscoe and Small, 2015).

Another well-studied patterning mechanism is Planar Pell Polarity (PCP). PCP shows cells what side is anterior, posterior, dorsal, and ventral. Polarity of an epithelial sheet gives rise to, for example, the direction of bristles on the *Drosophila* body (all hairs and bristles point posterior) (Myat et al., 2011). PCP is a well-studied subject and many of the cell surface proteins and underlying mechanisms are known (Peng and Axelrod, 2012).

An important feature in pattern formation is a symmetry break to differentiate one cell from neighbors in a homogeneous environment (Zou, 2020). Two neighboring cells that are identical can use a Delta-Notch signaling feedback loop between them to break this symmetry. This happens also in the *Drosophila* eye: A school example of epithelial organization, that is highly polarized with mirror-symmetry over the equator. The R3 and R4 photoreceptors in each ommatidium are vital in this polarity and PCP component Frizzled (Fz) regulates Delta-Notch signaling to determine the cell fate of photoreceptor R3 and R4 (Cooper and Bray, 1999). This mechanism can also yield a pattern in which each Delta-expressing cell in the epithelium is surrounded by cells with active Notch signaling. This contributes to the development of a well-ordered pattern and spacing of the aforementioned bristles on the *Drosophila* body (Cohen et al., 2010), and can be simulated in multi-cellular structures using synthetic cell-cell signaling (Toda et al., 2018). Furthermore, Delta-Notch signaling is found in the formation of stripes on zebra fish (Hamada et al., 2014). This is one example of how cell-cell signaling creates a symmetry break, discriminates self from others, and creates a pattern.

In this chapter I look into the organization of the lamina during scaffold formation and build towards an understanding of how the lamina can be formed from uniformly looking bundles to a patterned scaffold. First, I look at differentiating photoreceptors and their descend towards

the lamina plexus. Next, I investigate proteins and cell-surface molecules that localize on photoreceptors in the bundle and/or at the lamina plexus and their patterned expression at the lamina plexus. Lastly, I hypothesize how their expression may aid scaffold formation.

2.1 Photoreceptor bundles and their organization

There is a difference between the organization of R1-R6 in an ommatidium in the eye and their organization in a heel crescent at the lamina plexus; in the open trapezoid formation of rhabdomeres in the retina the R3 and R4 point *away* from the equator while in the crescent heel organization in the lamina the R3 and R4 point *towards* the equator (Horridge and Meinertzhagen, 1970; Meinertzhagen and O'Neil, 1991). There are two ways a bundle can rearrange its organization. Either photoreceptors shuffle, mingle, and braid to be organized at the level of the lamina plexus by an external factor to arrive in a rotated fashion. Alternatively, photoreceptors keep their relative position next to each other and rotate 180 degrees as a whole. In the latter scenario the intra-bundle organization stays intact. To test which of these two options is the case, one needs to obtain detailed information on the bundle organization. Photoreceptor bundles are so tightly organized in the optic stalk between the eye and the lamina that labeling of all photoreceptors with one antibody could not resolve individual axons inside the bundles. To overcome this problem, photoreceptors were labeled with a technique called MultiColor FlpOut (MCFO) (Nern et al., 2015). Normal Flp-FRT recombination is a site-directed recombination technique to alter DNA expression under controlled conditions *in vivo* (Cox, 1983; Theodosiou and Xu, 1998). MCFO is based on this technique and uses the flippase (Flp), to create multiple membrane-targeted and distinct epitope-tagged proteins that are sparsely and randomly expressed (see Figure 2.1). Figure 2.1 B (top) shows this technique as a schematic. Without a recombination event, the transcription terminator (stop-codon) flanked with FRT sites prevent transcription of the epitope. Upon Flp activation in a cell, this stop-codon is removed and the marker is expressed with 10xUAS activation. Under the GMR-Gal4 driver, this occurs in photoreceptors specifically. Three MCFO stop cassettes can give rise to a variety of colors depending on the number of recombination events (see Figure 2.1 B, bottom). Labeling the cell markers with different fluorescent secondary antibodies (post-experimentally rendered into different colors), multiple photoreceptors in a bundle can be visually distinguished from each other. In addition to the MCFO labeling, anti-chaoptin antibody (reveals actin) stains the membrane of all photoreceptors. Some photoreceptor membrane display extra brightness due to the blue channel

"leaking" into the chaoptin-obtained wavelength (see Figure 2.1 F). This occurred because the mouse and rat antibodies cross-reacted. This forms no problem for further analyses.

Heat-shock (Hs) duration is the main regulator of labeling density. A 5-8 minute Hs resulted in sparsely labeled photoreceptors in only primary colors (see Figure 2.1 A), while 20 minute Hs had still sparse labeling where all markers were consistently overlapping, resulting in an all white result (result not shown). A 12 minute Hs resulted in sparse photoreceptor labeling, with a diversity of overlap ranging from primary colors, to two and, in some cases, even three overlapping labels (see Figure 2.1 C). When taking an orthogonal cut through the optic lobe, photoreceptor bundles can be seen at the plane of focus. In Figure 2.1 D, it can be observed that photoreceptor axons, originating at different ommatidia, maintain their neighbor-to-neighbor organization. There is no braiding of neigboring bundles. In other words, the inter-bundle position does not change.

To investigate if braiding occurs within a bundle I needed bundles that contained several marked photoreceptors and follow their descent (see Figure 2.1 C). In the complete data set of six optic lobes, four bundles contained either 4 or 5 photoreceptors that were deferentially labeled. The labeling of the complete optic lobe was sparse enough to distinguish PRs axons in this bundle from neigboring bundles, dense enough to label 4 or 5 PRs in one bundle, and random enough to distinguish individual axons in one bundle. Figure 2.1 E shows the 3D visualization of the data, as well as the surface reconstruction of two bundles. The 3D surface reconstruction of labeled photoreceptors and subsequent analysis reveals that photoreceptors do not braid on their descent. Two out of four bundles show a single photoreceptor that did not "stay in line". Approaching the lamina, it moved towards a different position in the bundle, or to the complete outside of the bundle. While at first this suggests braiding, these photoreceptors can be identified as either an R7 or R8, determined from their location in the ommatidium where they occupy the center. In fact, all analysed bundles turned out to include an R7 or R8 photoreceptor (see Figure 2.1 F). This is a problem for the analysis since these photoreceptors do not terminate at the lamina plexus or obtain the R1-6 stereotypical organization. They do not need to stay in their neighbor-to-neighbor composition. R8 is the pioneer axon, leading the way during the initial photoreceptor descent, and R7 is the last photoreceptor to differentiate. Both pass through the lamina plexus on their way to the medulla. By excluding inner photoreceptors and considering labeled R1-R6 outer photoreceptors only, it reveals that these PRs always stay attached to each other and do not shift relative position. This adaptation did, however, change the number of PRs available for analysis to three, and in one case four, PRs per bundle.

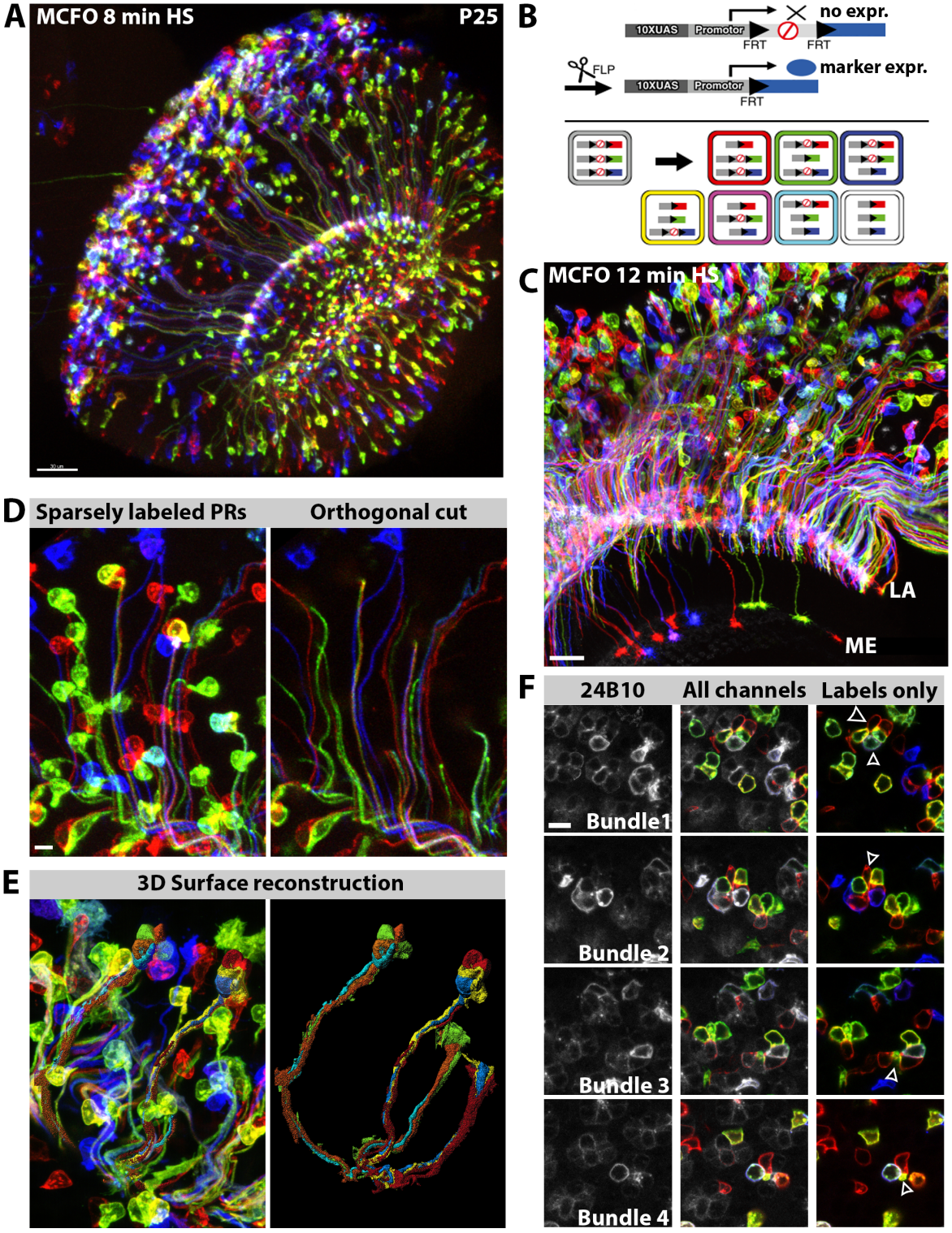

FIGURE 2.1: Sparsely and randomly labeled PRs reveal bundle organization

A) Overview of the optic lobe at P25. Photoreceptors are sparsely and randomly labeled using MultiColor FlpOut (MCFO) technique. A heat-shock of 8 minutes produces sparsely labeled photoreceptors with single labels (primary colors). Scale bar 30 μm. **B**) Top. Schematic of one MCFO reporter with 10 Upstream Activating Sequences (10XUAS) and a core promoter for GAL4-activated expression, a transcription terminator (STOP sign) flanked by Flp Recombination Target (FRT) sites, and an marker. Bottom. Potential marker combinations with three MCFO stop cassettes with different color markers: unlabeled (gray), single marker (red, green, blue), or combinations of two (yellow, magenta, cyan) or three (white) labels. Panel adapted from Nern et al. (2015). **C**) Part of the optic lobe showing retina on top, lamina (LA) and medulla (ME) with sparsely labeled photoreceptors with single and double labels (primary colors + mixed) produced by MCFO. Scale bar 20 μm. C) Selection of MCFO labeled photoreceptors (left) and showing only the axons (right) reveals no braiding between bundles. **D**) 3D surface reconstruction reveals a 180 degree rotation within a bundle, but no braiding. **E**) Four bundle examples. Cut through the photoreceptor cell bodies in the retina reveals the R7/R8 photoreceptors (indicated by white arrowheads). Scale bar 5 μm.

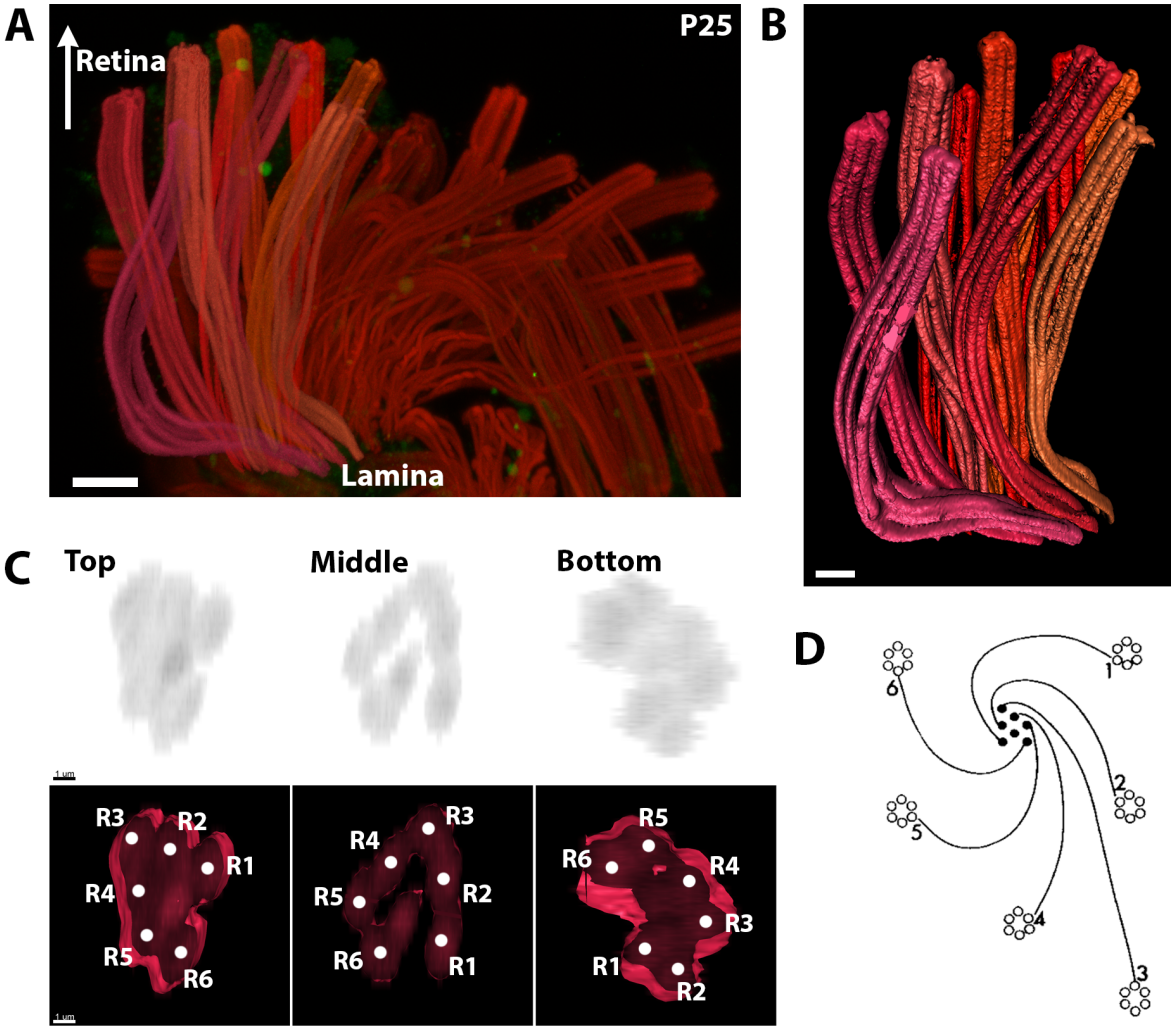

FIGURE 2.2: Bundle rotation between retina and lamina

A) Overview of remaining bundles after removal of retina and the majority of bundles. All photoreceptor bundles stained with anti-chaoptin. Scale bar 10 μm. **B**) 3D surface reconstruction of nine bundles. Colors on photoreceptor bundles are only meant to ease discrimination between them. Scale bar 5 μm. **C**) Cut through a bundle at three depths. *Top* resembles a cut through the bundle in the direction of the lamina, *middle* halfway the length of the bundle, and *bottom* close to the lamina. Dots in the bottom panels represent the middle of an axon with the indicated photoreceptor sub type (R1-R6) written. Note that relative position of R1-R6 stays intact. Scale bar 1 μm. **D**) Graphic representation of bundle rotation between the rhabdomeres in the eye and lamina cartridges at the lamina. Note the 180 degree rotation between retina and lamina. Panel adapted from Hardie (1983).

While spectacular images are obtained from the MCFO experiments, this elaborate method with sparse labeling, lengthy data acquisition and time consuming analyses proves inefficient to obtain absolute certainty in answering the question if photoreceptors braid during axon descent. On the other hand, staining all photoreceptors and considering all bundles would result in too crowded images, making it virtually impossible to identify individual axons in a bundle and assess the organization. To circumvent this problem, laminae were dissected very carefully to keep some bundles attached, while removing the outer retina and the majority of photoreceptor bundles attached to the lamina (see Figure 2.2). What remains is the optic lobe with the lamina attached and a small patch of bundles attached to the lamina. During one attempt, an estimated 30 (out of approximately 800) bundles remained attached, allowing for a detailed analysis of (only) a few bundles. Figure 2.2 A and B show the chaoptin staining (24B10 antibody) of all photoreceptors and 3D surface reconstruction of nine bundles. Figure 2.2 C shows a representative example of a descending bundle. All bundles show a stable, circular or oval organization along the length of the bundle. From the surface reconstruction of these bundles, it becomes clear that the complete bundle rotates, but that individual photoreceptor axons do not change location within the bundle. All nine bundles show no signs of braiding of photoreceptors, e.g. the intra-bundle organization is stable. Thus, the 180 degree rotation applies to the bundle, as illustrated by the model from Hardie (1983) in Figure 2.2 D, also at P25, while neighboring bundles do not switch position. Interestingly, not all bundles rotate in the same direction. Some rotate clock-wise, while others rotate counter-clockwise (data not shown). This does not depend on the position of the equator since these bundles do not project to an area of the lamina close to the equator.

2.2 Protein patterns at the lamina plexus

Once LN neurites have arrived to the lamina plexus, the lamina is made up of two cell types; photoreceptors with their stabilized heels and LN neurites. Together they create the scaffold. Each heel structure (of six heels from one bundle) contains L-cell neurites (from five LNs) in its center and obtains a horse shoe shape. It is a pre-pattern that is essential for further development of the fly visual system. It is unknown how this scaffold forms exactly, and how its structure is maintained over time. To investigate the presence of cell-adhesion molecules that could influence the pattern formation in the scaffold, an antibody screen of cell-surface proteins was performed that identified multiple hits. Strikingly, multiple cell-surface proteins create a pattern of their own at the lamina plexus. Their expression patterns are presented

in this chapter, and one particular protein is presented and discussed in depth in the Chapter 3.

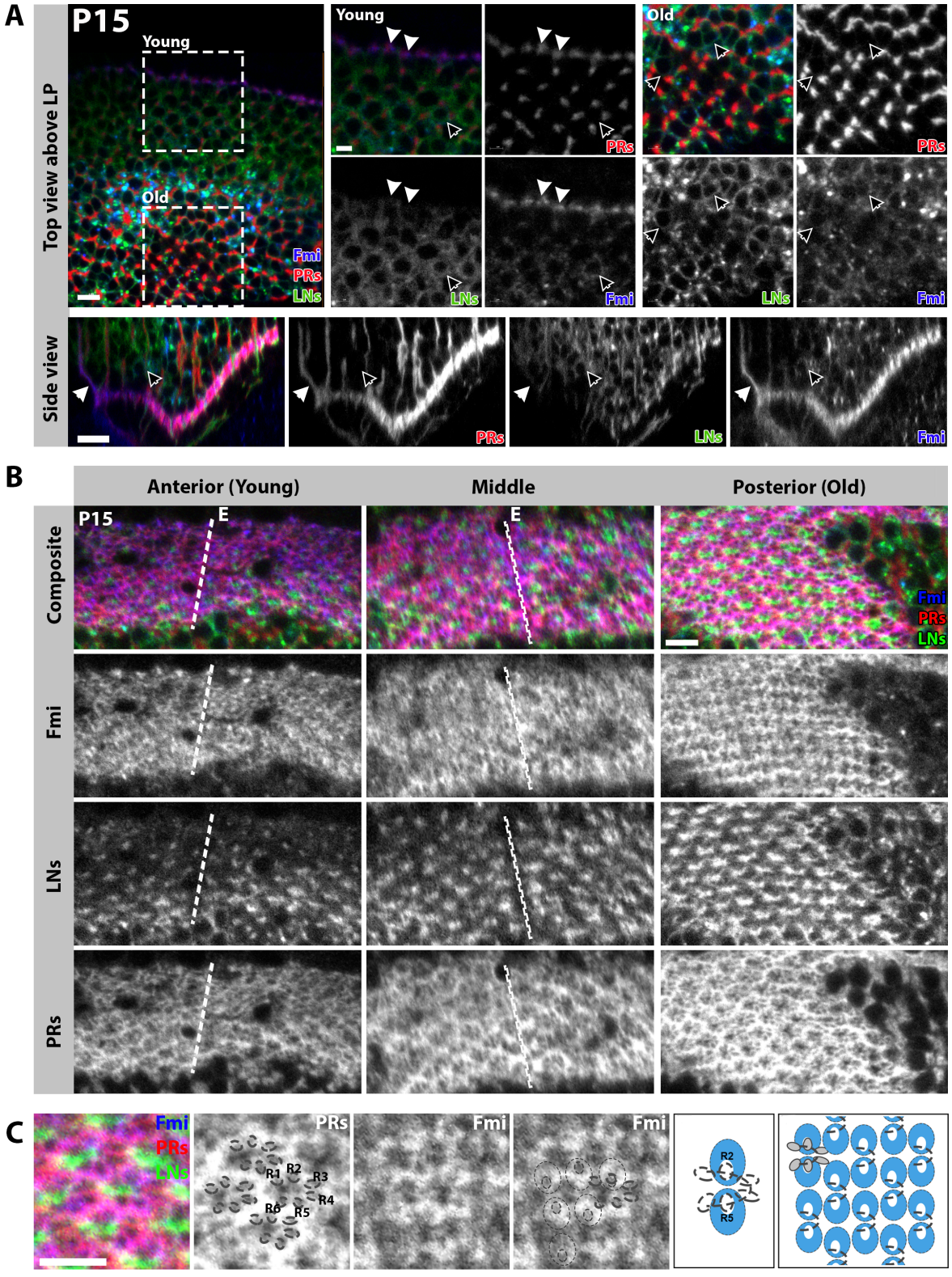

FIGURE 2.3: Flamingo localization during early development

A) Only the youngest row of incoming photoreceptor bundles strongly expresses Fmi. Anti-Fmi blue, Lamina Neurons green, photoreceptors red. Filled arrows point at youngest photoreceptor bundles that express Fmi. Open arrows point at L-cell cell bodies that express Fmi on the membrane. Images obtained from P10 pupae. **B**) Top view of the lamina plexus from anterior (youngest part of the lamina; left) to posterior (oldest part of the lamina; right). Dotted line marked with E indicates the location of the equator. **C**) Detail from the posterior lamina plexus. Photoreceptor heels are indicated with circles and Fmi localization is indicated with blue in the schematic on the right. Scale bar 5 μm.

Flamingo

The atypical cadherin Flamingo (Fmi), also named Starry Night (Stan), was first described in *Drosophila* as a component of the planar cell polarity pathway (PCP) (Chen and Clandinin, 2008; Das et al., 2002). At the lamina plexus, Fmi functions exclusively in PRs and has a patterned expression pattern. The expression of Fmi on descending photoreceptor bundles was first described by Lee et al. (2003) and is used as a marker to identify the most recently arriving bundles to the lamina (Umetsu et al., 2006). *Drosophila* Fmi mutants show target selection defects of photoreceptor axons (Chen and Clandinin, 2008; Lee et al., 2003), and when Fmi is over-expressed in R4 it causes neighboring photoreceptors to mis-target (Chen and Clandinin, 2008).

Figure 2.3 A shows that, indeed, Fmi staining of the lamina shows Fmi expression on the youngest bundles (most anterior), but not on older bundles. A few columns away from the youngest column, Fmi is expressed on the cell bodies of lamina neurons (see Figure 2.3 A). Figure 2.3 B shows that the expression of Fmi during development goes from unpatterned at the most anterior side (young), to nicely pattered at the older, more posterior part of the lamina plexus. Towards the older side it forms a clear expression pattern of horizontal and vertical lines that appears to overlap with photoreceptors. A more detailed analysis reveals that the strongest Fmi staining can be found around the heels of R2 and R5, with the larger bulk towards the outside of the heel structure (see Figure 2.3 C). On one "line" of Fmi, it alternates Fmi expression around R2 of the upper heel crescent and around R5 heels from a lower heel crescent. Thus, the photoreceptor scaffold of R2 and R5 in the heel organization at the lamina plexus creates the Flamingo pattern. This suggests that Fmi is involved in inter-bundle organization rather than in intra-bundle organization.

Ecad, Armadillo, and Sidekick

Armadillo (Arm) is a component in apical-basal polarization of epithelial cells during embryonic development (Huang et al., 2011) and a core component of the adherens junction (Cox et al., 1996). Other functions of Arm include the regulation of cell death (apoptosis)

during retinal development (Ahmed et al., 1998), and interactions in the Wingless signaling pathway as revealed by Noordermeer et al. (1994) in the *Drosophila* embryo.

With the performance of an antibody screen to check the expression profile of several membrane bound proteins, I discovered the patterned localization of Armadillo (see Supplementary Figure A.1). Arm localizes at the LN neurites in the LP, as well as in between photoreceptors where is appears as stripes. The patterned expression of Arm in the developing lamina in the *Drosophila* optic lobe is, to my knowledge, a novel finding and has not been reported before. Other proteins identified at the LP include Roundabout (Robo; involved in axon extension and turning (Kidd et al., 1999)), Fasciclin-2 (Fas2; involved in cell adhesion and neuron-glia interaction (Higgins et al., 2002)), and Disc large (Dlg; involved in cell polarity (Woods et al., 1996)). None of these proteins showed a particular pattern that involved photoreceptors.

As Arm is a polarization factor in embryonic development, it may also serve for polarization of the scaffold at the lamina plexus. To investigate the role of Arm at the LP, a timeline analysis was performed to investigate the time frame during which Arm is present in the lamina plexus. Figure 2.4 A shows anti-Arm antibody staining at different pupal ages (P20-P45). It shows that Arm is expressed in the scaffold, where it has the clearest patterned expression between heels around P20-P25. This is during scaffold formation and the start of photoreceptor extension. In time, this pattern is lost in late pupal stages. Arm in present at the center of cartridges in late pupal stages (P45), localizing at LN dendrites (see Figure 2.4 A).

Furthermore, Armadillo co-localizes with Sidekick [1] (Sdk; see Figure 4.1 B); a previously published homophilic adhesion molecule, in between photoreceptor heels (Astigarraga et al., 2018). Co-localization of Arm and Sdk was also previously reported in the *Drosophila* germband epithelia and genitalia epithelia, where they are involved in bicellular junction extension (Uechi and Kuranaga, 2019). In addition, immunoprecipitation with Sdk::YFP pulled out Armadillo, further suggesting an interaction between the two (Uechi and Kuranaga, 2019).

Figure 2.5 shows a comparison of three patterned proteins at the lamina plexus that have comparable expression patterns. E-cadherin (Ecad) staining reveals dots in between photoreceptor heels that appear circular (see Figure 2.5 top panels). Ecad exhibits a striking localization pattern, marking the adhesion surfaces of R1-R6 within the origination bundle. Per heel crescent it shows six markings. This pattern is similar to, but even more restricted than the cell adhesion molecule Sdk. Sdk staining reveals ellipsoids in between photoreceptor

[1] Armadillo-Sdk double staining shown in Figure 2.4 B performed by Monika Kauer.

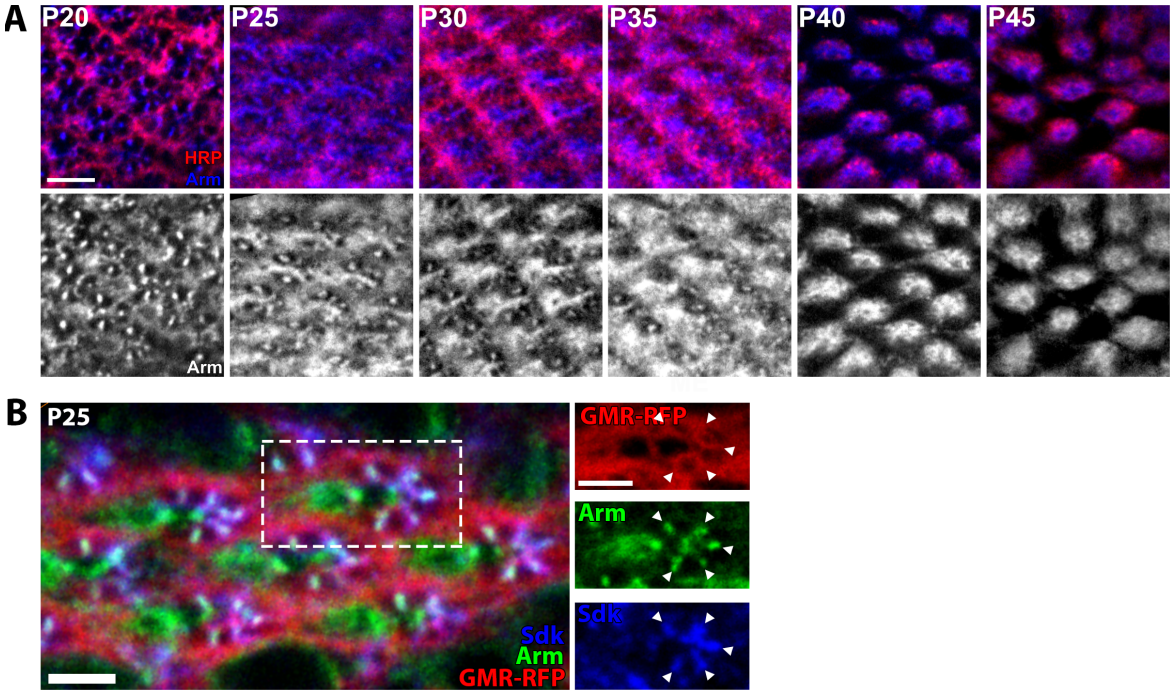

FIGURE 2.4: Armadillo localization at the LP during development

A) Timeline (P20-P45; 5 hour intervals) of dissected WT brains stained for HRP (neurons) and Armadillo reveals a pattern at the lamina plexus. HRP staining in red, Armadillo (Arm) in blue. **B**) Co-localization of Arm and Sidekick (Sdk) at the lamina plexus. Staining and panel by Monika Kauer. Scalebar 5 um.

heels. Per heel crescent it shows five markings; not between R1 and R6 (see Figure 2.5 middle panels). Armadillo staining reveals longer, stripe-like markings in between photoreceptor heels and also marks the neurites of LNs. Per heel crescent it shows five markings in between photoreceptor and one large marking at LNs (see Figure 2.5 bottom panels).

Sdk, Ecad and Arm are core components of adherens junctions, which serve key roles in numerous pattern formation processes (Cox et al., 1996; Finegan et al., 2019; Fung et al., 2009; Straub et al., 2011; Uechi and Kuranaga, 2019). Furthermore, Sdk, Ecad and Arm serve several functions during photoreceptor development (Ahmed et al., 1998; Astigarraga et al., 2018; Nguyen et al., 1997) In Chapter 3, the role of Sdk in lamina development is investigated more in depth.

2.3 Planar cell polarity is not involved in lamina patterning

A group of signaling molecules, including Frizzled (Fz), Dishevelled (Dsh), Flamingo (Fmi), Van Gogh (Vang), and Prickle (Pk) mediate planar cell polarity (PCP) signaling in developing *Drosophila* epithelial sheets. Like epithelial sheets, the lamina plexus is a single cell layer, with axons and neurites instead of epithelial cells. Because several PCP components are

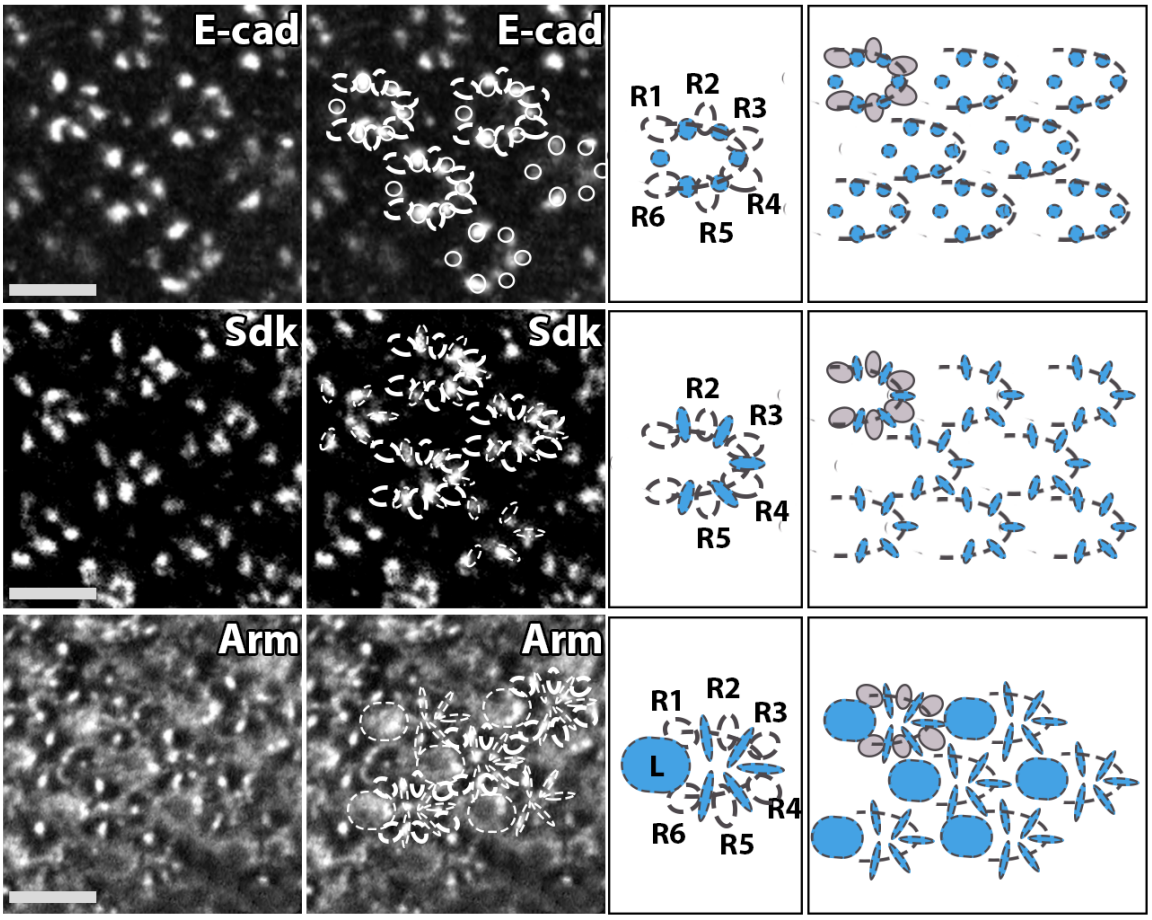

FIGURE 2.5: Schematic comparison of patterned proteins at the lamina at P25

Detailed section of the lamina plexus. Open circles represent photoreceptor heels (R1-R6), dotted outlines and light blue represents protein localization. Crescent line indicates the location of a heel crescent. **Top panels**) anti-E-cadherin staining. **Middle panels**) anti-Sidekick staining. **Bottom panels**) anti-Armadillo staining. Scale bar is 5μm.

identified at the lamina plexus (Fmi and Sdk; see Sections 2.2 and 2.2), and because of the asymmetric (polarized) organization of the axon scaffold during development, I investigated if scaffold formation is based on the principle of PCP. Therefore, GFP was expressed under known Fmi interaction partners within the PCP-pathway, e.g. Frizzled (Fz), Frizzled-2 (Fz-2), and Prickle (Pk) [2] (Struhl et al., 2012). The localization of the GFP signal within the developing optic lobe at P15 and P25 was assessed to discover if there is expression during scaffold formation [3].

After dissection at P15 and P25, brains were stained for Fmi and anti-GFP to increase the visibility of the GFP signal. Confocal images were taken of the complete optic lobe (see Figure 2.6 A) and show that Fz, Fz-2 and Pk are expressed in the optic lobe, but not at the

[2]Fz-Gal4, Fz2-Gal4, and Pk-Gal4 were kindly provided by Gary Struhl.
[3]PCP component localization experiments were conducted in collaboration with Melinda Kehribar.

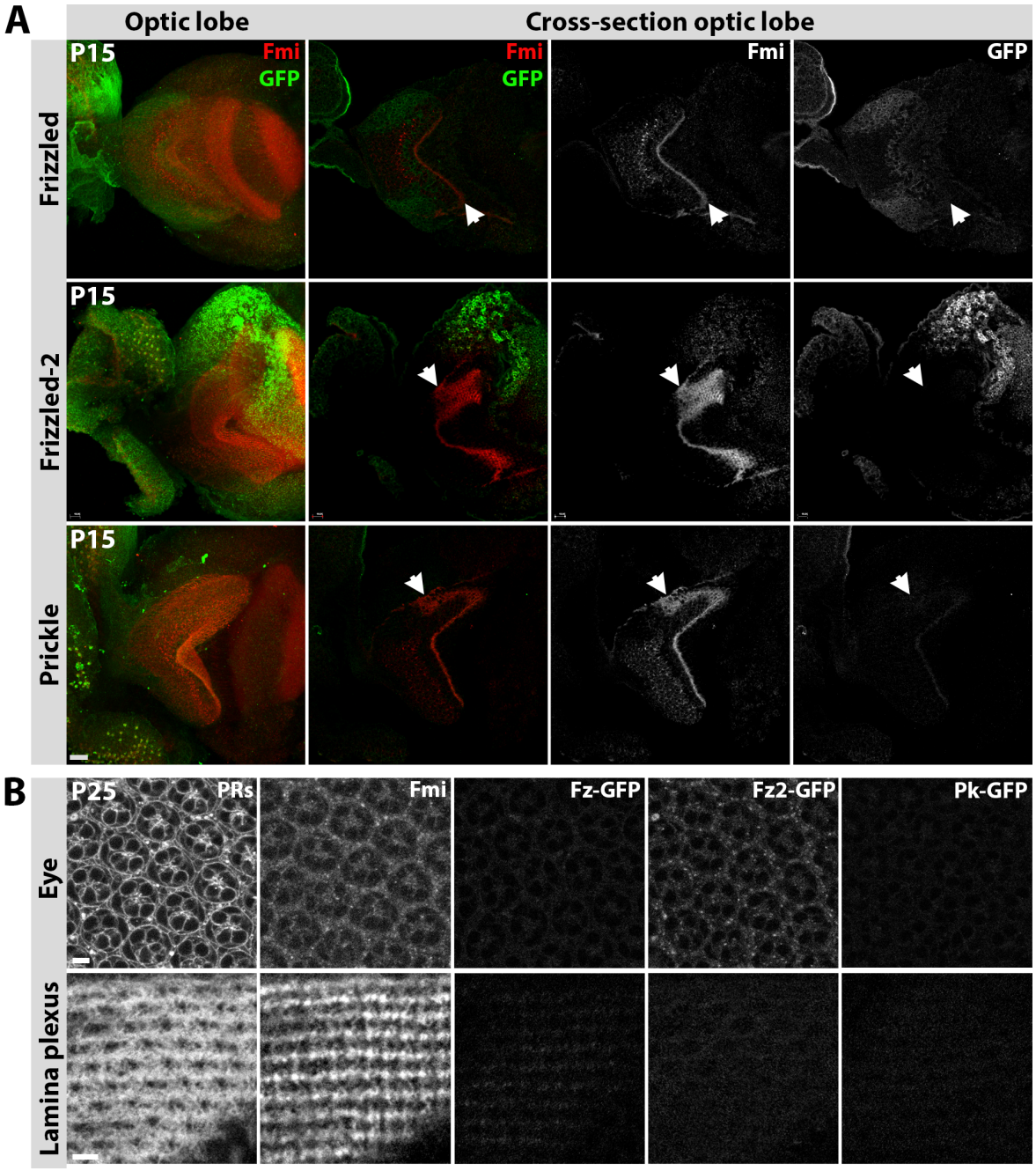

FIGURE 2.6: Expression of PCP components in the optic lobe

A) Expression of GFP under Fz-Gal4, Fz2-Gal4, or Pk-Gal4 driver in P15 optic lobes. Most left, stacked image. Right images, section through the optic lobe. Retina on the left side of every image. White arrows indicates the lamina plexus. GFP in green, anti-Fmi antibody staining in red. Scale bar 15 μm. **B**) Expression of GFP under Fz-Gal4, Fz2-Gal4, or Pk-Gal4 driver in P25 eye and lamina plexus. Most left is 24B10 staining to show photoreceptors and Fmi staining (second image). Scale bar 5 μm.

lamina plexus. All three proteins have expression in the eye, and Fz-2 shows a cluster of GFP-positive cells of an unknown cell-type on the dorsal side of optic lobe. However, non of the proteins is expressed at the LP at P15. At P25, confocal images of the retina show that Fmi and Fz-2 are expressed in inter-ommatidial cells and on the cell body of photoreceptors, but Fz and Pk have no expression here (see Figure 2.6 B, top panels). At the lamina plexus, only Fmi shows a pattern, and non of the other PCP components are present (see Figure 2.6 B, bottom panels). To exclude the possibility that the Gal4 drivers were not working properly, another experiment tested whether antibody labeling could identify Fz, Fz-2, or Pk protein in the lamina plexus. This resulted in a negative result (results not shown). While both Sdk and Fmi show distinct expression patterns, their interaction partners from the canonical PCP pathway could not be detected at the lamina plexus.

2.4 Conclusions and Discussion

Until recently, knowledge on the organization of a photoreceptor bundle during development of the visual system was based on suggestions from the early 70's and 90's, rather than experimentally shown (Horridge and Meinertzhagen, 1970; Meinertzhagen and O'Neil, 1991). Investigating the organization of photoreceptor bundles led to the following conclusions: 1) R1-R6 photoreceptors keep their relative position next to each other in a bundle, and 2) bundles cluster in superfascicles in which the neighbor-to-neighbor organization stays intact during descent, over the course of development and thereafter. Thus, both inter-bundle organization as well as intra-bundle organization are a representation of the inter-ommatidial and intra-ommatidial position, respectively. These conclusions are in line with a recent publication by Chang et al. (2018) who show the order of photoreceptor descent to the lamina using a sparse labeling technique.

Of course, the end-point organization does not tell how rotation happens during development, and up until this point there would be no technique to validate this due to technical constraints. Gal4-drivers are not active right after photoreceptor differentiation and live-imaging during this early stage of development is made virtually impossible due to rotation of the internal structures. For these reasons, it is not possible to observe the descent of photoreceptors to the lamina with live-imaging. The analysis of the early photoreceptor scaffold gives the closest means of determining the arrival of photoreceptors.

It is very likely that photoreceptors descent to the lamina in their order of differentiation. R8 is thereby the pioneer axon that leads the way to the lamina. Pioneer axons may not

always be needed for axon pathway formation. It has been suggested that the importance of pioneer axons in the CNS and PNS rather depends on the context (Lin et al., 1995). But in certain settings they have been shown vital to correct axon extension. In *C. elegans*, it was shown that pioneer axons create a guidance path along which later-outgrowing axons extend. Loss of function of FMI-1, a *Drosophila* Flamingo ortholog, in pioneer axons caused later-descending axons to separate from the pioneer axon and resulted in incorrect navigation to the brain (Steimel et al., 2010).

The localization of Fmi on the youngest arriving bundles (most anterior) is in line with findings that show that Fmi is expressed in pioneer axons (Lee et al., 2003). At the lamina plexus, I see a different pattern appear. No longer is Fmi only expressed in the most anterior bundle, but in a pattern across the lamina. The early expression pattern at the lamina plexus suggests the highest expression on the growth cones of R2 and R5 (see Figure 2.3). Schwabe et al. (2013) describe the localization and adhesive function of Fmi at the central part of the growth cone, and not at the periphery where extending filopodia sit. This is in line with my findings at P25. They do not describe a difference in expression on different photoreceptor sub types. I suggest, however, a higher expression on R2 and R5 that could build an interaction network between heel structures in the scaffold. These adhesive interactions could create a stable network of R2s and R5s that ensure an organized scaffold. Future research could aim to make a working computational model that builds a scaffold (or at least maintain a stable scaffold) using Fmi-adhesion as the main source of input information.

I determined that the Fmi pattern at the lamina plexus follows from the localization of R2/R5 between neigboring heel crescents in the scaffold. A regular scaffold means a regular Fmi pattern. In contrast to Fmi, Ecad, Sdk, and Arm localize within the heel crescent, in between photoreceptor heels. Their localization may have a function in cell-cell adhesion and form the "glue" in between photoreceptor heels that creates the typical crescent heel formation. It was suggested by (Lee et al., 2003) that Fmi on growth cones regulates appropriate outgrowth angles of R1–R6 growth cones during neural superposition sorting in the lamina. The hypothesis that Fmi regulates a regular pattern does not undermine this suggestion, as a regular pattern creates the foundation for correct extension angles.

Is is likely that all the patterned proteins investigated in this small essay are interdependent. I found, for instance, that RNAi expression of one of the proteins influences expression pattern and/or level of other proteins in a dependent way (see Supplementary Figure A.2). The dependence of Ecad expression of Arm levels was previously reported by Rogers et al. (2018), who demonstrate that the balance of Ecad and Ncad is dependent upon the availability

of β-catenin (Arm) proteins, and that alteration of either one modifies the proportions of differentiating cell types.

Sdk and Fmi are components of the planar cell polarity pathway that is involved in tissue patterning. Surprisingly, no PCP signaling pathway components were detected at the LP during scaffold formation. While Fz was reported to present itself at the lamina (Sato et al., 2006) (unpublished results), it was not detected with GFP expression under the Fz-Gal4 driver, nor with the anti-Fz antibody. Thus, although PCP signaling pathway components Fmi and Sdk are present at the LP during scaffold formation, they function in a non-canonical manner in a function that is not related to the classical PCP pathway.

Chapter 3 describes the localization of Sidekick protein and its influence on pattern formation during development in more detail.

Chapter 3

The role of Sidekick in adhesion and early pattern formation

Not only cells can organize themselves in an iterative pattern, but proteins can also be expressed in a patterned way (as presented in Section 2.2). Protein expression patterns can exercise many functions that may be crucial for polarity, cellular functions, or adhesion at distinct positions. Sidekick (Sdk) proteins are members of the immunoglobulin (Ig) superfamily that can mediate homophilic adhesion through their four N-terminal Ig domains (Goodman et al., 2016). The possible role for the adhesion molecule Sidekick in *Drosophila* development was first described by (Nguyen et al., 1997). In this first Sdk mutant study, it was reported that flies show defects in pattern formation in the eye disk. Nguyen and colleagues suggest that Sdk is needed at the ommatidial pre-cluster stage of development when the identity of R2, 3, 4, and 5 are defined. This implies that there is a very specific time slot for when Sdk is necessary; after R8 differentiation, and before R1-R6 differentiation (Nguyen et al., 1997). Newsome et al. (2000) suggest that Sdk functions as an adhesion molecule right around that time; not so much to organize the ommatidium, but because photoreceptors need adhesion to R8 to follow the extension of this pioneer axon into deeper layers in the brain. However likely this suggestion sounds, to my knowledge, experiments neither confirming or defying this hypothesis were ever published.

Instead, research focused on a possible role for Sdk at the photoreceptor growth cones in the lamina plexus. The localization of Sdk at the lamina plexus was reported first by Astigarraga et al. (2018). They show that Sdk localizes in between photoreceptor heels in the scaffold. During the sorting phase, the Sdk mutant displays photoreceptor extensions in the lamina that are not always directed towards the correct post-synaptic target, which results

in a mis-wired optic field and, subsequently, in impaired opto-motor behavior. In contrast to the full mutant, single R4 photoreceptors that lacked Sdk showed no defect in polarization (Astigarraga et al., 2018).

Astigarraga et al. also report the localization of Sdk on photoreceptor bundles and lamina neuron cell bodies above the lamina. They report a mutant phenotype where LNs penetrate the lamina at larval stage L3 and localize in or under the LP instead of above it. The Sdk mutant phenotype could be replicated by the expression of SdkRNAi in photoreceptors. In contrast, no gaps in the LP were observed with SdkRNAi expression in lamina neurons (NP6099-Gal4) or glia (Repo-Gal4). They conclude that Sdk functions only in photoreceptors. In succession, it suggests that homophilic adhesive properties of Sdk cannot influence the connection between pre-synaptic photoreceptors and post-synaptic lamina neurons; only between photoreceptors themselves. It is hypothesized that due to diminished homophilic adhesion between photoreceptors in Sdk mutant flies, gaps appear in the lamina and some lamina cells "fall through" (Astigarraga et al., 2018). This implies that the structural integrity of the lamina plexus, and thereby the early pattern, is dependent on Sdk. Surprisingly, the photoreceptor scaffold at the lamina plexus is not shown in their publication.

Other studies also imply a function for Sdk in normal cell arrangements. In epithelial sheets, the localization of Sdk was pinpointed to tri-cellular adherens junctions where it is able to organize cell-cell contacts and rearrangements. It could be found at contact points between either three cells at tri-cellular junctions or two cells (Finegan et al., 2019). Differential localization of Sdk to regions experiencing higher tension implies that Sdk can respond to different tension and contractility (Letizia et al., 2019), thus maintaining the structural integrity in that way. Moreover, in developmental stages with cell-rearrangements or tissue rotation, Sdk is required for bi-cellular junction extension (Uechi and Kuranaga, 2019).

Taken together, this suggests that there is a broad function for Sdk in adhesion, structural integrity, and regular patterning of a tissue. In this chapter, I discuss the role of Sdk at the level of early bundle configuration and the formation of the lamina scaffold. Moreover, the possible role for Sdk that may explain the reported mis-wiring phenotype by Astigarraga et al. (2018) is investigates. I hypothesize that an early role for Sdk in adhesion and bundle organization is important for the later stability of the lamina structure. In this chapter, I first discuss the WT localization of Sdk during development, after which I investigate the role of Sdk in 1) bundle organization, 2) scaffold formation, and 3) single photoreceptor extension angles.

3.1 Sidekick localization during development of the optic lobe

To be able to understand the function of Sdk during development, the expression profile of Sdk in the *Drosophila* visual system is investigated with a timeline analysis. Dissected brains from wild-type (WT) animals at different developmental time points were stained with the anti-Sdk antibody[1] to obtain a timeline of Sdk expression. Figure 3.1 shows that the Sdk localization in the retina, on photoreceptor bundles, and at the lamina plexus is transient. In the eye, Sdk is present in inter-ommatidial cells and in between photoreceptors. The latter is most clearly noticeable around P40-P50 (see Figure 3.1 B). No Sdk is present in the adult eye (data not shown). From the larval stage L3, very early in visual map formation, up until around P40, there is a clear presence of the protein at the lamina plexus. As early as P15, a pattern appears that covers the lamina plexus (see Figure 3.1 C). Like published by Astigarraga et al. (2018), Sdk localizes in between the heels of photoreceptors, except for the space between R1 and R6 of the same bundle. This iterative pattern on every heel crescent is maintained over the course of photoreceptor extension (P20-P40). Around P45 the Sdk signal weakens and is less clearly visible between the heels. It is still present on photoreceptor growth cones, but it lacks the stereotypical pattern that it has before. Around P50–when columns are formed, photoreceptors stabilize at the target, and synapse formation starts–the signal fades away. At the adult lamina, any remaining Sdk signal coming from Sdk staining could no longer be detected.

Sdk is present on bundles of photoreceptors throughout development. Sdk is observed on bundles; especially on the young bundles that are descending (anterior side), or just have descended onto the lamina (see Figure 3.2 B). Moreover, Sdk localizes to the cell body of lamina neurons. This was previously described by Astigarraga et al. (2018).

3.2 Sdk mutant displays lamina scaffolding defects

Late developmental defects were mapped (photoreceptor extension, final wiring, and behavioral defects) by Astigarraga et al. (2018). To investigate the role of Sdk during development, I dissected $Sdk^{\Delta 15}$ mutant animals[2]. To test the mutant and to reproduce the reported phenotype, adult brains were stained with 24B10 antibody to see all photoreceptors in the cartridges. The lamina looks disturbed with uneven spacing between cartridges and hypo- or hyper-innervation of cartridges (see Supplementary Figure A.3). Defects, apparent at the

[1] Anti-Sidekick antibody was kindly provided by Jessica Treisman.
[2] *Drosophila* flies mutant for Sdk were provided by Jessica Treisman.

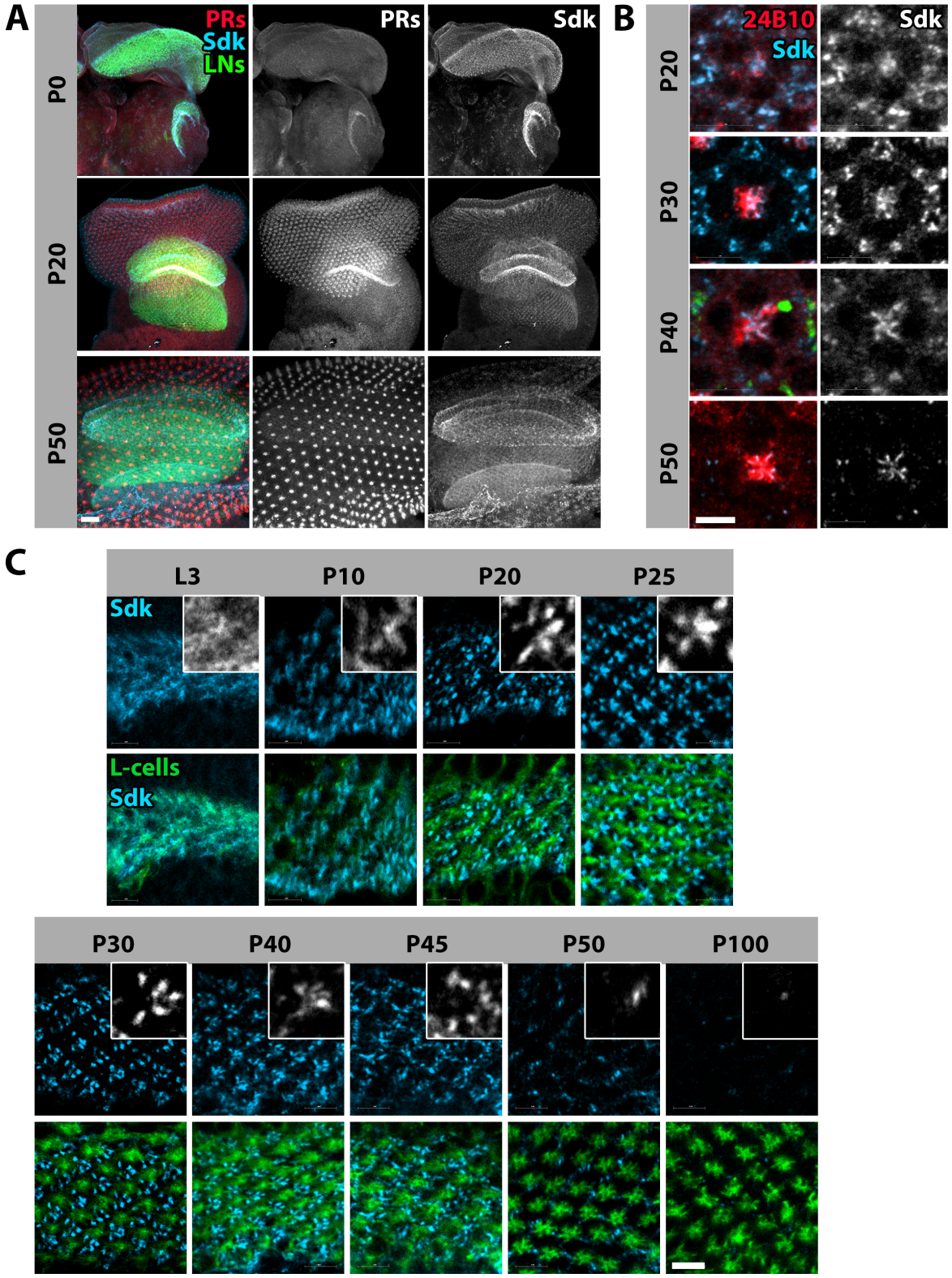

FIGURE 3.1: Sdk expression profile in the *Drosophila* visual system

A) Overview of Sdk localization during of the optic lobe at P0, P20, and P50. Photoreceptors red; Lamina neurons green; Anti-Sdk antibody staining blue. Scale bar 15 μm. **B**) Sdk localization during development of the eye. Representative ommatidium at P20, P30, P40, and P50. Scale bar 5 μm. **C**) Sdk localization during development of the lamina between larval stage (L3) and adult (P100). Cross-sections of the lamina plexus at each time point. Lamina Neurons in green; Anti-Sdk antibody staining in blue. Scale bar 5 μm.

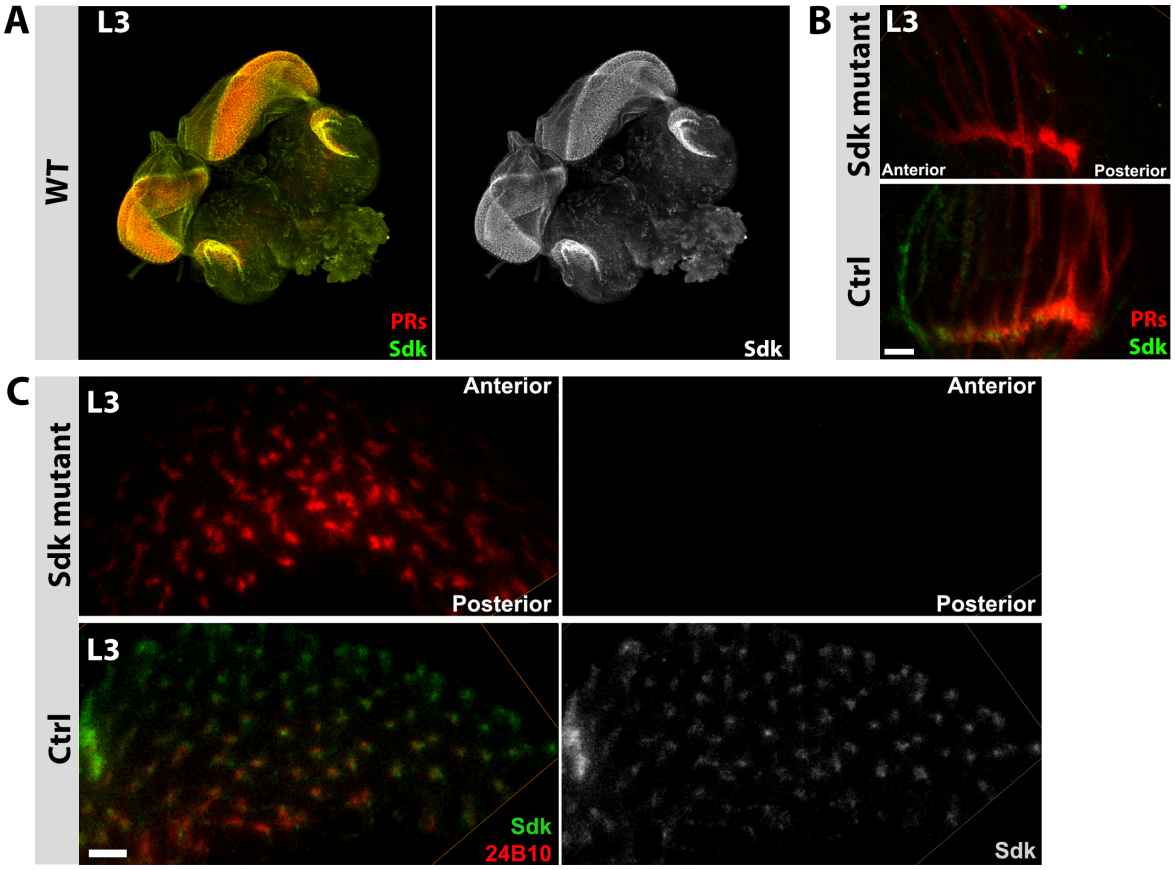

FIGURE 3.2: Sidekick mutant phenotype at larval stage L3

A) WT expression of Sdk in the optic lobe of the L3 larvae. Photoreceptors red, Sdk green. **B**) Comparison of WT and Sdk mutant lamina development. A transversal cut through the lamina shows incoming photoreceptor bundles and a side view of the lamina plexus. **C**) Comparison of WT and Sdk mutant bundles. Images taken 2 μm above the lamina plexus. 24B10 staining (photoreceptors) red, Sdk green. Scale bar 5 μm.

end of a developmental program, may have an early cause. They can carry over from early to subsequent developmental steps. Yet, from adult analyses it remains unclear how the formation of lamina is affected during development.

To replicate findings from Astigarraga et al. (2018) and to investigate if Sdk has an early role during development, the formation of the scaffold at the lamina plexus was visualized and WT and the Sdk mutant compared. Figure 3.2 B presents a side view of the LP at larval stage L3 and shows that the scaffold forms in a similar way as the WT, but with a slight developmental delay. It is smaller in size, with less photoreceptor bundles that have descended from the eye to the lamina plexus. Figure 3.2 C presents a cross-section of bundles 2μm above the lamina plexus and shows the difference in the number of descended bundles at Ls. The exact quantification of this delay is difficult. Yet, these images are comparable with previously published results (Astigarraga et al., 2018). Furthermore, bundles seem less evenly spaced on their descent to the LP, when compared to WT (see Figures 3.2 B and C).

There are noticeable gaps in the lamina, comparable to the phenotype that was described by Astigarraga et al. (2018) where LNs passed through the LP. In summary, the $Sdk^{\Delta 15}$ mutant has the same phenotype as reported in published work and can be used for further experiments.

The organization of the LP is easier to assess at a later time of development, when more PRs have stabilized their heels at the LP and the LP is less curved. Hence, the lamina plexus was further investigated at P20-P25, when a proper scaffold has formed. Dissected brains were stained with anti-chaoptin (24B10) and anti-Sdk antibodies to visualize all photoreceptors and (the lack of) Sdk. In WT, the scaffold consists of photoreceptor heels that form crescent shapes that lay as fish scales organized in a two-dimensional plane. From the orientation of the heel crescents one can determine the location of the equator, which is towards the bend side of the crescent. In Figure 3.3 (top left panels) it can be observed that in the $Sdk^{\Delta 15}$ mutant, the scaffold is not properly organized. From the organization of the heels, one cannot determine the location of the equator.

Moreover, I investigated the localization of other proteins that present themselves in a pattern at the LP during development (see Figure 3.3 bottom panels). Namely Armadillo (Arm), Flamingo (Fmi), and E-cadherin (Ecad). I found that their expression pattern is disturbed when they normally co-localize with Sdk. This is the case for Arm and Ecad. Arm in WT is expressed in the neurites of lamina neurons and in between photoreceptor heels (like Sdk; see Section 2.2). In the Sdk mutant, Arm is still expressed in lamina neurons, but the expression in dots between heels is lost. The remaining signal in between photoreceptors are likely protrusions of lamina neurites that still have Arm on their membrane. Ecad has a dotted pattern across the lamina plexus, very similar to Sdk in WT (see Section 2.2 and Figure 2.5). The dots are smaller, but co-localize. In the Sdk mutant, the Ecad signal is almost completely lost. Fmi is not affected in the expression intensity, nor in expression profile. In WT, Fmi is expressed at R2 and R5 -and less at R1 and R6- and this expression is maintained in the Sdk mutant. The reason that the pattern is not observed in the Sdk mutant is because photoreceptors are not localized correctly. Hence, the localization of Fmi seems disturbed, but is actually intact.

3.3 Bundle rotation is affected in the Sdk mutant

In the previous section, it was shown that the $Sdk^{\Delta 15}$ mutant has a scaffolding defect at the LP. Scaffolding defects could arise from a mis-orientation of incoming bundles. To investigate

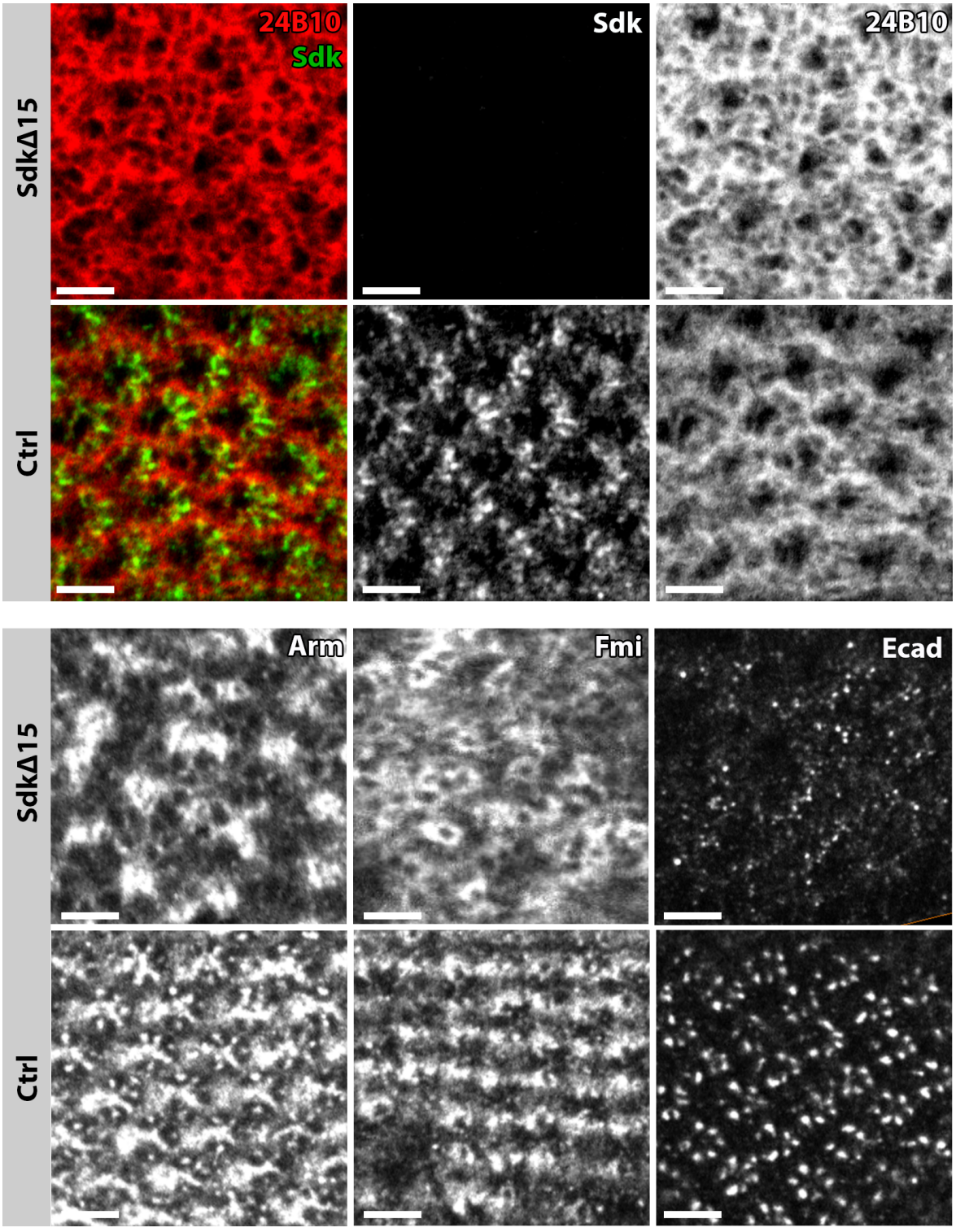

FIGURE 3.3: Patterned proteins are affected in the Sdk mutant

The Sdk mutant alters the expression of other patterned proteins at the lamina plexus. **Top panels**: 24B10 staining of all photoreceptors reveals the disorganization of photoreceptors in the Sdk mutant. All photoreceptors in red, anti-Sdk antibody staining in green. **Bottom panels**: the expression of other proteins that co-localize with Sdk have an altered expression in the Sdk mutant. Both Ecad and Arm expression are diminished. Fmi expression is unaffected, though the disorganization of photoreceptors results in a disorganization of the Fmi pattern. All scale bars 5 μm.

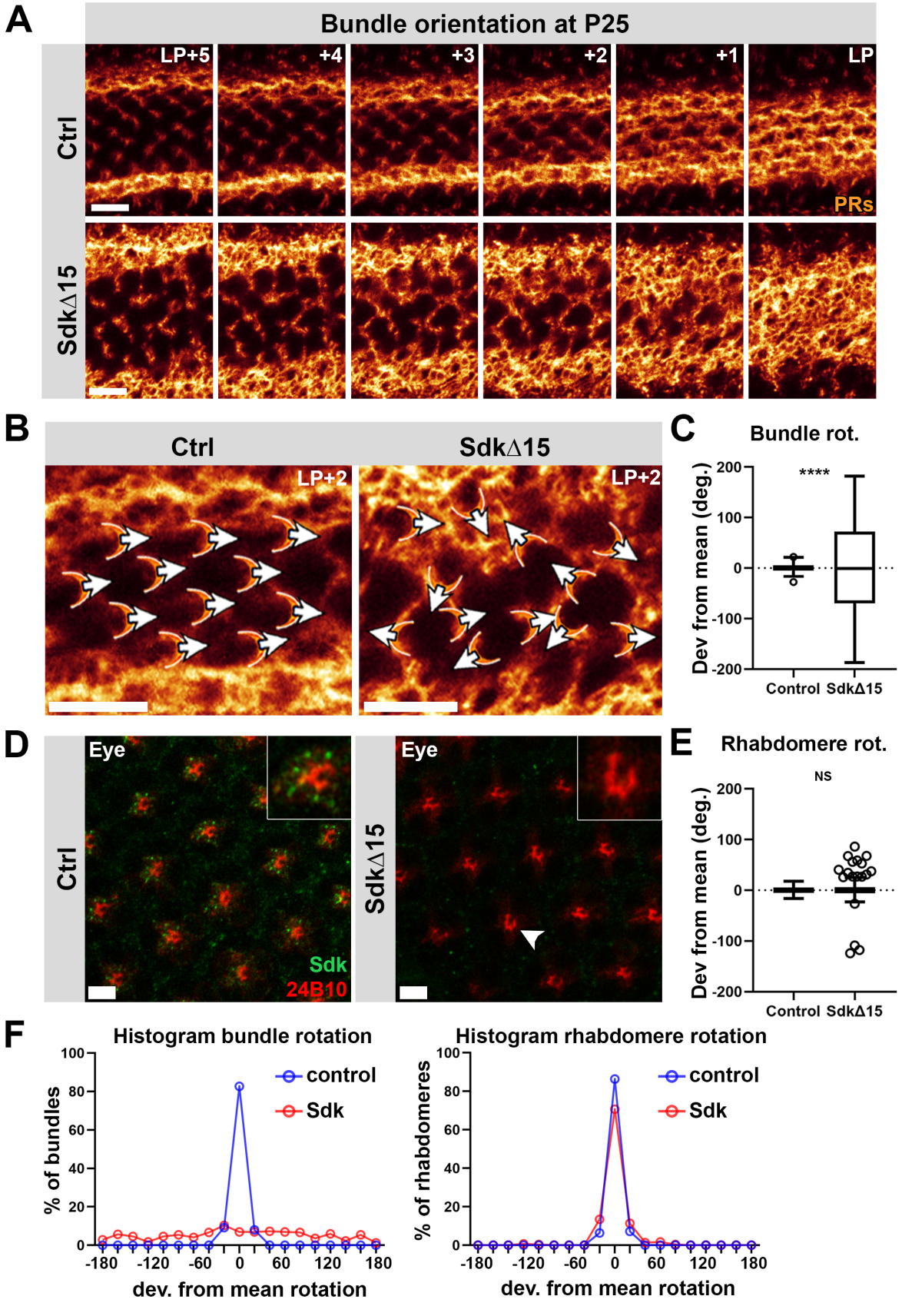

FIGURE 3.4: Arrival of bundles to the LP in the Sdk mutant

A) Top view of lamina plexus. Comparison between WT and Sdk mutant. From left to right; from 5 μm above the lamina plexus to a cross section of photoreceptor at the LP. **B**) Overlay of image taken on 2 μm above the lamina plexus with crescents and arrows to indicate the bundle orientation. **C**) Actin staining (red) and Sdk staining (green) of the eye shows the orientation of ommatidia in WT and Sdk mutant flies. Significance: **** = p-value <0.0001, NS = non significant. Scale bar in all instances 5 μm. **C**) Quantification of orientation of bundles at the lamina plexus ($N = 260$ and $N = 386$ for control and experiment, respectively) **D**) Actin staining (24B10) of rhabdomeres in the eye reveal single instances of ommatidial rotation (white arrowhead). **E**) Quantification of orientation of ommatidia in the eye ($N = 125$ and $N = 290$ for control and experiment, respectively). F) Histogram of bundle orientation (left) and rhabdomere orientation (right). Data binned in 20 degree bins between -180 and 180 degrees. Control in blue, Sdk mutant in red.

if this is the case in the Sdk mutant, photoreceptor bundles were traced back up to 10μm above the lamina at P25 when bundles are easy to follow above the LP. At this level, their bundle organization and orientation can be reliably assessed as crescent shapes in WT animals. In WT, some bundles cluster together above the lamina plexus, but during their descent they rotate and eventually arrive with even spacing between bundles to the lamina plexus (see Figure 3.4 A). At 2μm above the lamina plexus one can clearly see that bundles organize in structures that "scale" the lamina like the scales on a fish. In contrast, the orientation of bundles in the Sdk mutant appears to be completely random. (see Figure 3.4 A-B). To quantify the results, the orientation of bundles at 2μm above that lamina plexus were measured and normalized to the mean orientation of bundles. Significant differences between experiment and control were found: Firstly, the experimental data did not follow a normal distribution, and secondly, the range of data points was broader for the Sdk mutant, than for control (see Figure 3.4 C). An F-test for testing equal variance between groups showed a highly significant difference between experiment and control bundles (p-value <0.0001 with a control group of $N = 260$ and an experimental group $N = 386$).

The cause of a wrong orientation of bundles at the lamina plexus could be an organization defect of ommatidia in the eye that translates to the lamina. An eye phenotype was indeed reported by Nguyen et al. (1997). They describe that in some ommatidia an extra photoreceptor differentiates in between R3 and R4 in the Sdk mutant, and in some there is an extra inner photoreceptor (R7 or R8). In approximately 10% of ommatidia they encountered these "mystery cells" (Nguyen et al., 1997). The appearance of extra "mystery cells" was also found by Astigarraga et al. (2018), but they report that it does not occur in more than 5% of ommatidia. Their finding, that removal of Sdk affects development and connectivity of deeper layers in the optic lobe, is therefore not likely caused by extra mystery cells. Letizia et al. (2019) show a graph where around 35% of ommatidia have extra cells. These are not only photoreceptors, but mainly inter-ommatidial cells. I also observed Sdk localization in inter-ommatidial cells during development at P20 and P30 (see Figure 3.4 B). Nguyen et al. (1997) discovered more defects linked to mutant Sdk animals; some ommatidia fuse, 0.4% of cone

cells was missing, and bristles were not always aligned or even absent or doubled, they observed a rough eye. Lastly, they found an ommatidial orientation defect, which was not described in more detail than this.

To assess if there is a correlation between the defects in bundle orientation and ommatidial orientation in the $Sdk^{\Delta 15}$ mutant, P50 eyes were stained with 24B10 to visualize actin within rhabdomeres and their orientation is presented in see Figure 3.4 D. The hypothesis is that if this should give the same amount of mis-orientation as in the lamina, this could explain the bundle rotation phenotype in the lamina. If not, the defect likely originates downstream of the eye, in the inter-bundle organization. Results show that the orientation of ommatidia is surprisingly normal in the $Sdk^{\Delta 15}$ mutant. Mistakes were found in 18 out of 290 (6.2%) ommatidia. The box plot that represents these results shows these instances as outliers from the main data set (see Figure 3.4 E). When outliers are removed, the control and experimental data set have a similar spread of data as the WT control (F-test for equal variance; p-value $= 0.43$, not significant at $\alpha = 0.05$; control group $N = 125$; experimental group $N = 290$). A distribution of the data shown as a histogram in Figure 3.4 F, shows that experimental data for bundle orientation is equally distributed along the Y-axis. The range in which orientations are found (standard deviation between +180 and -180 degrees deviation from the mean) is similar to a total circle of 360 degrees which indicates that rotation is presumably random. In contrast, the bundle orientation in the control experiment has a sharp peak, indicating a narrow distribution of angles (over 80% of data points fall within this bin). This suggests that the orientation of bundles has a preferred direction around this value. For the rhabdomere orientation a similar peak is observed, to the same height (80%) for the control (see Figure 3.4 F). For the Sdk mutant this is similar. Around 70% of data points were collected within this bin. From this, it is concluded there is no correlation between rhabdomere orientation in the eye and the rotation of the bundle. The mistakes that were found in ommatidial rotation could contribute to mis-orientation of bundles at the level of the lamina. They do, however, not explain it.

3.4 Bundle orientation defects are found in Sdk clonal patches

To investigate the role of Sdk during development further, Sdk mutant clones in varying sizes were created using the MARCM technique; Mosaic Analysis with Repressible Cell Marker (Lee and Luo, 2001). With this technique to create clones during development, mitotic recombination during cell divisions is used as a means to make post-mitotic cells either homozygous mutant for a gene (including a cell membrane marker), or homozygous WT. This allows

for the analysis of labeled mutant neurons within an otherwise phenotypically wild-type brain. The duration of a heat shock during development determines the number of clonal cells and therefore the size of the clone. I wanted to investigate if Sdk acts bundle-autonomous, or even photoreceptor autonomous. Clonal bundles were created with the aim to analyse what would happen to the bundle orientation when neighboring bundles are WT. Single photoreceptor clones were created to analyse what would happen to bundle orientation if just some photoreceptors are mutant for Sdk. A 15 minute heat shock was used to induce single PR clones and a 1-3 hours heat shock to obtain clonal patches within the lamina. Sdk mutant clones are positively labeled with GFP.

A clonal patch is considered small if it contains 2-10 neighboring bundles that contain mutant photoreceptors, and large between 10 and 25 neighboring bundles. In these mutant patches one can analyse the bundle orientation upon their arrival at the lamina plexus by looking at the bundle orientation above the lamina plexus (see Figure 3.7 A). From the 3D analysis of fixed tissue imaged with confocal microscopy as shown in Figure 3.5 A, it is clear that the bundle orientation defects that were observe in the full Sdk mutant are also present in clonal patches. Figure 3.7 B shows that the orientation defect is clearly limited to a patch in which bundles contain Sdk mutant photoreceptors (blue arrows) and does not affect bundles that are on the outside of the clonal patch (white arrows). Moreover, it seems that bundle orientation defects occur more often at the center of a mutant patch, and less often at the borders. For the quantification, the bundle orientation was measured for all mutant bundles in a patch and the equal number of WT neighbors as a control. Data was normalized to the mean across the WT neighbors in one sample. A statistical analysis shows that this data does not follow a normal distribution, and that there are outliers (indicated with dots outside the boxplots in Figure 3.7 C). Outliers are not removed from the data set since these are the mis-oriented bundles and them sticking out of the data is expected. A boxplot of the data shows that the bundles that contain mutant PRs have a broader distribution of bundle orientation at the arrival point in the lamina plexus than that of their WT neighbors. The standard deviation for the experiment is 39.81, while the standard deviation for the WT bundles is 13.01 ($N = 49$ for both experiment and control). Moreover, the data distribution of larger clonal patches is broader than that of small clonal patches (see Figure 3.7 C). The standard deviation is 54.07 for large patches and 24.38 for small patches ($N = 21$ and $N = 27$ large and small patches, respectively). Thus, the spread of data is caused by the size of the clone, where a larger clone causes more deviation from the mean bundle orientation. One might consider that neighboring WT photoreceptors have a positive influence on bundle orientation because rotation defects are more often observed at the center of a large clone.

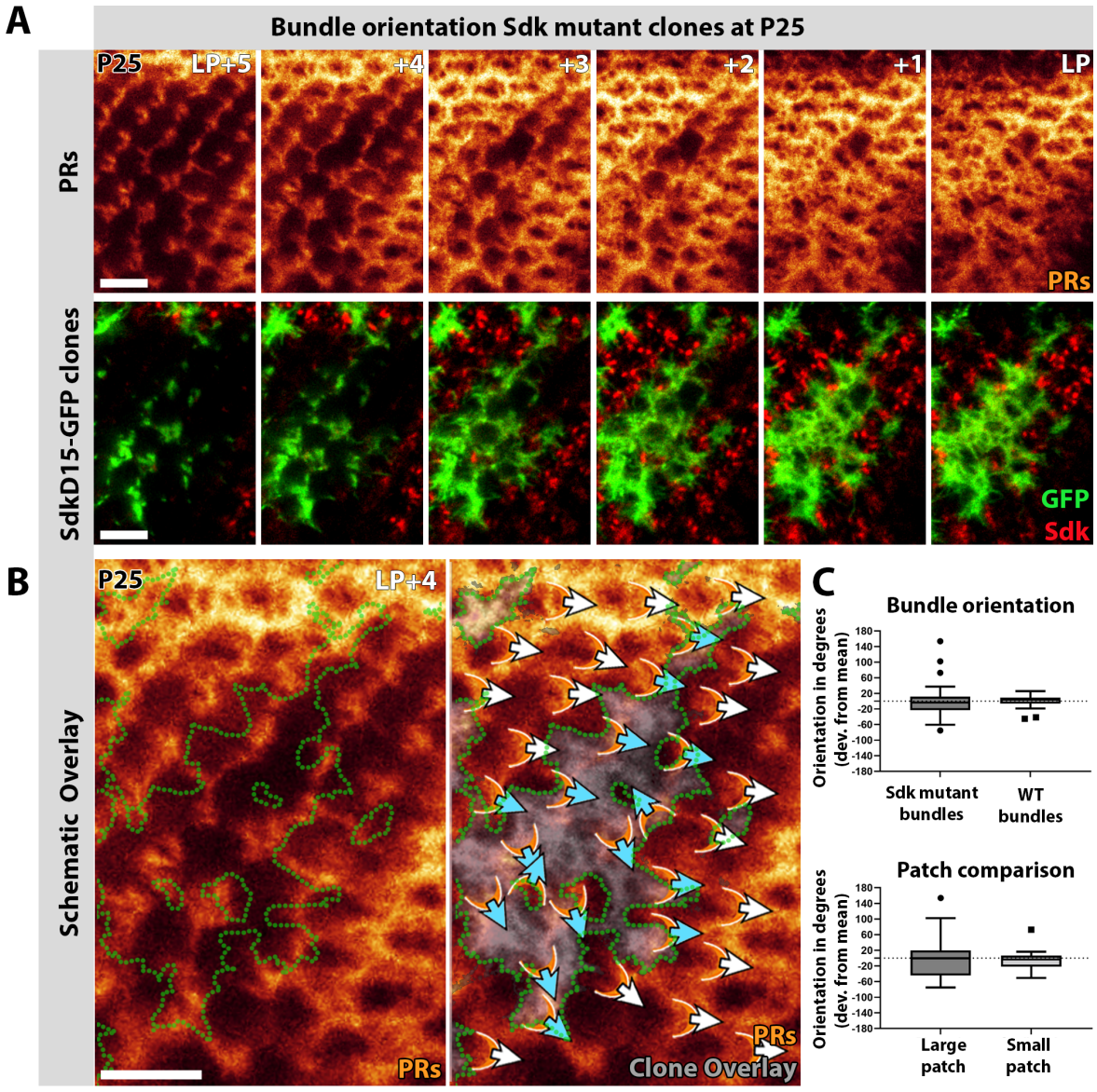

FIGURE 3.5: Photoreceptor bundles show rotation defects at Sdk clonal patches

A) Top view of lamina plexus. Comparison between WT and Sdk mutant. From left to right; from 5 μm above the lamina plexus to a cross section of photoreceptor at the LP. All photoreceptors in glow. GFP expressing Sdk mutant clones in green. Anti-Sdk antibody staining in red.**B**) Left: Overlay of image taken on 4 μm above the lamina plexus with the clonal patch outline (green dotted shape). Right: Overlay of the same image with crescents and arrows to indicate the bundle orientation. Blue arrows indicate bundles that contain Sdk mutant photoreceptors. White arrows indicate bundles outside of the clonal area (grey overlay) Scale bar 5 μm. **C**) Top: Quantification of orientation of bundles at the lamina plexus ($N = 49$ for both control and experiment). Outliers represented as dots. Bottom: Comparison of orientation of bundles in large and small patches. ($N = 21$ for large patches, $N = 27$ for small patches)

However, there are also observations of single mutant bundles that have orientation defects in a WT environment.

Thus, at the level of the lamina plexus, disruption of the scaffold is almost exclusively observed in the mutant patches. In these patches, where many Sdk clones are close to each another, the GMR::Tom channel (photoreceptor scaffold) shows that crescent structures are not properly spaced and that heel crescents are mis-oriented. This is comparable to the full Sdk mutant and it is likely, just like in the full Sdk mutant, caused by the arrival of mis-oriented bundles. To verify this hypothesis, one should look at both the lamina and the eye of the same brain in Sdk MARCM experiment and compare the orientation of ommatidia with the orientation of bundles in the lamina.

3.5 Bundle adhesion is affected in the Sdk mutant

Since Sdk was described to be an adhesion molecule and defects in bundle orientation were observed above the lamina plexus, the next experiment focused on bundle adhesion in the $Sdk^{\Delta 15}$ mutant. Pupae at P20 stage were dissected and stained with the 24B10 antibody to visualize photoreceptors and thereby the organization of bundles between 10 and 2μm above the lamina plexus. Following the bundles reveals multiple examples of photoreceptors that detach from bundles at some level above the lamina plexus. To investigate if detached photoreceptors can re-attach after detachment, bundles were investigated with 3D data reconstruction and visualization software. Figure 3.6 shows that some photoreceptors are detached from a bundle for several micrometers before re-attaching to the same bundle (red highlights). Others detach from their bundle to re-attach to a different bundle (yellow highlights). There are also cases where detached photoreceptors, or photoreceptor pairs, do not re-attach to a bundle, but arrive to the lamina plexus alone or as a pair (data not shown). Lastly, many bundles do not show detachments. Since photoreceptors are still able to form a bundle with their photoreceptor neighbors and (in general) can maintain adhesion to a bundle during their descent, this suggests that Sdk has a redundant function in bundle adhesion. Most likely it is not the only adhesive molecule than maintains the structural integrity of a bundle.

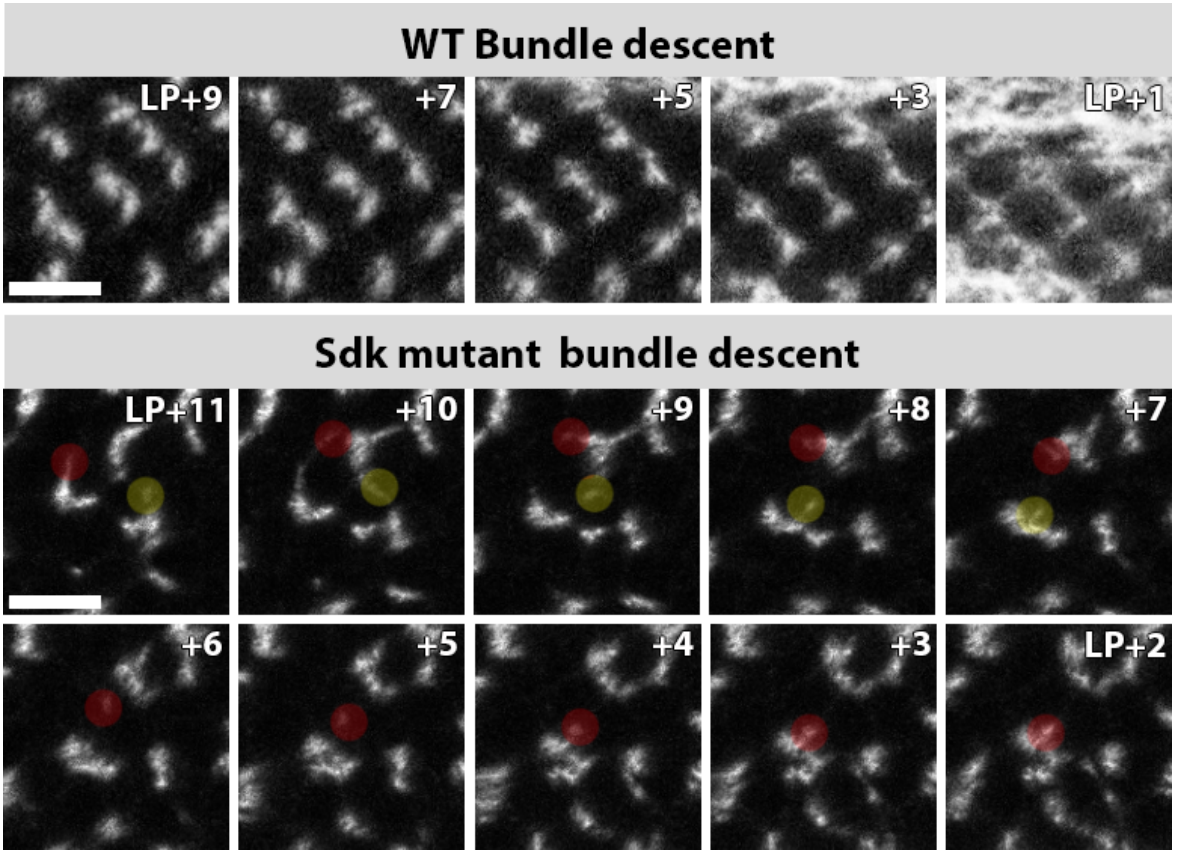

FIGURE 3.6: Photoreceptors have reduced bundle adhesion in the Sdk mutant
24B10 (anti-chaoptin) antibody staining reveals the orientation of bundles above the lamina plexus (LP). LP+# indicates the distance between the image plane of focus and the LP in μm. **Top panels** show WT bundle descent. Note the orientation of bundles in crescents that point towards the right of the frame (towards equator). **Bottom panels** show bundle descent in the $Sdk^{\Delta 15}$ mutant. Red circles highlight photoreceptors that detach from a bundle and re-attach to the same bundle at a closer distance to the LP. Yellow circles highlight photoreceptors that detach from one bundle and re-attach to a different bundle. Note that the orientation of bundles at +3 and +2μm above the LP have no stereotypical organization. Scale bar 5 μm.

3.6 Superposition sorting in the full mutant, and single Sdk mutant clones

Astigarraga et al. (2018) state that the full Sdk mutant gives a mis-wiring phenotype due to lack a of Sdk for adhesion and stabilization in the heel crescent. In contrast, sparse photoreceptors (all R4s expressing SdkRNAi under the mδ05-Gal4 driver) do not copy this phenotype. The authors conclude that neighboring photoreceptors still express Sdk and this is what prevents mis-wiring, thus suggesting a non-autonomous effect during the extension phase. Both SdkRNAi in R4 as well as R4 extension angles in the mutant are documented at P40. No earlier developmental data of photoreceptor extension or scaffold formation is included in their publication. In the previous sections, the early defect in bundle adhesion and bundle orientation upon arrival at the LP is discussed. This prevents a normal scaffold

of photoreceptors to be formed at the LP. Hence, it is not surprising that photoreceptor extension angles are wrong when the early developmental pattern of bundle arrival, and stabilization in the scaffold are affected by a lack of Sdk. Thus hypothesizing a early role for Sdk in scaffold formation rather than a role during photoreceptor extension.

To test this hypothesis, the extension angles of single Sdk mutant photoreceptors in a WT background were analysed. If extension angles would be incorrect in a normal scaffold, where Sdk is missing from single photoreceptors only, this would imply an effect on extension angles. Moreover, with this analysis one can assess the extension of all photoreceptor sub types, and not only R4s, so to exclude that the effect is driven by the mδ05-Gal4 driver.

First, to confirm that single mutants for Sdk do not induce structural defects in the lamina plexus, the scaffold structure was investigated in the lamina where single clones were created with the MARCM technique. With a heat shock of 60 minutes, single cell clones and small patches were created in the lamina plexus. Supplementary Figure A.4 confirms that single mutant photoreceptors in a heel structure do not disrupt the structure of the lamina plexus.

Next, to investigate if mutant photoreceptors could extend in a correct angle, single Sdk mutant photoreceptor clones were created in an otherwise WT looking brain. Figure 3.7 A shows examples of Sdk mutant photoreceptor clones that extend in a correct direction. In these cases there is no defect in outgrowth angle. Not with single, or with multiple mutants per bundle. Heel position could be reliably detected either in between Sdk dots, or otherwise in the GMR-Tom channel that shows the photoreceptor heel positions in the scaffold. A statistical analysis is not performed due to the low number of photoreceptors marked in this experiment.

In rare cases, it is possible that Sdk mutant photoreceptors do extend in a wrong direction. Supplementary Figure A.5 shows a single mutant photoreceptor that is extending from heel position R4 in a incorrect angle for an R4. The correct direction would be to the right, towards the equator. The heel position could be reliably positioned in between two Sdk dots that had lower Sdk staining intensity, indicating the reduction of Sdk. No neighboring photoreceptors were mutant for Sdk. It is, however, unclear if this GFP labeled Sdk clone is actually an R4 that extends wrong or that it is an R6 that extends in the correct direction, but has a wrong heel position. In the latter case this could be explained by the reduction of Sdk that would have led to the separation of the photoreceptor from the bundle and the reattachment to the bundle in a wrong position. There would be shuffling or braiding of photoreceptors during the descent in this case. This could, however, not be traced from the available data.

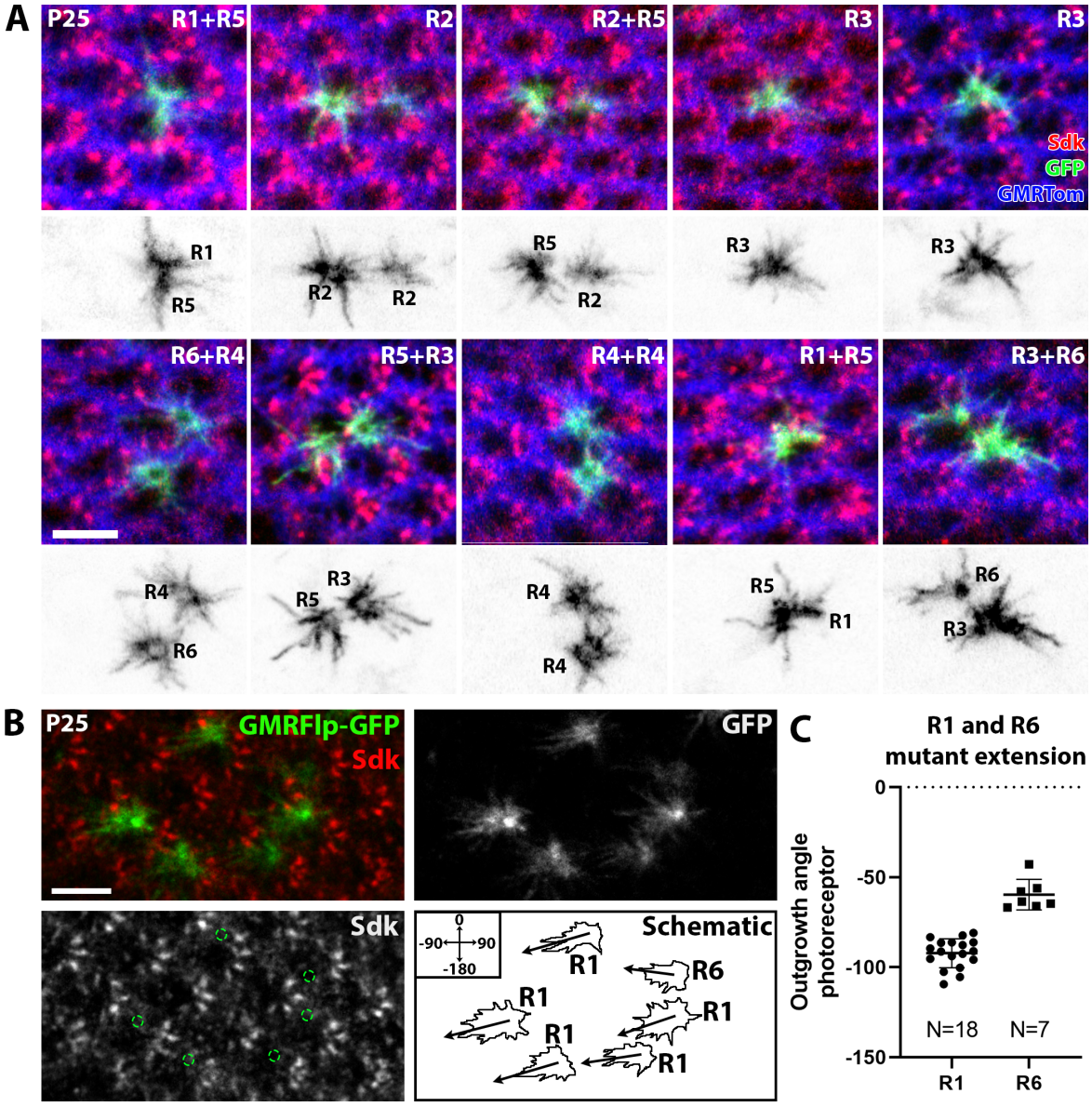

FIGURE 3.7: Single Sdk mutant photoreceptors maintain correct extension angles

A) Ten panels showing the top view of the lamina plexus with single photoreceptor MARCM clones, mutant for Sdk express GFP. GMR::Tom in blue; Anti-Sdk antibody staining in red; GFP in green. Underneath each panel the single GFP channel and the notation of PR sub type. R-cell sub type written down close to the heel position of the photoreceptor. **B**) Sdk mutant photoreceptors created with GMR-Flp typically creates R1 and R6 clones only. Green circles in the Sdk channel represent the heel positions of Sdk mutant clones and are always in either the R1 or R6 position. Scale bar 5 μm **C**) Graph of extension angles of mutant R1 and R6 photoreceptors. Dots represent individual data points.

A different approach is needed to confirm which photoreceptors are mutant. Using GMR-Flp to induce clones typically creates R1 and R6 clones only. Confocal images taken from P25 brains, stained with 24B10 and Sdk antibodies, as presented in Figure 3.7 B show that non of the mutant photoreceptors has a different heel position than their own R1 and R6 positions. In other words, these PRs did not shift position within a bundle due to reduced Sdk adhesion. Furthermore, quantification and statistical analysis of their extension angles shows they are perfectly clustered together for R1s and R6s (see Figure 3.7 C). This means that the extension angles are not affected by the reduction of Sdk in the heel crescent. While this does not exclude the possibility that in rare cases photoreceptor bundles shuffle because of reduced Sdk levels, I find that there is no evidence to expect this is the case for single mutants created with GMR-Flp.

3.7 Conclusions and Discussion

As suggested by an overview of recent literature, Sdk seems to have a substantial role in cell-cell adhesion, structural integrity, and regular patterning of the *Drosophila* lamina during development of the visual map.

I found that the $Sdk^{\Delta 15}$ mutant reveals an early-stage defect in bundle orientation that cannot be attributed to orientation of ommatidia in the eye. Due to developmental constraints, the scaffold at the lamina plexus (P25) and the orientation of rhabdomeres (visible after P40) cannot be assessed at the same time or in the same brain. It could, however, be deducted from the statistical analysis of their orientation at different times of development that they are unrelated. The spread of data points from the eye analysis is incomparable to that of the orientation of bundles (see Figure 3.4). Thus, it is concluded that an organization defect of photoreceptor bundles in the $Sdk^{\Delta 15}$ mutant is unlikely caused by ommatidial rotation errors in the eye, but is instead a defect that arises at the level of the bundle. Hence, Sdk has a role in the regulation of bundle orientation.

Newsome et al. (2000) suggests that Sdk may function as an adhesion molecule for photoreceptor adhesion to R8 to follow the extension of this pioneer axon into deeper layers in the brain. In the Sdk mutant, detachments of single photoreceptors from bundles are regularly observed. Many, but not all, re-attach to their own bundle, or attach to other bundles. Some stay single and arrive as a single axon to the lamina plexus where it is incorporated into the distorted scaffold (see Figure 3.4). However, the fact that not all photoreceptors arrive as single axons to the lamina means that there is still adhesion between photoreceptors in a

bundle. Thus, the adhesion strength may be reduced in the Sdk mutant, but not absent. This means that Sdk acts as a redundant adhesive force in bundles and that a different adhesive molecule is present to maintain bundle adhesion in the absence of Sdk.

There are few possible candidates for this. For instance, Ecad and Fmi; proteins that are discussed in Chapter 2. Cadherins are adhesion molecules and have been shown essential in cell-cell adhesion in multiple systems (Das et al., 2002). Further research should investigate if the Ecad-Sdk double mutant displays a phenotype in bundle adhesion that is worse than the partial detachment phenotype in the Sdk mutant. This could confirm the redundant role of Sdk in bundle adhesion. Similarly, one could investigate the Fmi-Sdk double mutant since Fmi is expressed in arriving bundles and believed to aid adhesion to R8 (Lee et al., 2003; Steimel et al., 2010).

I observed a rare case of extension angle defects of single Sdk mutant photoreceptors in a WT background and a normal scaffold. This low penetrance phenotype could be caused by the reduction of Sdk at the LP. However, there are at least two other proteins (Armadillo and E-cadherin) that have an expression profile similar to Sdk, and which expression is disturbed in the Sdk mutant. While vertebrate Sdk 1 and 2 are described as trans-membrane Ig super-family molecules that mediate homophilic adhesion *in vitro* (Yamagata et al., 2002), there are indications that *Drosophila* Sdk has heterophilic interaction partners too. Immunoprecipitation of Sdk isolated from *Drosophila* showed a interaction with E-cadherin and β-catenin, better known as Armadillo (Uechi and Kuranaga, 2019). Thereby are cadherins and cathenins both part of the membrane adherens junctions in between cells in epithelial sheets and regulate cell-cell adhesion (Nagafuchi and Takeichi, 1989). Moreover, it was shown that both Ecad and Arm patterns are down regulated or lost in the LP in the Sdk mutant. Taken together, their co-localization and interaction may indicate a dependence on Sdk expression in an unknown regulatory pathway. Either of these proteins may contribute to bundle adhesion and/or stable photoreceptor extension during development. Another possibility, as discussed in Section 3.6, could be that the observed photoreceptors have a correct extension angle according to their sub type, but they reside at the wrong photoreceptor position in the heel crescent. Detachment of PRs from a bundle and subsequent re-attachment might create intra-bundle shuffling in these cases. By creating clones of a known sub type (R1+R6) no evidence was found to support this hypothesis. Although, it might be so rare, that one could only find an example of shuffling if looking at a larger number of cases. This would create a very interesting show case if extension angles would indeed only depend on photoreceptor identity, and are independent of the position in a heel crescent. It becomes even harder to imagine mechanisms underlying robust superposition sorting in that case.

Knock-out/knock-down experiments in developmental biology regularly influence the end-point organization of a neural structure. Without tracing the cause of defects, proteins can be blamed to be causative to these defects, and final wiring defects attributed to their necessity. However, to fully understand protein function during development it is essential to pinpoint the stage at which (the lack of) a certain protein disturb a process. Therefore, it is an interesting and challenging next step to consider growth cone dynamics during the extension phase in the Sdk mutant with live-imaging. An attempt to create flies suitable for live-imaging was taken, but unsuccessful. This fly would be genetically designed to be either 1) a full Sdk mutant, 2) create Sdk clones with HsFlp, or 3) create clones in R1 and R6 using GMRFlp. Furthermore, clones would be labeled with GFP. The mδ05::Tom fusion protein would label individual R4s to assess any non-intrinsic defect (if neighboring cells are mutant). After the live-imaging experiment, the lamina could be fixated and stained with DCSP-2 or 24B10 (depending on the developmental time) and imaged with confocal microscopy to obtain a complete overview of the wiring state of the lamina. It appears promising to follow up on the extension angle phenotype reported by Astigarraga et al. (2018). One should be able to discriminate between incorrect extension angles that originate at the beginning of the extension phase, and initial extensions that are correct and obtain later defects. Because of the defects in the scaffold, it seems likely that initial extension angles are already wrong, but for now this remains to be shown.

Taken together, I find very early developmental errors that could be translated to later-stage developmental defects and could explain motion-vision defects that are published by Astigarraga et al. (2018). In their published schematic model they hinted on a defect in heel organization at the lamina plexus, but did not include data to support this. I confirm that the Sdk mutant has an early developmental defect in pattern formation at the LP. The full Sdk mutant, as well as patches of Sdk mutant clones influence the lay-out of the lamina plexus drastically. This seems to be caused by a defect in bundle rotation which appears to have happened at random. The scaffold of photoreceptors is therefore also stabilized in a random organization instead of in the stereotypical organization that we know from the WT LP. Hence, the inter-bundle organization is affected on the level of bundle orientation, while the neighbor-to-neighbor localization is unaffected. Moreover, the detachment of photoreceptors from a bundle likely alters the organization of R1-R6 within a bundle (intra-bundle organization). It is not be surprising that outgrowth direction of photoreceptors in the Sdk mutant (published data by Astigarraga et al. (2018)) is disturbed, and R4s in the Sdk mutant appear to have random extension angles, based on extending from a mis-organized environment. In this case, the developmental outcome seems already determined with the scaffolding

of the lamina plexus, which is greatly disturbed in Sdk mutant animals. It is likely that later developmental defects can be attributed to these early defects and are not caused by late developmental processes of photoreceptor extension or adhesion to a target. I propose that all later occurring defects are secondary defects that arise from primary defects in bundle adhesion, intra-bundle organization, bundle orientation and scaffold stabilization. The inter-bundle organization (neighboring bundles in the lamina represent neighboring ommatidia in the eye) seems to be unaffected in the Sdk mutant. Live imaging of single labeled PRs in the Sdk mutant background is needed to confirm the hypothesis that scaffold formation is the root of wrong photoreceptor polarization.

Chapter 4

Structural organization and sorting without target cells

Lamina neurons (LNs) are the main synaptic partners of photoreceptors (PRs) that terminate in the lamina (Meinertzhagen and O'Neil, 1991). It is well-established that PRs initial descent to the lamina depends on the presence of glia. R1-6 terminate in between layers of marginal and epithelial glia (Poeck et al., 2001). LNs do not contribute to this process, as removal of LNs does not result in overshooting of PR axons. The basic organization of the lamina plexus during development comprises of photoreceptor axons and LN neurites. Because of their necessity as a post-synaptic partner, it is not uncommon to assume that the organization of the lamina scaffold in early development is also dependent on the presence of LNs. Yet, what the organization of the lamina looks like in a scenario without LNs has not been investigated so far.

After scaffold formation and prior to column- and synapse formation, photoreceptor axons are sorted in a developmental synaptic pre-specification step; neural superposition sorting. During superposition sorting, photoreceptor axons make transient contacts with many potential post-synaptic elements but establish synapses only with appropriate partners. Since LNs are identical across the scaffold, it is unclear how photoreceptors would recognize their correct target and discriminate it from other LN clusters. Moreover, a computational model of neural superposition sorting–based on assumptions of set outgrowth angles, velocity, and photoreceptor's capacity of recognizing a "stop signal" when they reach other photoreceptors–suggests that post-synaptic LNs are dispensable during the sorting process (Langen et al.,

2015). Thus, the question is if photoreceptors could indeed function in a developmental environment when their post-synaptic partners are missing. Ultimately, it is unknown if LNs are necessary at all to guide photoreceptor sorting.

In this chapter, the structural organization of the lamina plexus is examined when LNs are either silenced or missing from the scaffold. The possibilities for either silencing LN dynamics or depleting the lamina from LNs[1] are explored together with their consequences on the scaffold organization. Moreover, it is investigated how the removal of LNs affects the wiring capability of photoreceptors in the lamina plexus. Lastly, the consequences of changes during scaffold formation for the subsequent developmental steps are investigated; e.g. the extension phase of neural superposition sorting, and the adult wiring pattern.

4.1 Analysis of a scaffold without lamina neurons

Visually, one can easily tell if a pattern is regular, irregular, contains just one mistake, or is a total chaos. Humans have a wide range of recognizing patterns and classifying patters as regular (Chetverikov, 2000). Quantifying the quality of a pattern, however, requires more effort. In a search for pattern markers in the lamina, an antibody screen revealed that Armadillo (Arm), a *Drosophila* homolog of β-catenin, localizes on lamina neurons and at cell-cell junctions between photoreceptor heels (see Section 2.2). Both Arm and Sdk localize in between photoreceptor heels in the lamina plexus during scaffold formation and the extension phase of neural superposition sorting (see Chapter 2). Arm and Sdk localization are used interchangeably to assist the quantification of the lamina pattern. By drawing a connection between the markings between photoreceptor R1-R2 and R5-R6, a vertical line is obtained that represents the orientation of a heel crescent. Arm/Sdk localization was used to analyze photoreceptor heel position, assign photoreceptor sub type identity, count photoreceptor heels, measure spacing between bundles and assess the regularity of the scaffold by measuring the angles between bundles, and quantify rotation of heel structures[2] (see Figure 4.1).

4.2 Silencing lamina neuron membrane dynamics

In order to investigate the role of LNs during scaffold formation specifically, the temperature sensitive dominant negative form of Shibire (Shibire^{ts}); the *Drosophila* homolog of dynamin

[1] Smoothened-RNAi experiment that depletes the lamina from LNs was performed by Egemen Agi.
[2] The analysis of scaffold organization was conducted jointly with Egemen Agi and Monika Kauer.

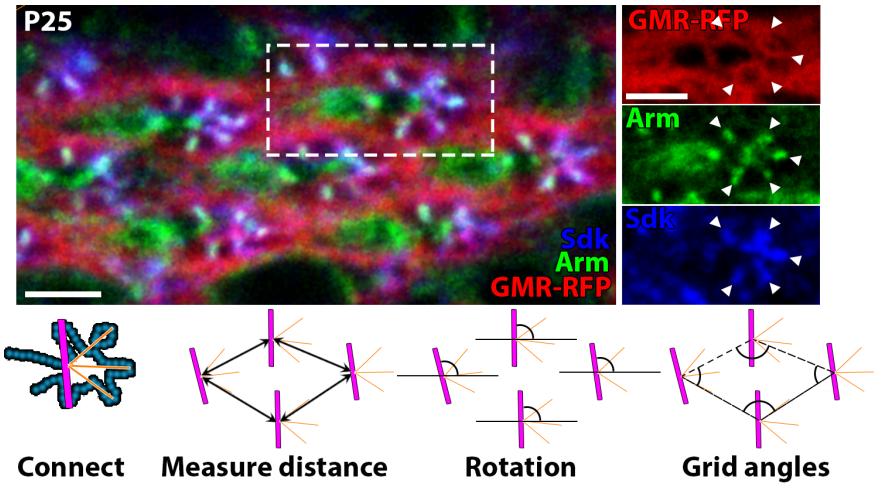

FIGURE 4.1: The use of Armadillo and Sidekick labeling for scaffold analysis

Top) The co-localizing antibody staining of Armadillo (Arm) and Sidekick (Sdk) label vertices in between photoreceptor heels in the lamina plexus. Arrows point towards co-localization in between photoreceptor heels. Scalebar 3 μm. Antibody staining and figure made by Monika Kauer. **Bottom**) Connecting these Arm/Sdk dots creates a K-shaped guide that enables measurements within the scaffold and quantification of the grid; the distances between heel structures, the orientation (rotation) of heels structures, and the angles between heel structures.

(Gonzalez-Bellido et al., 2009), is used to silence membrane dynamics. Shibire is required for fission of invaginated membrane during endocytosis (Kroll et al., 2015). Shibire^{ts} blocks vesicle recycling at a restrictive temperature (31°C), while it functions as wild type at permissive temperatures (RT/ 22°C) (Gonzalez-Bellido et al., 2009; Luo et al., 2008). The blocking of membrane dynamics by Shibire^{ts} is also reversible, as the dominant negative mutant protein goes back to functioning like WT in permissive temperature, so the block on endocytosis is released almost instantaneously (Luo et al., 2008). Blocking membrane dynamics specifically between P0 and P25 by expressing it under the L-cell specific driver 9B08-Gal4 would block LN's ability to interact with other cells; meaning photoreceptors during the scaffold formation phase.

To investigate the role of LNs during photoreceptor arrival at the lamina plexus, and during scaffold formation P0 pupae were kept at 31°C for 20 hours, and dissected immediately afterwards. Developmental stage after Heat-shock (Hs) corresponds with WT P25 at 25°C. Brains were stained with anti-Arm antibody and prepared for confocal microscopy. GMR::tdTomato fusion protein enables visualization of photoreceptors. Figure 4.2 A shows top-view images of the lamina plexus, and show that PRs are able to target to the lamina when LNs' membrane dynamics are blocked during the scaffolding phase. This is to be expected since a similar result was published by Poeck et al. (2001). It can be observed in Figure 4.2 A that expression of Shibire^{ts} and a 20 hour Hs result in LNs that have lost all their membrane protrusions and have shrunken back to small "blob-like" structures. Meanwhile, the PRs are organized

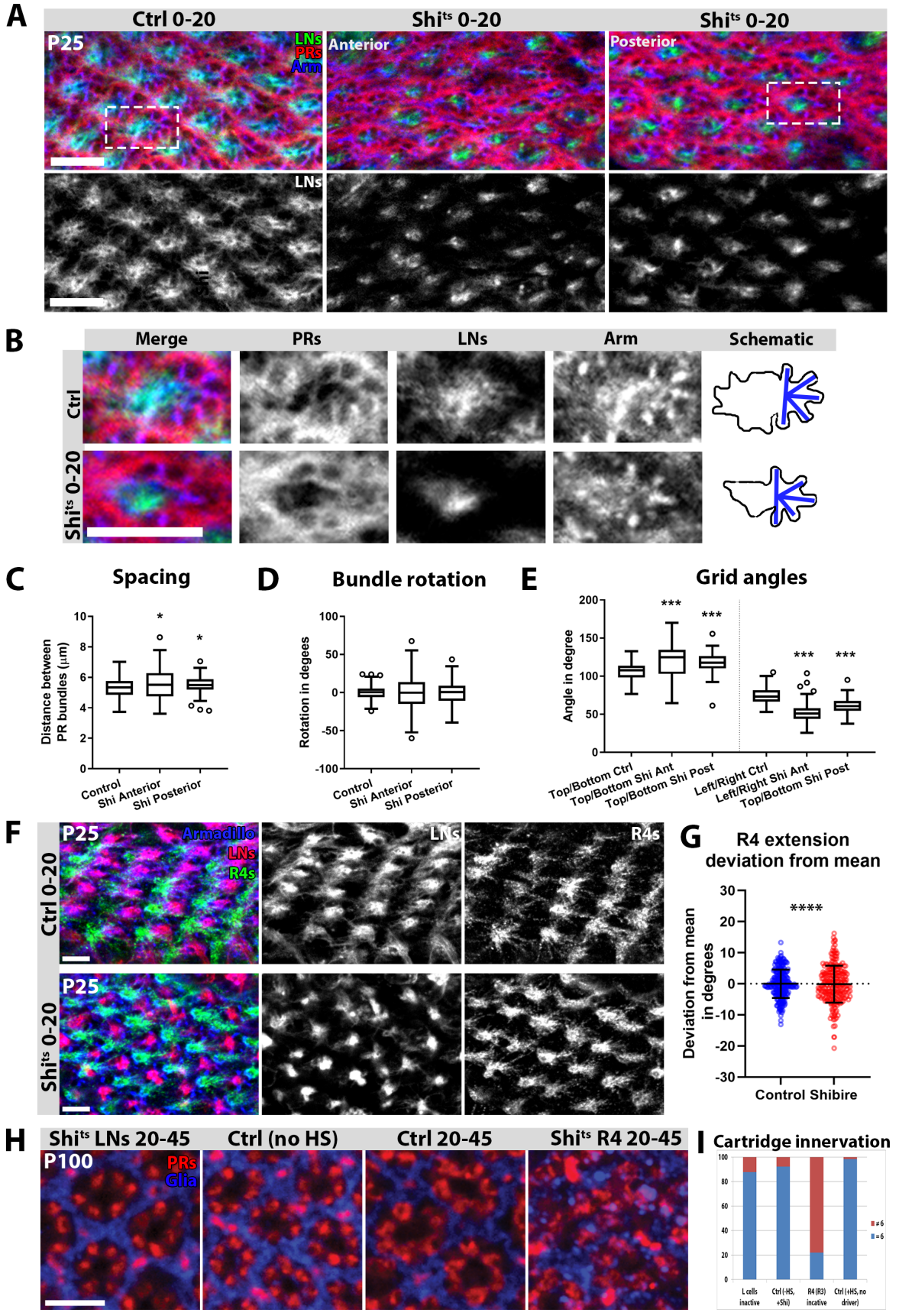

FIGURE 4.2: LN dynamics blocked during scaffold formation with Shibire DN expression

A) Confocal microscopy image of lamina plexus from top. Control animals were heat shocked at 31°C from P0 for 20 hours and dissected immediately after, just like the experiment. Boxed areas are enlarged in B. All photoreceptors (GMR-Tom) in red, LNs (9B08-GFP) in green, anti-Armadillo antibody staining in blue. **B**) Example of analysis from Shibire experiment, posterior lamina. Quantification of the scaffold is performed by the analysis of Armadillo staining. Angles were determined by drawing in a reference line between membrane between R1-R2 and R5-R6, and connecting the other membranes, stained by Armadillo, with the centre of this line. Spacing of heel structures was measured as the diagonal distance between center of Arm lines. C-E) Quantification of Armadillo staining in the lamina plexus. **C**) Graph representing the spacing of heel structures in the lamina plexus. **D**) Rotation of heel structures measured from Arm reference line, and normalized for the mean rotation in each sample. **E**) Grid angles measured the angles between heel structures. All measurements from the centre of the reference line. **F**) R4 extensions in the LP in Shibire^{ts} background. LNs in red, R4s in green and Arm staining in blue. **G**) Quantification of R4 extensions in in Shibire^{ts} background. **** represents a p-value <0.0001 for the F-test (for testing equal variance between groups). Dots represent individual data points. Graph shows mean +/- SD. **H**) Adult outcome after sorting (31°C for 25 hours staring at P20) at restrictive temperature. All photoreceptors in red, glia in blue. Experiment by Egemen Agi. **I**) Quantification of sorting outcome after sorting at restrictive temperature. Analysis by Egemen Agi. All scale bars 5 μm.

in a crescent around them, comparable to WT. To analyse the scaffold, the quantification methods as described in Section 4.1 were used. Figure 4.2 B shows the Armadillo staining is intact in the Shibire^{ts} experiment and can be used for scaffold analysis. Quantification shows that the blocking of membrane activity has an effect on the spacing of heel crescents in the heel spacing at the lamina plexus (see Figure 4.2 C). While the mean distribution of distances between heel structures was not significantly altered, the spread of data points indicates that the variability of the scaffold increased. The angles measured between heel crescents is closely related to this variable (see Figure 4.2 E). Differences are especially noticeable at the younger anterior side of the lamina plexus. The difference between the anterior and posterior side of the lamina in experimental conditions differ significantly from each other. It must be noted, that the most anterior side of the lamina in WT is also less stereotypically organized than the posterior side at P25 (see Figure 2.3). Possibly, this effect is strengthened by the loss of membrane dynamics at LN cell bodies in between photoreceptor bundles. On the younger side, LNs have been exposed to a longer heat shock before sorted into columns in between PR bundles. However, this hypothesis cannot be confirmed from this data set. Further analysis of the scaffold reveals that, in addition to a more variable spacing, the rotation is also more variable (see Figure 4.2 D). Again, the variability is larger at the anterior side of the lamina. While this is quantifiable data, visually, the organization of photoreceptors seems largely unaffected by the inability of LNs to interact, or by their morphological shape-change. The crescent heel structures in the experiment look comparable to WT P25.

How individual photoreceptor outgrowth angles are affected by the inability of LNs to interact with them was investigated in a similar experiment. Instead of labeling all photoreceptors with GMR::Tomato, only one PR sub type (R4) was labeled with under the mδ05::Tomato.

Animals were heat shocked from P0 for 20 hours to block membrane dynamics with Shibire^{ts} and dissected immediately afterwards. The polarization of R4 extension was measured and compared to the control which was heat shocked, but did not contain the dominant negative Shibire^{ts} (see Figure 4.2 F). Results show that the extension of R4 photoreceptors is hardly affected by the silencing of LN membrane dynamics during scaffold formation. The "blob"-like LNs do not change the R4 extension angles. The quantification of these angles are represented in Figure 4.2 G. Both experimental and control data follows a normal distribution ($N = 231$ for experiment, $N = 243$ for control). This shows that there is a general angle that the R4s extend in, and the extension angles are not random. The F-test for equal variance reveals a statistically significant difference in the variance between groups (p-value <0.0001 ; standard deviation for experiment = 5.94, standard deviation for control = 4.58). This indicates that the null-hypothesis, that the variance is the same between groups, can be rejected. In summary, extension angles experience more variation in their polarization angle compared to control when LN membrane dynamics are blocked, but extend in a generally correct direction.

Lastly, it is investigated what happens to photoreceptor sorting in the absence of LN dynamics. To this end, pupae expressing Shibire^{ts} under the 9B08 driver were heat shocked at 31°C for 20 hours during the sorting period between P20-P45 [3] [4]. After Hs, pupae were returned to 25°C incubator and dissected upon eclosion. In this experiment, the scaffolding phase is unaffected, while LNs' membrane dynamics are blocked during the sorting phase. The adult laminae were stained with 24B10 (all photoreceptors) and with anti-ebony antibody (glia) to more easily discriminate cartridges from one another. Results show that the adult cartridges do not display any organizational defects when LN membrane dynamics were blocked with Shibire^{ts} during sorting. They are comparable to control when there was Shibire^{ts} in the animal, but no Hs and to the control where there was a Hs, but no Shibire^{ts}. The positive control is the expression of Shibire^{ts} in R4 using the mδ05-Gal4 driver. In these animals, the R4 photoreceptor dynamics were blocked during the sorting phase and this resulted in incorrect cartridge innervation (see Figure 4.2 H-I for the quantification). In summary, photoreceptor sorting towards the correct target appears unaffected when LN membrane dynamics are blocked during the extension phase.

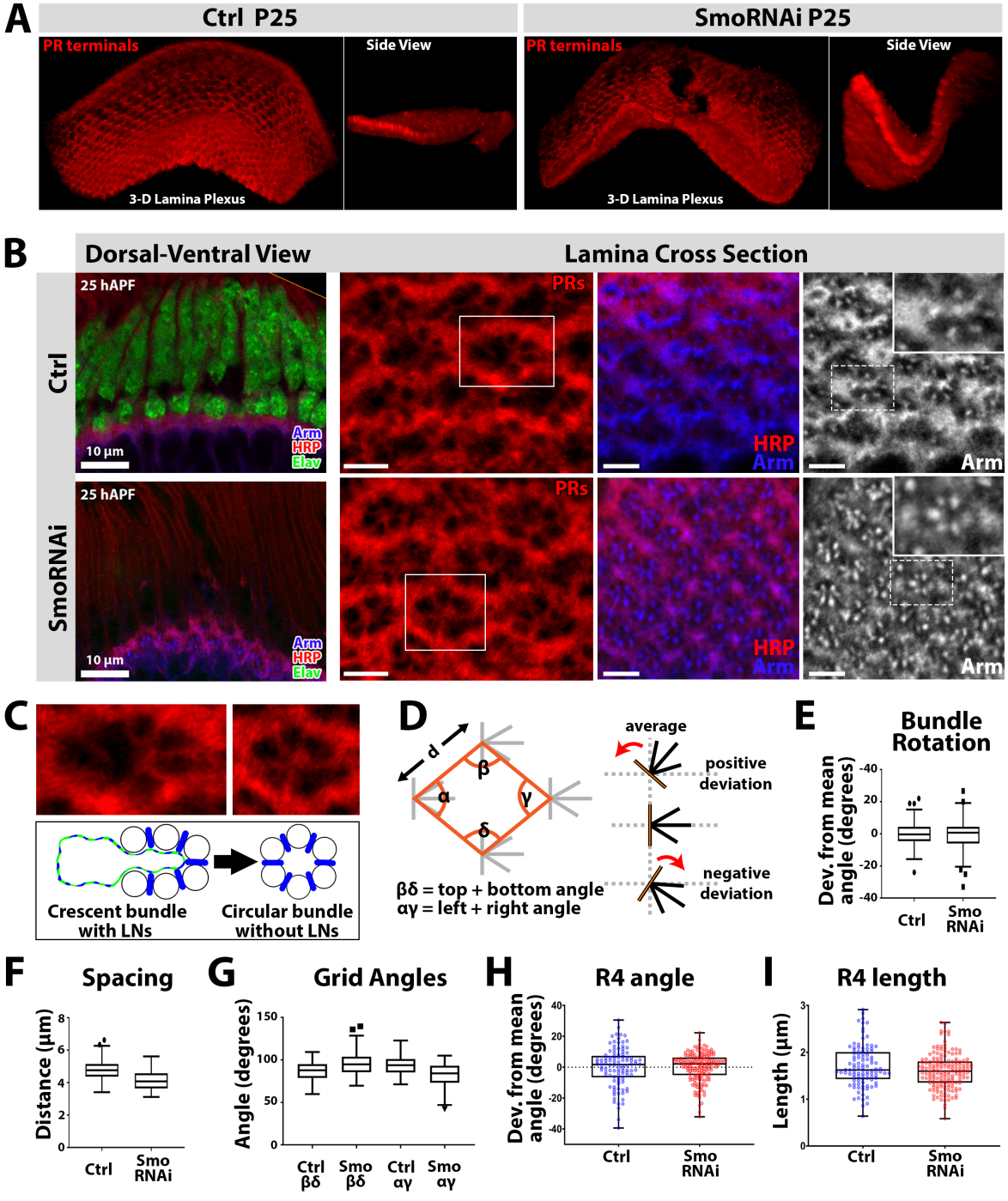

FIGURE 4.3: SmoRNAi-induced changes in the photoreceptor scaffold

The expression of SmoRNAi in LNs prevents their differentiation and causes changes in the lamina plexus. All data from fixed tissue at P25. **A**) A 3D reconstruction of the lamina plexus shows the different lay-out of the lamina in the absence of LNs. **B**) A side view (left most panel) and top view of the lamina plexus reveals a different, still organized, scaffold. LNs in green, photoreceptors (stained with HRP) in red, Arm staining in blue. Contents of squares are enlarged in most right panel (Arm channel) and in C. Scale bar 5 μm if indicated in the figure. **C**) Organizational change of photoreceptor heels from crescent to circular from B as well as a schematic representation. **D**) Schematic of Arm quantification. E-G) Boxplots as mean +/- SD, individual dots represent outliers identified with Tukey-test. H-I) Boxplot as mean +/- SD, individual dots represent individual data points. $N = 102$ for control, $N = 162$ for experiment. **E**) Graph representing bundle rotation. **F**) Graph representing heel structure spacing. **G**) Graph representing grid angles as explained in D. **H**) Graph representing R4 extension angles at P25 measured from fixed data. **I**) Graph representing R4 length at P25 measured from fixed data. Data obtained by Egemen Agi.

4.3 SmoRNAi prevents differentiation of lamina precursors

In the previous section, the membrane dynamics of LNs were blocked during scaffold formation and photoreceptor sorting to investigate their role during these processes. While this approach may have blocked the ability for LNs to interact with photoreceptors, it does not rule out a possible passive role for LNs. In theory, photoreceptors could use LNs as positional markers in the lamina by their sheer presence. To test the requirement of LNs for scaffold formation, the differentiation of lamina precursor cells (LPCs) into lamina neurons was prevented. Differentiation of LPCs into LNs is initiated by photoreceptors through signaling via wrapping glia that surround photoreceptor bundles (Fernandes et al., 2017). Upon differentiation, LNs migrate to localize in between photoreceptor bundles. A few hours later, they extend their neurites to the lamina plexus where photoreceptors and LN neurites form a stable scaffold that forms the canvas for photoreceptor sorting (see Figure 1.2 A). LPCs that are mutant for Smoothened (Smo) are unable to respond to the differentiation cue (Hedgehog signaling; Hh) from photoreceptors. Smo encodes an essential component of the Hh receptor, and knocking down Smo blocks the ability of LPCs to receive and transduce the Hh signal. In turn, the inability to respond to Hh signaling blocks their differentiation and inhibits migration into columns (Umetsu et al., 2006). Thus, with the expression of SmoRNAi under an LN-specific driver (NP6099-Gal4), LPCs are prevented to enter the LN columns that are normally formed in between PR bundles[5]. Figure 4.3 B shows a side view of the LP when Smo is knocked-down in LNs. Although not all LPCs have been prevented from column entry, it is observed frequently that lamina patches are deprived LPCs and consequently no LN neurites enter the LP.

[3]Shibire^{ts} experiment between P20-P45 was performed by Egemen Agi.

[4]A 20 hours Heat-shock at 31°C starting at P20 results in a developmental stage that represents P45 of development at 25°C.

[5]Smoothened-RNAi experiment was designed and performed by Egemen Agi.

To investigate the effect of removal of LNs from the lamina, fixed brains were stained with multiple antibodies to assess the lay-out of the lamina. A side view of the lamina in the absence of LNs, presented in Figure 4.3 A, shows increased curvature of the lamina compared to WT. Occasionally, gaps are observed in the lamina in the experimental condition, while this is not observed in WT. Moreover, bundle spacing is altered above the lamina, as can be observed in Figure 4.3 B. As a result of lacking LNs in between the photoreceptor bundles, they are not spaced apart and cluster together more than in WT. This effect is also visible at the lamina plexus; the spacing of heel structure is decreased. In all, two main changes in the lamina scaffold are observed when there are no LNs. 1) The spacing between heel structures; this decreased when LNs were absent, but the variation was not significantly different than in WT (see Figure 4.3 F). Changes seen in the grid angles are related to this decrease in spacing, which change the dimensions of the lamina plexus slightly differently along the anterior-posterior axes than it does along the dorsal-ventral axis (see Figure 4.3 G). 2) The crescent organization of the heel structure is changed into a circular one (see Figure 4.3 B-C). When neurites of LNs do not occupy the centre of a heel structure, it is not pried open. Instead of the well-known horse-shoe shape, the axons occupy a circular organization and R1 and R6 of every bundle now touch each other. Figure 4.3 B (right panels; Armadillo channel) shows that an extra dot in between R1 and R6 is present that is either not present or undetectable in WT.

Even though there are differences to WT, the seemingly flawless patterning of the structure is striking. A top view of the lamina plexus shows a surprisingly organized layout. 24B10 staining, as well as Arm staining shows the organization of photoreceptor axon in a neatly organized scaffold (see Figure 4.3 B). Moreover, the mean bundle rotation was not altered (see Figure 4.3 E). This suggests that in WT, LNs space and physically separate bundles from each other, but that PRs are capable of self-organization of a regular structure and LNs are not required for PR scaffold formation.

After scaffold formation, photoreceptors extend their growth cones in cell-type specific angles to reach their post-synaptic partners during the sorting phase of neural superposition sorting (Langen et al., 2015). It is unknown if, and how, this developmental step is influenced by the presence of LNs. To investigate how PRs extend their growth cones in an environment without LNs, the directional extension of growth cones was assessed by labeling only one R-cell sub type, R4, using the mδ05-CD4::tdeGFP fusion protein. In WT, this driver expresses GFP in R4 photoreceptors in the eye and their axons in the lamina in a very regular pattern (see Supplementary Figure A.6). In the eye, R4s point away from the equator, while R4s growth cones extend towards the equator in the lamina. R4 extension angles of WT photoreceptors

were measured in the experiment where SmoRNAi is expressed by an LN specific driver, which results in patches of lamina that are depleted from LN neurites. R4s in this environment showed no defects in their initial extension angle. Figure 4.3 H-J show the quantification of the R4 extensions measured from fixed data. Like in WT, the R4s front of the growth cone extend away from the heel and grow in a linear fashion towards the equator. Thus, despite the observed changes in the spacing and basic scaffold of the bundles (crescent to circular) that may have an influence on R4 extension, the extension angles are remarkably robust (see Figure 4.3 H; no statistically significant difference). In the experiment, it was observed that R4 extensions are shorter than in control (see Figure 4.3 I; unpaired T-test, p-value = 0.034; F-test for equal variance, p-value = 0.025). It is possible that this is a consequence of missing LNs and a smaller scaffold.

4.4 Photoreceptor dynamics in an altered environment

In contrast to the limited effect of removal of LNs on the scaffold observed at P25, the lack of LNs in the lamina caused by expression of SmoRNAi in LNs has a disastrous effect on the final organization of cartridges; the end result of sorting. At P50, the part of the lamina plexus where there are no LNs appears disrupted. It shows cartridges that have differing numbers of PR terminals and even fused cartridges (see Supplementary Figure A.7). The observations that the scaffold is organized and extensions of R4s at P25 are normal (see Section 4.3) while the endpoint of superposition sorting is badly affected may suggest a late role for LNs in the wiring process of the lamina. Still, it does not distinguish between a photoreceptor targeting defect or a target adhesion defect, nor pinpoints a time of development at which LNs are required. To distinguish between these two processes and to see how wiring defects arise during sorting, live-imaging is needed to assess the photoreceptor sorting process during development[6].

Live imaging of R4 PRs allows for the observation of the directed R4 extensions over the course of 20 hours. Figure 4.4 A shows snapshots from the live imaging data set. R4 growth cones extend away from the heel in a linear fashion towards the equator (at the right of every image). Analysis of R4 extensions shows that R4 behavior is not affected at early stages (P25-P35). Up to this time point, R4s extend correctly, have no extensions longer than the control, and stop extending without having reached an LN cluster. Similar to the images obtained from fixed brains, there is a slight decrease in the length of R4s (see Figure 4.4 C). This can be explained by the decreased spacing in the lamina plexus (see Figure 4.4 B).

[6]Live imaging data for the SmoRNAi experiment was obtained by Egemen Agi.

Indeed, when the relative length of R4s is plotted as a percentage of the distance between bundles this shows no significant difference between experiment and control (see Figure 4.4 D). A combination of these results suggests that R4s can extend in the right direction, across the appropriate distance, have normal dynamics, and can reach their correct target region at the time they are supposed to stop extending any further. It suggests that LNs are not required for correct photoreceptor extension between the onset of extension until, at least, P36.

From P38-40 onward, defects arise in R4 directional extension and their ability to adhere. Some R4s retract after initially arriving at the correct cartridge location, some of them go to different target regions, while others can stay at the correct location and wire correctly (see Figure 4.4 A and E). The quantification of R4 targeting in the lamina is shown in Figure 4.4 F. After an initial phase of correct extension of R4, incorrect targeting and retractions start occurring at P36. Over time, the defects increase and reach approximately 50% of R4 that are incorrectly extended at the end of the sorting phase. The non-predictability of this process might suggest a stochastic adhesion defect. Because the LNs are not available as a target to adhere to, photoreceptors may have extended the correct distance and in the correct angle, but cannot stay extended without connecting to some force that keeps them in place.

4.5 Conclusions and Discussion

Poeck et al. (2001) showed that photoreceptors do not need LNs to be able to arrive and stabilize at the LP. However, it remained unclear how photoreceptors would cope without LNs in subsequent stages of development. This chapter showed that photoreceptors, by themselves, can create a patterned scaffold at the lamina in the absence of LNs. Even though changes in heel spacing (smaller) and the organization of a heel structure (from crescent to circular) are striking and obvious, the lamina plexus is surprisingly well organized: as well as can be expected from a structure from which a complete cell type is pulled that normally makes up a large proportion of that structure. The fact that the scaffold is more compact when LNs are missing is presumably related to the fact that an entire cell type is missing from this part of the lamina. From these findings, two things can be concluded. 1) LNs play no active role in the formation of the scaffold, and 2) creation of the scaffold is a process that is highly robust and resistant to one of the harshest perturbations possible.

If one considers neural superposition sorting as an algorithm, the scaffolding step, with its stereotype pattern, is a great way to reduce developmental noise. The robustness of this

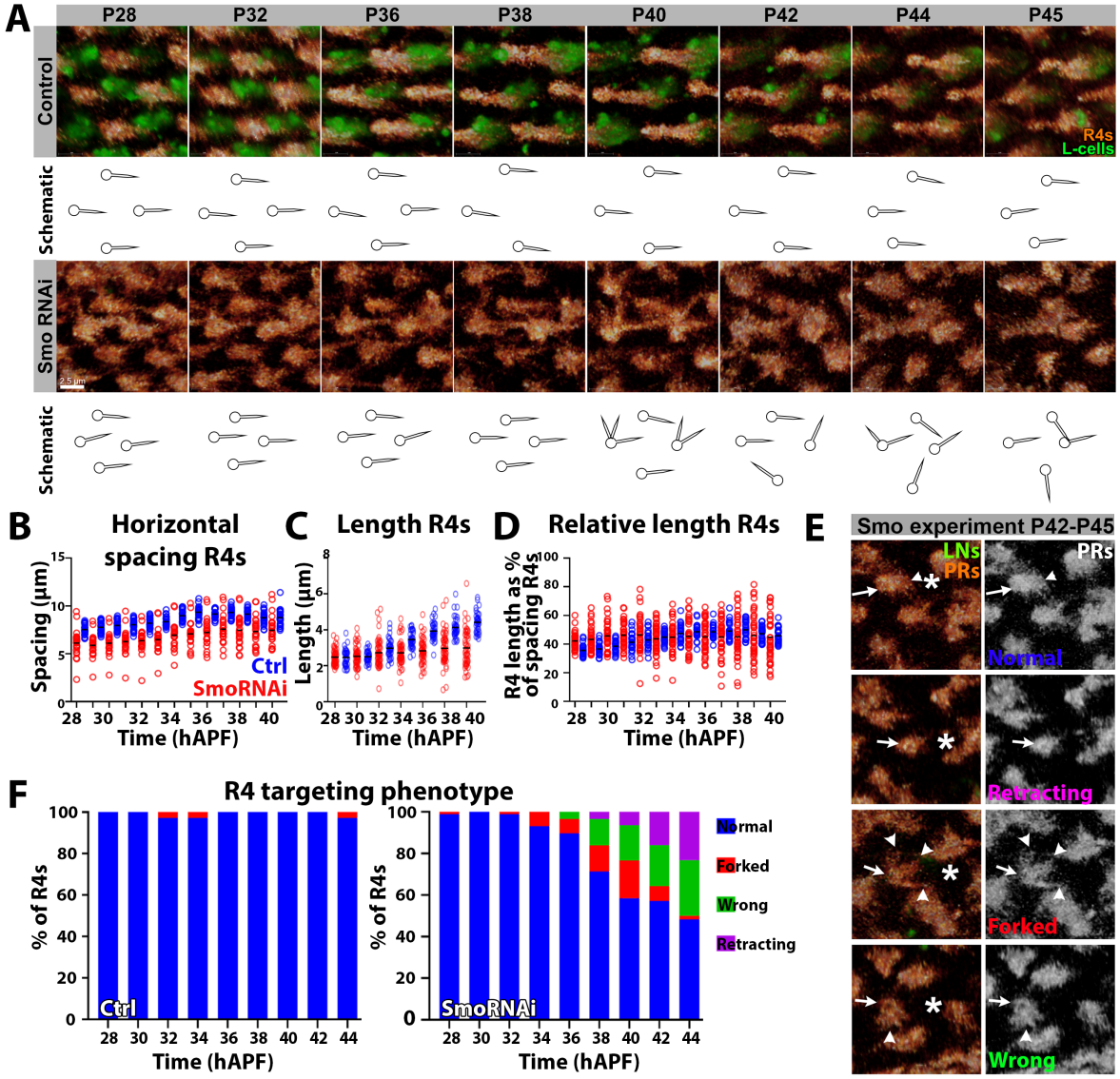

FIGURE 4.4: R4 extensions in environment without LNs

Comparison of R4 extension in WT lamina plexus and environment where LNs are absent due to SmoRNAi expression that prevents their differentiation. **A**) Snapshots from live imaging data set between P28-P45. R4s in glow, LNs in green. Underneath snapshots are schematic representations of R4 extensions. The circle represents the heel position, the spike the R4 extending front of the growth cone. Scale bar 2.5 μm. **B-D**) Data in graphs obtained from analysis of the live imaging data set. Black horizontal bar represents the mean, dots represent all individual data points. control in blue, experiment in red. **B**) Graph representing the horizontal distances between R4 heels over time. **C**) Graph representing the R4 length over time. **D**) Graph representing the relative R4 length over time calculated by dividing data from C by B. **E**) Photoreceptors experience stabilization defect at the end of the sorting phase. From top to bottom are examples showing normal targeting, retraction of the growth cone, a forked growth cone, and wrong targeting. All images are snapshots from the lamina between P42-P45. Arrows indicate the R4 heel position, arrowheads indicate the tip of the growth cone, asterisk represents the correct targeting location if LNs would have been present. **F**) Quantification of R4 targeting as indicated in E. Normal targeting in blue, forked growth cones in red, extensions in wrong direction in green, retractions in magenta. Data obtained by Egemen Agi.

step ensures that any developmental noise from a previous step is carried over into the next. Indeed, in the analysis on photoreceptor growth cone extensions (by R4 visualization) there is hardly any noticeable defect in the altered, but perfectly patterned lamina. As a side note, it should be considered that R4s might not be influenced the most by the change from crescent to circular heel structure. Rather, R1 and R6 would. Ideally, to solve this problem, one would create GMR-Flp clones in R1 and R6 and assess their extension angle in the SmoRNAi experiment. This is, however, not possible due to the fact that the Gal4-UAS system is already in use for the expression of SmoRNAi (UAS) by the NP6099 driver (Gal4). Alternative driver systems, like LexA-LexAop or the Q-system (Potter and Luo, 2011; Potter et al., 2010), could be a solution in this situation, but currently do not have the right drivers to perform these experiments.

One observation that stands out is that R4s have shorter extensions in the absence of LNs. Because the scaffold is smaller due to the missing cell type, the photoreceptors do not have to extend so far. But how do they "know" this? It was previously suggested that extension angle, and growth speed are cell-intrinsic properties of photoreceptors that are specific for each sub type (Ji et al., 2021; Langen et al., 2015). Growth cone extension length may, however, be a feature that is not programmed in detail, but does also depend on the environment. The shorter length of extensions in the SmoRNAi experiment implies that photoreceptors do not use the target to decide how far they should extend. It is possible that PR axons use filopodia on their growth cone to sense when they have extended far enough. With the notion that adaptation of extension length happens in an environment without LNs, LNs cannot be the cue that filopodia sense to stop growing. The mathematical model from Langen et al. (2015) already hinted at this possibility. Their models suggest that a stop-rule could instead consist of the sensing of other growth cone fronts that extend towards a target area. Alternatively, it is possible that growth cones use filopodia on their growth cone to sense the next heel structure as a positional marker to guide this extension-limiting decision. This possibility is discussed in more detail in Chapter 6.

While the start of the extension phase knows no defects to the R4 extension angles, this changes over time. Before P35, the sorting phase seems to run completely independent of LNs. After this time, photoreceptors start showing behaviours unknown in WT; retractions and growth cones that change direction and turn in alternative directions. This suggests that LNs are necessary from P35 onward for stabilization of the growth cone at the correct target. If the target is not available, stabilization is less likely to succeed and growth cones that cannot adhere retract back to their anchoring points (heels) or search for alternative adhesion points in the direct surroundings. It is unclear why certain photoreceptors can keep their correct

extension after P35, while others can't. Furthermore, it is unclear why certain growth cones can change direction and try to adhere to alternative targets while others immediately retract. This may be a case of individual growth cone dynamics, their overlap with other filopodia, and their ability to stabilize individual or several filopodia. At this point it is unclear what the stabilization mechanism would be, or what photoreceptors can adhere to when LNs are not present. More about stabilization of growth cones is discussed in Chapter 5 and 6.

The synaptic circuit in the lamina has been determined by electron microscopy (EM) reconstruction and show that among ten different neural types, LNs are the main post-synaptic partner of PRs, that primarily make synapses with L1-L3 (Meinertzhagen and O'Neil, 1991). R1-R6 form tetrad-synapses which include an invariant pair of L1 and L2 and two variable elements out of the lamina neuron L3, amacrine cells and/or glia. It is remarkable to see that photoreceptors in an environment that are devoid of LNs can still form clusters of photoreceptors that resemble cartridges. From this observation the question rises if PRs form synapses in this case, and if so, with whom? A quantitative ultra-structural analysis of 60 mutants revealed that the average number of synapses per photoreceptor terminal is mostly stable (Hiesinger et al., 2006). Their analysis shows that cartridges may have abnormal photoreceptor innervation (more or less PRs per cartridge than the normal 6), but synapse number is normal in most mutants. The total number of synapses in a cartridge is dependent on the number of pre-synaptic PRs, rather than the number of post-synaptic LNs. Furthermore, the over-expression of the transcription factor Runt in PRs, induces the R1-R6 axons to overshoot the lamina and instead target the medulla. It was shown that in this artificial target zone, where their main post-synaptic partners are not present, PRs do form their usual tetrad-synapses with alternative partners (Edwards and Meinertzhagen, 2009). These are, however, all cases in which LNs or alternative partners are available and did not involve any case in which the complete post-synaptic target was absent. One may argue that this provides evidence that neurons make synapses in all cases, even with themselves if need be (autapses). Self-innervation could be the case in the SmoRNAi experiment as well. This is, however, not yet investigated and requires serial EM to identify the number of and location of synapses reliably.

In summary: The removal of all LNs from the lamina creates a different, but stable and organized scaffold. PRs are capable of forming an organized scaffold by themselves. Growth cones can extend correctly and independently from any input coming from LNs at the start of the extension phase. Thus, it seems that a stable and organized scaffold is a prerequisite for normal neural superposition sorting. Wiring defects occur late, and not in all cases. One of the questions that arises from these conclusions is if photoreceptors are still able to create

a scaffold in an uneven environment. Does this create an uneven scaffold? Chapter 5 goes into this, and related questions.

Chapter 5

The effect of a structurally disrupted scaffold on photoreceptor extensions

Photoreceptor axons connect with their post-synaptic targets in the lamina in an organized way, following the principle of neural superposition sorting Kirschfeld and Franceschini (1968). An organized environment, e.g. a regular scaffold, may be key for correct axon sorting.

Programmed cell death (or apoptosis) is an active regulatory mechanism to kill cells. A famous example of naturally occurring apoptosis during vertebrate embryonic development is inter-digit apoptosis, which shapes digits and separates fingers and toes (Chen and Zhao, 1998). During development of the *Drosophila* visual system, apoptosis regulates, amongst others, the correct number of inter-ommatidial cells in the retina (Brachmann and Cagan, 2003), as well as the correct number of LN cell bodies in a column in between photoreceptors (Huang et al., 1998). Apoptosis can be artificially induced by over-expression of certain apoptosis-enhancers. Examples are Reaper (White et al., 1996) and Hid (Roman and Davis, 2002), reported to be very potent apoptosis enhancing genes. In the light of proteins discussed in Chapter 2, it is interesting to note that over-expression of Armadillo was reported to induce neuronal apoptosis during retinal development (Ahmed et al., 1998).

Results presented in Chapter 4 show that the complete loss of lamina neurons from the lamina creates an organized, yet smaller, sorting field. In this altered scaffold, photoreceptor extension angles are not affected during the initial phase of axon sorting. This may be explained by the regularity of the scaffold. In this chapter, apoptosis-induction is used as a method to make the scaffold more irregular. It is investigated if this change in scaffold regularity results in alterations in photoreceptor extensions during the subsequent sorting phase. Lastly, it is

hypothesized how a feedback mechanism among photoreceptors can account for alterations in the scaffold and correct extension angles to ensure robust wiring.

5.1 Ablation of post-mitotic lamina neurons

In contrast to prohibiting differentiation of lamina precursor cells, as described in Chapter 4, killing post-mitotic lamina cells turned out to be more complicated than initially expected. The complete ablation of LNs by the expression of an apoptotic enhancer, has never succeeded with the genetic tools available[1]. The most lethal gene is UAS-Reaper; reported to be a very potent apoptosis enhancing gene (White et al., 1996). The expression of Reaper, even under a restricted driver, leads to death of the organism at the larval or pupal stage. The second most effective killing strategy–that does not kill the entire animal or ablates the complete eye–is the UAS-Hid apoptotic enhancer. Roman and Davis (2002) show that the cell specific activation of Hid in photoreceptors leads to disruption of the adult eye. Figure 5.1 shows that Hid expressed under the LN-specific 9B08-Gal4 driver at 29C in male flies (most optimal conditions) results in sparse killing of LNs.

To stress the cells and achieve more cell killing, crosses were kept at 29°C at all times. Since development at 29°C is faster than at 25°C, pupae which were kept at 29C were dissected after 20 hours[2]. Only male pupae or male adult laminae are analysed because the eyGal80 construct in the 9B08-GAL4 stocks suppressed the expression of UAS-hid and prevented cell killing in female flies (see Figure 5.1 A).

To assess the timing of the cell-killing experiment, the ablation of LNs from the scaffold at P25 and adult cartridges are compared. This is important since increased killing during the time P25-P50 may disturb neural superposition sorting in an other way then just the loss of cells from the scaffold. In the lamina, every cluster (P25) and cartridge (after P50) contains neurites coming from 5 LNs; L1-L5 (Meinertzhagen and O'Neil, 1991). UAS-Hid crossed to Ey-Gal80; UAS-CD4::tdGFP; 9B08-Gal4 over-expresses Hid as well as GFP in LNs, allowing the visual inspection of LNs in the lamina plexus. Figure 5.1 B shows that in this experiment, most adult cartridges look like WT (mean = 75.79 percent; standard deviation = 9.26). In other words, killing affects approximately 25% of the total number of cartridges, and not every cluster of LNs is affected equally. Only 1-2 percent of cartridges is

[1] Ablation experiments included expression of UAS-Reaper, UAS-Grim, UAS-Skl, UAS-Dronk, UAS-Dark, and UAS-Hid in combination with different drivers: ey-Gal4, mδ05-Gal4, GMR-Gal4, 27G05-Gal4, 9B08-Gal4, and at increasing temperatures (25-29-31°C).

[2] P20 dissections from pupae kept at 29°C will be referred to as P25 for clarity, because it represents the developmental stage that is normally reached after 25 hours of development at 25°C.

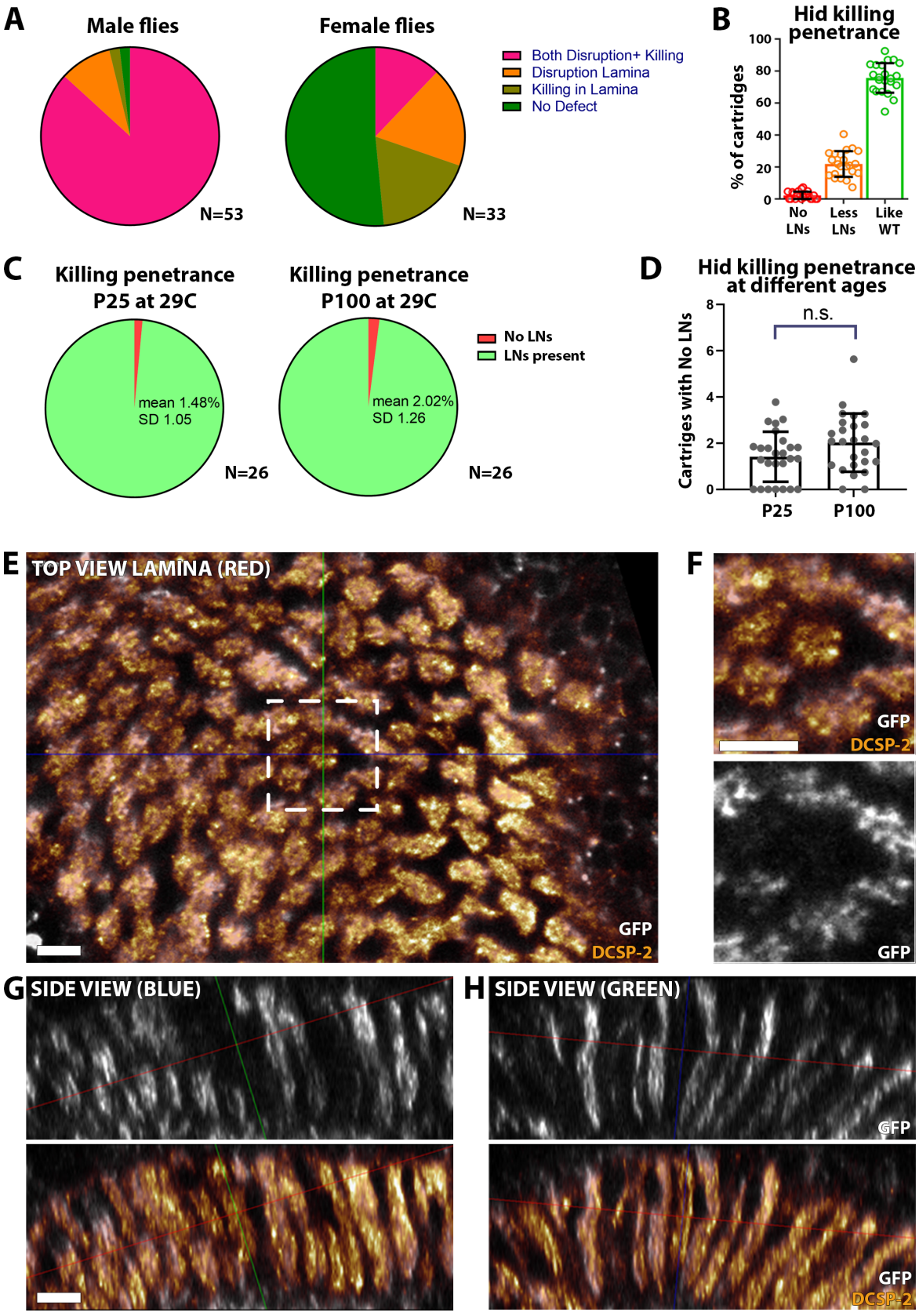

FIGURE 5.1: Hid expression induces sparse killing of LNs

A-D) Statistics from Hid over-expression (OE) experiments where UAS-Hid is expressed under the 9B08-Gal4 driver at 29°C. *N* represents the number of animals. **A**) Pie charts representing the part of experimental laminae disrupted by OE of Hid in male and female flies. **B**) Bar graph of the killing penetrance of Hid OE within affected laminae. Dots represent individual data points. **C**) Pie charts representing the killing penetrance of Hid over-expression within affected laminae. Killing (red) assessed as the ablation of all lamina neurons from a heel structure (P25) or a cartridge (P100). *N* represents the number of animals. **D**) Graph representing the killing penetrance of Hid over-expression within affected laminae at P25 and P100. Dots represent individual data points. **E**) Top view of lamina at P100. Photoreceptors (DCSP-2 staining) in glow, LNs in white. White box is enlarged in F. Green line indicates the cut through the lamina as shown in G. Blue line indicates the cut through the lamina as shown in H.**F**) Detail of a cartridge which is deprived of LNs and contains photoreceptors only. **G**) Orthogonal cut through the lamina cartridge along the blue line indicated in E and H. Green line cuts through the cartridge deprived of LNs. **H**) Orthogonal cut through the lamina cartridge along the green line indicated in E and G. Blue line cuts through the cartridge deprived of LNs. Red line indicates the cut through the lamina as shown in E.

completely devoid of LNs (see Figure 5.1 C-D). There is no statistically significant difference in killing penetrance between P25 and P100 (mean = 1.48% and standard deviation = 1.05 at P25; mean = 2.02% percent and standard deviation = 1.32 at P100). These results implicate that cell killing occurs early in development and does not continue over time. No LNs in a cartridge means that neurites of all five LNs are absent from the lamina. Figures 5.1 E-H show a 3D assessment of an adult cartridge devoid of LNs. A cut through all three axes shows that neurites are absent over the complete length of the cartridge. This is a representative example of cartridges devoid of all LNs. Thus, the over-expression of Hid is a validated method to sparsely remove LNs from the lamina early without affecting LN viability in later developmental stages.

5.2 Sparse ablation of LNs increases scaffold variability

To investigate the role of sparsely ablated LNs on the developmental pattern at the lamina plexus, brains were dissected at P25 and stained with 24B10 to analyze the scaffold. Figure Figure 5.2 A shows that, when all LNs of one cluster were ablated, the same change in heel organization is observed as in the SmoRNAi experiment at P25; from crescent to circular (see Section 4.3 and Figure 4.3). Measurements of the distances between heel structures shows no statistically significant difference between experiment and control (see Figure 5.2 C-D). In fact, the rarity of LN gaps in the lamina plexus make most comparisons between experimental and control conditions non-significant because only 1-2% of the lamina is affected (see Figure 5.2 C-F). There is, however, a significant increase in the variance of scaffold angles (see Figure 5.2 F), meaning that there is evidence for a broader distribution of data that corresponds to an increased variability in the scaffold. Around 77% of LN clusters looked unaffected in their size, while the remaining 23% was smaller due to the partial killing of LNs and their

absence from the lamina plexus (see Figure 5.1 B). This fraction of LNs might explain the increase in variability in the scaffold. Hence, the sparse ablation of LNs from the scaffold observed at P25 results in a lamina plexus that is less stereotyped and structured than the WT variant. Data on distances between bundles, bundle rotation, and angles in the grid were not significantly different, but the distribution was broader, making the scaffold organization of the lamina less regular than both WT and complete ablation of LNs in the SmoRNAi experiments. Therefore, Hid over-expression as a method, allows for the investigation into the role of structural organization in the process of photoreceptor sorting.

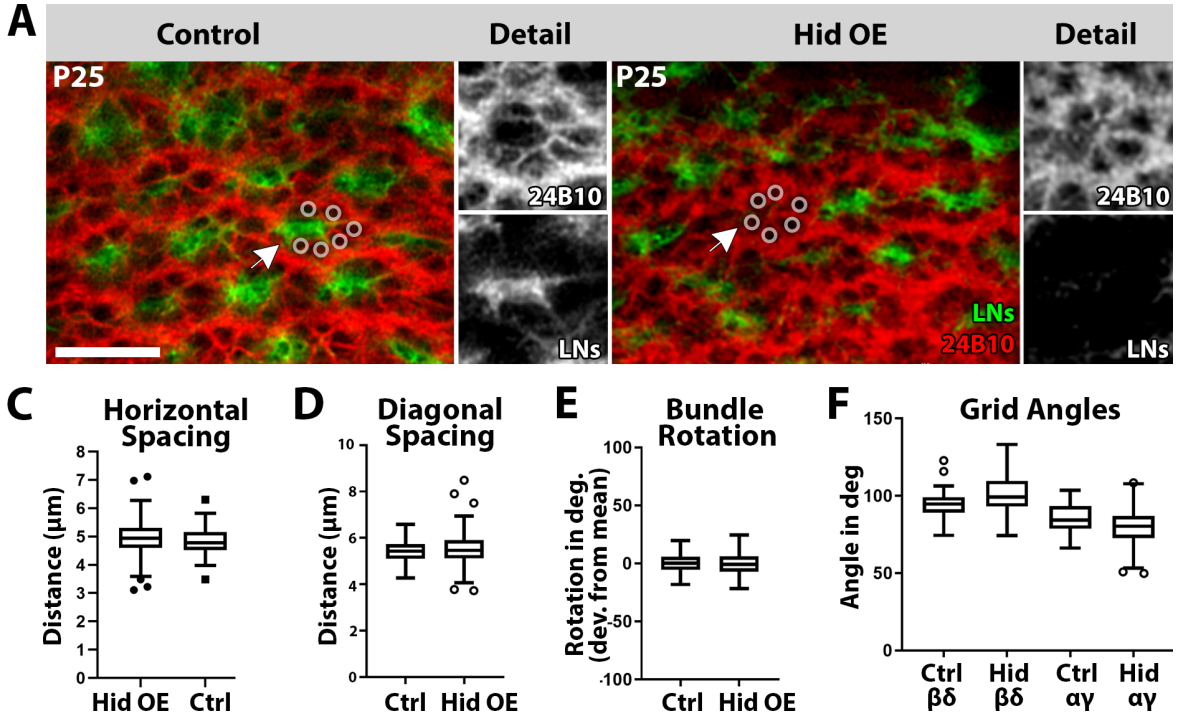

FIGURE 5.2: Scaffold organization in Hid over-expression experiment

A) Top view of lamina plexus at P25. Photoreceptors (24B10 staining), red; lamina neurons, green. Arrows indicate the heels structures shown in more detail in side panels. All scale bars 5 μm. **B**) Graph of killing penetrance in the Hid over-expression experiment organized for LN presence. **C**) Graph of horizontal distances between heel structures in the scaffold. All graphs showing mean +/- SD. Dots represent outliers. **D**) Graph of horizontal distances between heel structures in the scaffold. **E**) Graph of bundle rotation measured from Armadillo staining. **F**) Graph of angles measured in between 4 heel structures. β and γ are angles left and right, α and δ are the top and bottom angles.

5.3 Variability in the scaffold is corrected at the level of R4s

To examine if increased variability in the scaffold affects photoreceptor extension angles during superposition sorting, the extension angles of R4 photoreceptors in the Hid OE experiment were measured. The hypothesis is that if photoreceptor extension relies on a invariable starting point in a regular scaffold, R4 extension angles should show an increase in variability

in the Hid OE experiment. In addition to the findings from the SmoRNAi experiment, this would further suggest a role for the scaffold on subsequent extension angles rather than the presence of LNs as targets. To this end, GFP is expressed in the R4 photoreceptor sub type with the mδ05-Gal4 driver. The extension angles are analysed at P25, during the extension phase. Images taken from the lamina are aligned so that the equator is always on the right side. Measured extension angles are corrected for the mean extension angle for all laminae. Figure 5.3 A shows that R4 extension angles are extending in a correct direction. R4 angles are measured and quantified following the approach discussed in Section 4.1; with the aid of Armadillo staining (see Figure 5.3 B). Results show no obvious defects in R4 extension direction at P25 (see Figure 5.3 C). Statistical tests to compare control and Hid OE experiment show that there is no statistically significant difference between R4s that are extending *towards* a target area without LNs, with less LNs, and areas which look like WT (ANOVA; p-value >0.05; data not shown). Alternatively, R4s that extend *away* from a heel structure without LNs to the other classes, are also not significantly different (ANOVA; p-value >0.05; data not shown). Thus, the extension direction of R4s in laminae with sparsely killed LNs is similar to that of R4s in WT and show no changes based on the presence of LNs in the home, or the target area. The asterisk in Figure 5.3 C refers to weak evidence for significant difference between the variance of data of R4 extension angles of control and experimental conditions (F-test for equal variance; p-value = 0.0435. Interestingly, when the data is separated into the three classes (red, orange and green represent LNs "like WT", "Less LNs" and "No LNs", respectively), this indicates that most variance comes from the cluster "like WT" (see Figure 5.3 C). Thus, the slight increase in variance within the data set does not arise from clusters without LNs, but from other factors, possibly the variability of the scaffold caused by the incomplete removal of LNs.

To investigate if the variability of the scaffold influences the variance of extension angles, both the bundle rotation and the R4 extensions are considered. Bundle rotation is measure using the Arm/Sdk staining as explained in Section 4.1. Figure 5.3 B illustrates that connecting the Arm staining between R1-2 and R5-6 obtains a vertical line (next referred to as Arm line). The deviation of the Arm line from the mean indicates the bundle rotation deviation (see Figure 5.3 D). An unpaired T-test on bundle rotation shows no significant difference between experiment and control (unpaired T-test; p-value = 0.29; N = 76 for control and N = 122 for experiment). Next, in Figure 5.3 E, the bundle rotation is plotted against the R4 extension angles. Hypothesizing that increased bundle rotation results in more variation in the scaffold organization and could influence R4 extension angles. Moreover, the influence of LN presence was taken into account by registering the LN classification of the home, and the

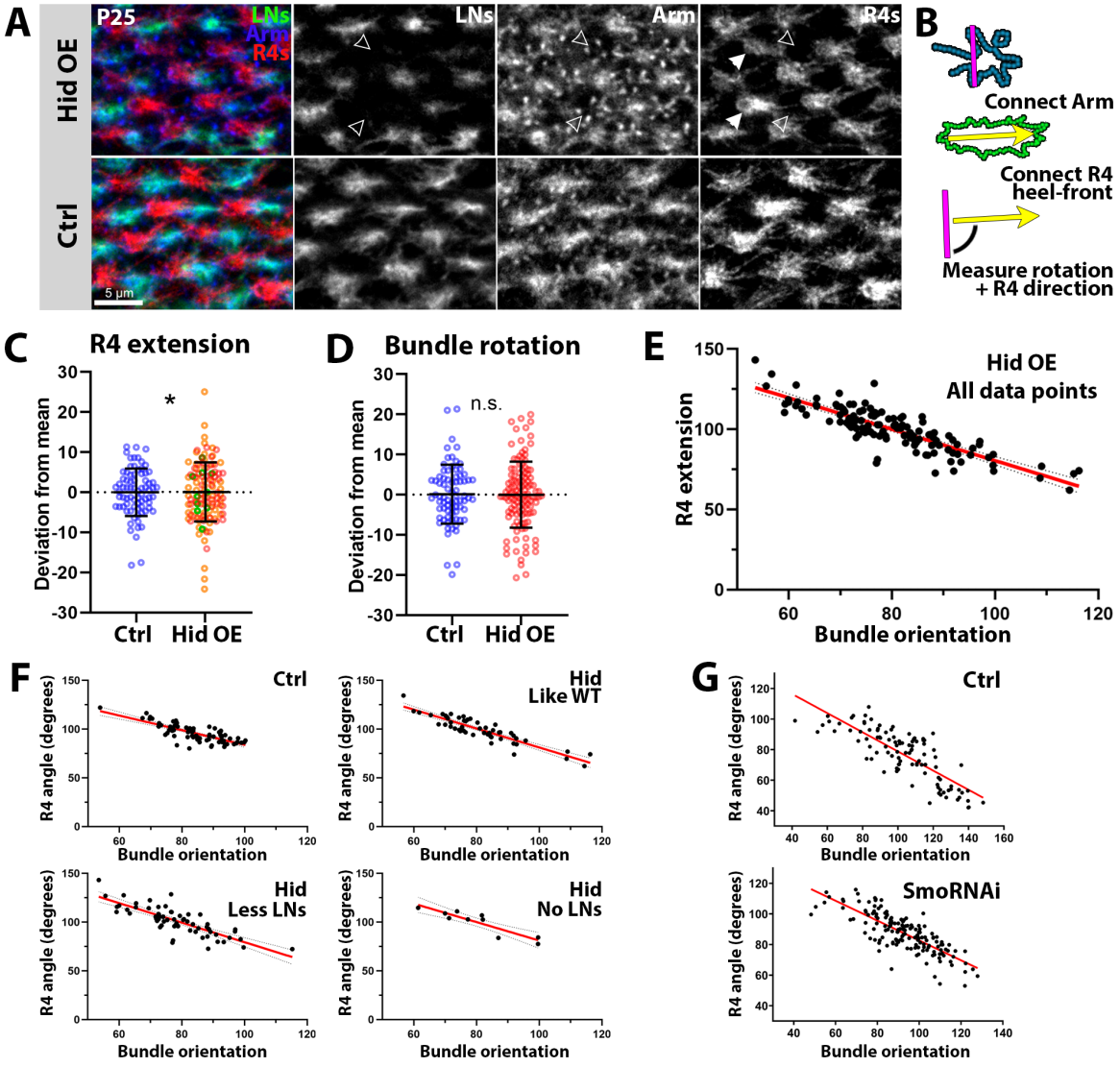

FIGURE 5.3: Photoreceptor extensions in a disorganized environment

A) Fixed images of R4 growth cone extension in Hid experiment at P25. R4s, UAS-CD4::tdTom x mδ05-Gal4 in red; ani-Armadillo staining in blue; LNs, UAS-CD4::tdGFP x 9B08-Gal4 in green. Black arrowheads indicate clusters without LNs. White arrowheads indicate R4s extending towards target areas without LNs. Scale bar 5 μm. **B**) Schematic representation of extension angle and bundle rotation analysis. **C**) Graph of R4 extension angles. Dots represent individual data points. $N = 69$ for control, $N = 141$ for experiment. Experimental data points are separated in 3 classes. "Like WT" in orange, "Less LNs" in red, "No LNs" in green. **D**) Graph of bundle rotation measured using the Arm line shown in B. **E**) Linear regression drawn through Hid OE data. Dots are individual data points. **F**) Linear regression drawn through control experiment data, and Hid OE data that is separated by LN presence. **G**) Linear regression drawn through SmoRNAi data and its respective control.

target area.

In this occasion, the relative extension angle is measured as the angle between the R4 extension (line from heel to front of the growth cone) and the Arm line (see Figure 5.3 B). There are two possible scenarios for the relative extension angle: 1) The relative extension angle is stable, e.g. R4 extension relies on the bundle orientation in the scaffold. 2) The relative extension angle is variable, e.g. that R4 extension is independent from the bundle orientation in the scaffold. Results, plotted in a correlation graph in Figure 5.3 E, indicate that the latter hypothesis is true. Plotting the distribution of bundle rotation against the relative R4 extension angles resulted in a negative correlation between the two. The sign of the correlation coefficient represents the direction of the relationship. The negative correlation coefficient indicates that when the value of bundle rotation decreases (rotation counter-clockwise), the value of the relative extension angle (between bundle and R4 extension) increases. This negative relationships produces a downward slope on the scatter plot. Simple linear regression analysis found a slope of -0.73 for all Hid data points combined (red line in the scatter plots). Data split into classes (see Figure 5.3 F), shows the slope for LN classification "Less LNs" of -0.82 ($N = 51$), and -0.83 for "No LNs" ($N = 10$). Hid OE data classified as "Like WT" ($N = 61$) has a slope of -0.65 in the presence of normal looking LNs. This is comparable to control data (-0.61; $N = 76$). All slopes are significantly different from 0 (p-value <0.0001). Hence, the relative extension angle of R4 is variable and, at least partially, counters the rotation of the bundle. Returning to the SmoRNAi experiment, SmoRNAi data on R4 extension and bundle rotation were compared in this manner and a similar negative relationship was found[3] (see Figure 5.3 G). Slopes are -0.65 for SmoRNAi experiment ($N = 161$) and -0.63 for control ($N = 102$).

5.4 live-imaging of R4s reveals a late stabilization defect

Next, the question is how the scaffold develops over time and if the correction of photoreceptor angles (as shown in Section 4.4) is persistent over the entire period of photoreceptor extension. Therefore, live-imaging of R4 photoreceptors in a background of sparsely ablated LNs, induced by Hid over-expression was performed[4]. One image stack was taken every 60 minutes for 19 hours between P27 and P46. Figure 5.4 A shows snapshots every 5 hours from live-imaging data of R4 extensions where LNs are labeled with GFP. It shows a comparison of R4 extensions in control (upper panels; GFP expression in LNs under 9B08-Gal4 driver) and

[3]Linear regression analysis of SmoRNAi data performed by Egemen Agi.
[4]Live-imaging data for the Hid OE experiment was obtained by Egemen Agi.

Hid over-expression (OE) experiment (bottom panels; Hid+GFP expression under 9B08-Gal4 driver). Figure 5.4 A shows that R4 extension angles are similar for experiment and control early in the sorting phase, and comparable to the R4 extension angles observed in fixed images (see Figure 5.3). Moreover, especially in the earlier time points (P25-P30), the heel positions in the scaffold are comparatively normal. The localization of LN clusters looks abnormal and is discussed in more detail in Chapter 6. Figure 5.4 B shows that spacing within the scaffold, measured as the distances between R4 heels, is similar between the experiment and control in the time points P25 to P38. However, this changes, as time passes. In control data (blue in Figure 5.3 B), one can observe slight curve in the heel spacing graph, due to the expansion of the lamina and the subsequent tightening of cartridges. In contrast, this is not observe this in the experimental data set (red), where the average heel spacing remained around 5 μm. Comparable to the fixed images taken at P25 (see Figure 5.3 A), spacing between heels (see Figure 5.4 B) was comparable to the distances measured in control, but with more variance in the data. The variance within the experimental data set increases over time. Initially, there is a non-significant difference between the spacing of heels in control and experiment. However, from P38 onward, there is a persistent statistically significant difference in the variance between control and experiment (F-test for equal variance; p-value <0.05 for P38 and P40; p-value <0.01 for P42, P44, and P46).

To assess the targeting accuracy of R4 photoreceptors in the live-imaging data set, the distance between the tip of the R4 growth cone and the centre of the LN cluster towards it is extending is measured (see Figure 5.4 C). Surprisingly, the distance from tip to the target of control photoreceptors, from early in the extension phase on, is less than 2 μm. This suggests that the extension towards the target not a process that takes 20 hours (between P20 and P40), but ends earlier. This would be at least true for R4, visualized during this experiment. It was expected that the distance would decrease over time (because photoreceptors extend towards the target during the extension phase). Yet, distances did not decrease until the very last hours of superposition sorting. This is when growth cones have stopped lateral extension, and instead are "diving" into the cartridge. For the experimental condition, the tip to target distance shows an increase in variance over time (F-test for equal variance, p-value <0.01 for all time points). For clarification, when clusters of LNs are completely missing from the lamina, these R4s are not taken into account since the location of the appropriate target cannot be reliably appointed. While there is no significant differences between control ($N = 49$) and experiment ($N = 57$) in the distance from the R4 tip to the LN target during the main part of the sorting phase, they do start to deviate in the last two time points.

To evaluate whether this finding means that R4s are mis-targeting in the Hid over-expression

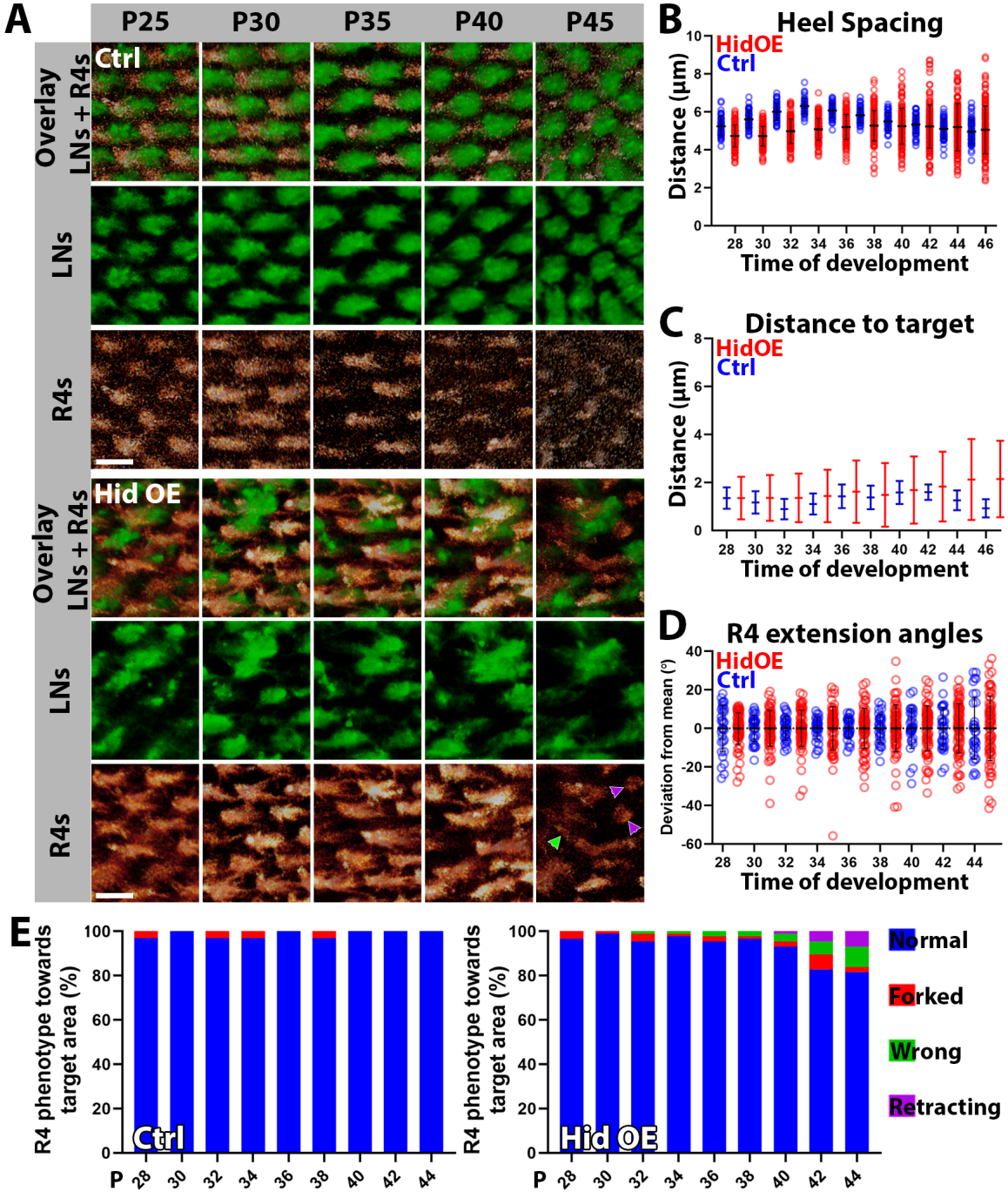

FIGURE 5.4: live-imaging R4 photoreceptors in the Hid over-expression experiment

A) Snapshots from live-imaging data, every 5 hours; P25-P45. R4 photoreceptors in glow, LNs in green. Scale bar 5 μm. Data obtained by Egemen Agi. **B-D**) Quantified measurements from live-imaging data. Graph shows mean +/- SD. In case of dots: every dot represents a data point. **B**) Spacing of photoreceptor heels measured from live-imaging data. Diagonal distances between the center of the R4 heels measured every 2 hours. $N = 82$ for control, $N = 87$ for experiment. **C**) Quantification of R4 extension towards target areas. Distance between R4 growth cone tip and centre of L-cell. $N = 82$ for control, $N = 79$ for experiment. **D**) Quantification of R4 extension angles (corrected for the mean). $N = 82$ for control, $N = 87$ for experiment. **E**) R4 targeting phenotype classified as: blue, normal extension angle towards target area; red, growth cone is forked; green, growth cone extension in wrong direction; magenta, growth cone is retracting, or has retracted. $N = 82$ for control, $N = 87$ for experiment. Data analysis in collaboration with Monika Kauer.

experiment, the analysis is extended to include R4 extension angles (see Figure 5.4 D) and the R4 targeting phenotype (see Figure 5.4 E). As can be observed in Figure 5.4 A, early time points show correct R4 extension angles (blue in Figure 5.4 E), while P40 and P45 show growth cones that are not all aligned. It can be deducted from Figure 5.4 D that the R4 extension angles in the Hid OE experiment have a larger variance in the data that increases over time[5]. While most R4s still extend correctly, even in these later time points, some growth cones extend in wrong directions, touching incorrect LN clusters (see Figure 5.4 A, green arrowhead), others retract (violet arrowheads). Eventually, approximately 80% of growth cones targets to the correct LN cluster in the Hid OE experiment, while the remaining 20% ends up in the incorrect location (see Figure 5.4 E and Supplementary Figure A.8). Mis-targeting, retraction, and splitting the growth cone (forked phenotype) are phenotypes found in Hid as well as in the SmoRNAi experiment. Supplementary Figure A.9 presents an overview of R4 targeting phenotypes in both SmoRNAi and Hid OE experiment. All PR behaviors described are observed at the end of the targeting phase (P42-P45) in both experiments and not before P38, except for forking, which happens throughout development and is sometimes also observed in control experiments.

5.5 Adult outcome after sorting in a distorted field

Lastly, the influence of sparse LN killing on the final lamina wiring is investigated. P100 brains (from newly hatched adults) were stained with either 24B10 or DCSP-2 to visualize photoreceptors, LNs expressed GFP under the 9B08-Gal4 driver. Fixed images of the adult lamina show a sorting defect in the experimental condition (see Figure 5.5 A). WT cartridges are evenly spaced and always contain six photoreceptors. The exception of this rule is the equator area, where cartridges contain seven or eight axons (Langen et al., 2015). Wiring mistakes at the equator are also described by Meinertzhagen (1972). In Figure 5.5 A, it can be observed that lamina neurites are organized in a star-shape in the middle of a WT cartridge. In contrast, in the Hid OE experiment there is uneven spacing of cartridges and they often contain more or less than six photoreceptors (hyper- or hypo-innervation, respectively). In addition to missing LNs from some cartridges, cartridges that do contain LNs are often fused. With visual inspection, the presence of LN neurites can be clustered into four bins. Either neurites are 1) completely absent from the cartridge ("No LNs"), 2) some neurites are present

[5]Extension angles at P44 are less reliably measured because the growth cone has stopped lateral extension and is now "diving" into the cartridge. Extension in the Z-axis, rather than on the imaged plane of focus. Time point P46 is removed from the data set for this reason.

("Less LNs"), 3) neurites are visually indistinguishable from WT ("Like WT"), or 4) neurites of two or more cartridges are fused (see Figure 5.5 B).

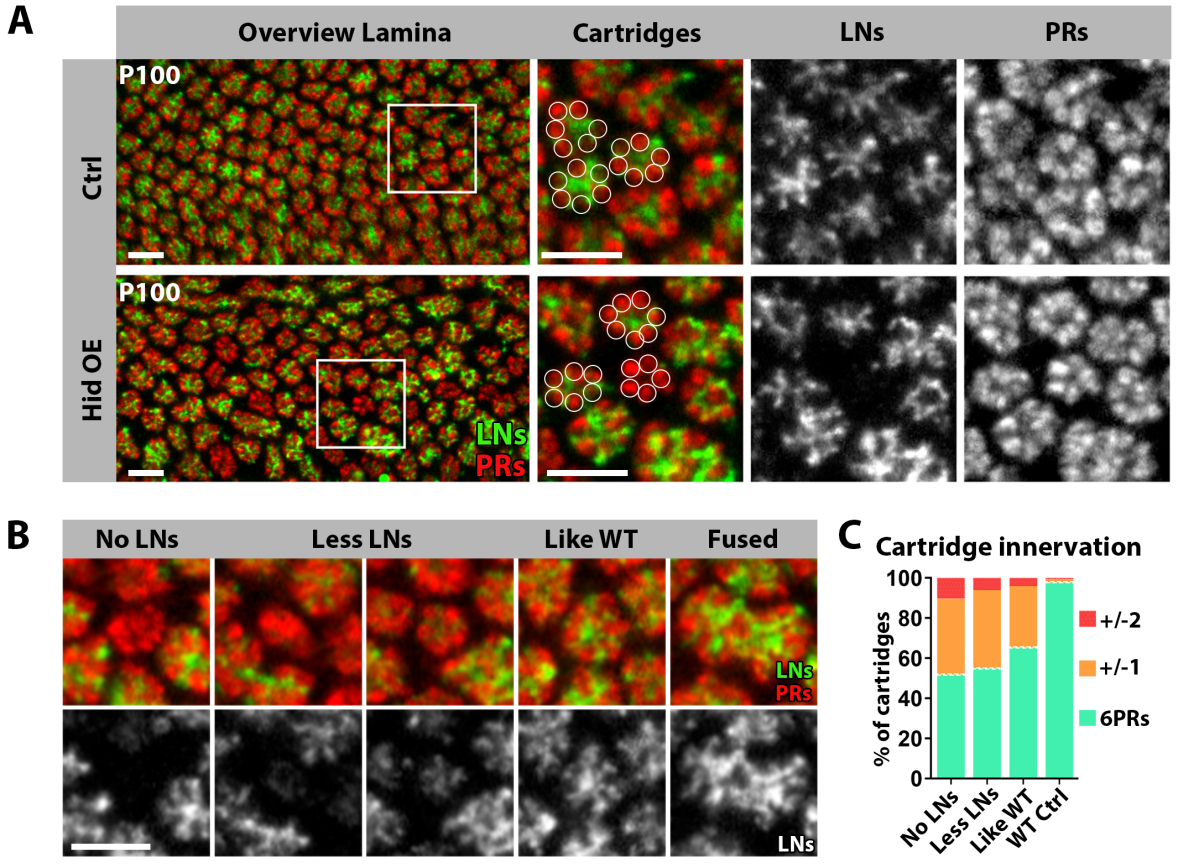

FIGURE 5.5: Hid over-expression results in a mis-wired adult lamina.

A) Overview of lamina with adult cartridges in Hid OE experiment. Squares are shown in more detail on the right. DCSP-2 staining marks photoreceptors, GFP marks neurites of LNs located at the center of each cartridge. Three cartridges are filled with circles representing the outline of photoreceptor axons. Scale bar 5 μ **B**) Classification of LN killing based on the presence of LN neurites. All representative images. **C**) Graph representing cartridge innervation by photoreceptors. Cartridges classified as indicated in B with the exception of Fused cartridges.

To analyse if the presence of LN neurites is instructive for photoreceptor wiring, photoreceptor axons were counted in each cartridge and this information was linked to the presence of LNs in that cartridge, e.g its classification. For this analysis of cartridge innervation, fused cartridges are not considered since their number of axons would always exceed six and skew the distribution excessively to one side. Figure 5.5 C presents the quantification analysis of the number of photoreceptor axons per cartridge and shows that an approximate of 50% of cartridges has the correct number of photoreceptors in the Hid OE experiment, even when LNs are not present. Meaning that photoreceptors do not only cluster together in cartridges without LNs, but also have the correct number of axons in approximately 50% of cases. The presence of clusters of PRs in "empty" cartridges is striking yet not unexpected given this is also observed in the SmoRNAi experiments, where all LN neurites are missing from the

lamina (see Supplementary Figure A.7). Moreover, considering the distribution of data in other columns of the graph, this suggest that LNs do contribute to the process of cartridge formation. When some LNs are present ("Less LNs"), the percentage of cartridges containing the correct number of photoreceptors is slightly higher than when there are no LNs; around 56%. Moreover, when LNs within a cartridge are "like WT" (either because the cartridge contained neurites of all five LNs, or otherwise because it could not visually be discriminated from this), 62% of cartridges have six photoreceptors, e.g. above average. For both cases, this corresponds to a statistically significant difference compared to cartridges with no LNs (see Figure 5.5 C). As a side note: while the presence of six photoreceptors per cartridge might represent a well organized lamina, it does not necessarily mean that cartridges are wired correctly. They could still contain photoreceptors of the wrong identity, or from the incorrect origination bundle. This cannot be distinguished in this analysis.

5.6 Late stabilization defects through Ncad deficiency

In the previously described experiments (the SmoRNAi experiments from Chapter 4 as well as the Hid OE experiment in this chapter), conclusions lean toward an understanding of photoreceptors being able to extend their growth cone in a target-oriented direction either without their post-synaptic partners actually present or only partially available. With LNs being dispensable in this scenario, this also implies that any molecule expressed by LNs or carried on their cell-membrane, is dispensable during this period. This contradicts studies that conclude that the adhesion molecule N-cadherin (Ncad) is necessary in both the photoreceptors and the post-synaptic target for correct target selection (Schwabe et al., 2013) and subsequent wiring (Prakash et al., 2005; Schwabe et al., 2014).

With the use of live-imaging it was observed that PRs have a late stabilization defect at the lamina when no, or less LNs are available; photoreceptors that initially extended correctly start retracting and turning in the late stage of photoreceptor sorting. To investigate the disconnect between the data presented here and published results, the role of the adhesion molecule Ncad during photoreceptor extension and stabilization at LNs must be investigated. Thus, the next questions are if Ncad is present at a lamina without LNs, and what photoreceptor behaviour looks like in the absence of Ncad.

It has been shown that Ncad is expressed in R7, R8, L1–L5, and Mi1 neurons (Lee et al., 2001; Nern et al., 2008), and in outer photoreceptors R1/R6 during distinct phases of development (Prakash et al., 2005). It was shown that Ncad is required in both PRs and LNs

to wire the lamina correctly (Prakash et al., 2005). Specifically, Ncad expression in L1-L5 (the LNs) regulates column formation in the lamina (Schwabe et al., 2014) using differential adhesion. Similar suggestions have been made for the medulla (Trush et al., 2019). The differential adhesion hypothesis (DAH), advanced in the 1960s, proposes that mixtures of cell populations organize themselves according to their inter-cellular adhesive properties: the less adhesive cell population is located at the periphery and surrounds the more adhesive cells (Steinberg, 1975, 2007). In case of lamina cartridges, this means that photoreceptors surround the LNs in a cartridge. The question is how the DAH would work in the context of our ablation experiments; in the partial or complete absence of LNs. In these cases I observe the stabilization of PRs in clusters in a majority of cases despite the absence of LNs.

To investigate this, first it was examined if the adhesion molecule Ncad is present when LNs are ablated. To investigate the localization of Ncad in the Hid OE experiment, when LNs are partially absent from the scaffold, laminae were stained with an anti-Ncad antibody at different developmental time points. LNs are visualized by the expression of GFP, and all photoreceptors are stained with the anti-chaoptin (24B10) antibody to visualize photoreceptors. The resulting images reveal that Ncad is present in locations with less and even without LNs at every time point assessed (examples indicated by white arrows, see Figure 5.6 A); from the start of extension (P25), throughout the sorting phase (P35), at the start of column formation (P50), and in adult cartridges (P100). This shows that photoreceptors have access to Ncad even when Ncad is not expressed by the target L-cell. It confirms that Ncad is expressed by photoreceptors R1-R6, as reported by (Prakash et al., 2005), and that this may be enough adhesion for photoreceptors to adhere to in the absence or reduction in the number of LNs at the lamina.

There is, however, an adhesion defect in the SmoRNAi experiment as well as in the Hid OE experiment in which a part of the extended photoreceptors deviates from the intended target. The percentage of mis-sorting (50% in SmoRNAi vs. 20% in the Hid OE, respectively) may be influenced by the presence of LNs, and thus by Ncad. From these results the hypothesis rises that a higher content of LNs/Ncad at the target location decreases the mis-sorting, because Ncad is required for differential adhesion to reliably form a cartridge. To investigate how differential adhesion, or more accurately; the lack of differential adhesion, affects lamina cartridges formation, NcadRNAi was expressed in LNs and development of the lamina during the extension and stabilization phase was monitored with live-imaging[6]. Figure 5.6 B shows snapshots from the live-imaging data set in which R4 photoreceptors (visualized by the expression of GFP) extend in a background of NcadRNAi expressed in LNs. It was observed

[6]Live-imaging data for the NcadRNAi experiment was obtained by Egemen Agi.

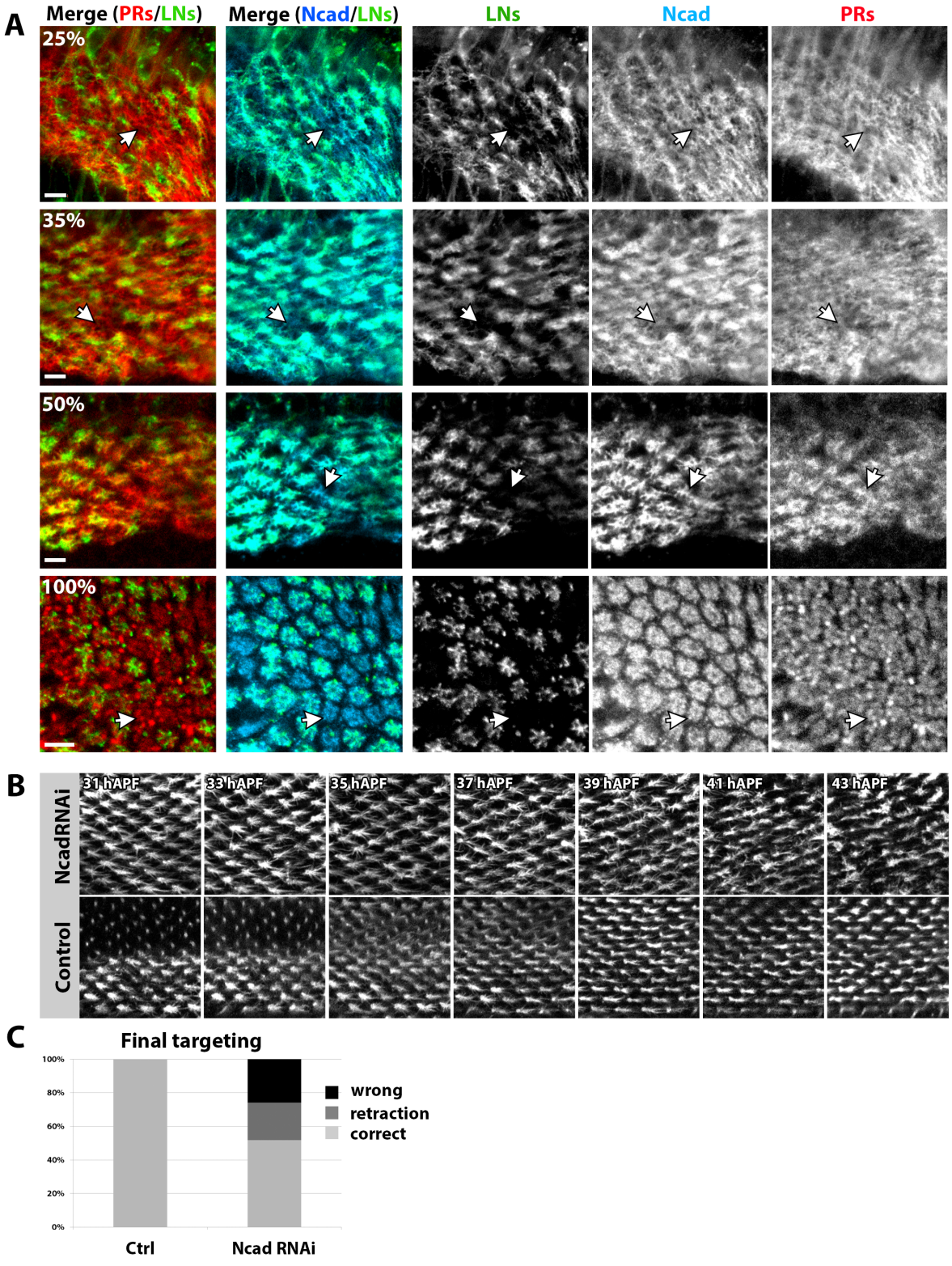

FIGURE 5.6: Ncad is involved in photoreceptor adhesion.

A) anti-Ncad antibody staining of laminae in the Hid over-expression experiment reveal no gaps where LNs are absent. Fixed images at P25, P35, P50 and adult stage (P100). All photoreceptors in red, LNs in green, Ncad staining in cyan. Scale bar 5 μm **B**) Snaphots from live-imaging between P31 en P45. R4 photoreceptors initially extend correctly (to the equator on the right of every image) when NcadRNAi is expressed in LNs, comparable to control. live-imaging obtained by Egemen Agi. **C**) Quantification of R4 final targeting. Black is wrong, dark grey is retracted, light grey is correct. Quantification by Egemen Agi.

that R4s can target correctly until 35 hAPF, but adhere to the correct target location only in approximately 50% of cases (see Figure 5.6 B-C). Adhesion in the absence of Ncad at LNs resulted in a stochastic distribution (50/50) between correct and incorrect adhesion, where incorrect adhesion was also divided 50/50 over retraction and choosing an incorrect target location[7].

In conclusion, PR targeting is initially correct, but PRs can only stochastically attach to their correct target location in the absence of Ncad from LNs. In this way, the results from expressing NcadRNAi in LNs are comparable to the results from the SmoRNAi experiment where LNs are absent. The NcadRNAi experiment phenocopies the timing of adhesion defects onset (P35-P38), as well as the incorrect targeting rate. The Hid OE has a milder mis-sorting phenotype, suggesting that the presence of LNs/Ncad helps with the photoreceptor adhesion to the target and is required for photoreceptor stabilization starting at the second half of the extension phase.

5.7 Conclusions and Discussion

In this chapter, a method was presented with which one can increase the variability in the scaffold. Instead of a overall decrease in heel distances and a change of photoreceptor heel structures from crescent to circular in all heel structures. Compared to observations in the SmoRNAi experiments in Chapter 4 (see Section 4.3), Hid over-expression results in a broader phenotypic range. LN cluster size is variable due to sparse killing, and therefore changes distances withing the scaffold dynamically. Furthermore, its low penetrance changes only a small subset of photoreceptor heels to circular organizations. The low percentage of LN killing was therefore both a curse and a blessing. A curse, since finding clusters of LNs that are totally ablated from the lamina is so difficult and, hence, statistical power is low. A blessing, because it allowed for analysis of a non-stereotype photoreceptor environment. This allowed for the examination at photoreceptor behavior in a perturbed environment without interfering with the molecular lay-out of the lamina.

[7]Quantification of R4 targeting in the NcadRNAi experiment by Egemen Agi.

Fixed, as well as live-imaging data, shows that initial photoreceptor extension angles are correct. Photoreceptors in the Hid OE experiment can be mis-targeting, or retract back to the heel, but do so only very late in the extension process. This is a phenomenon that was observed both in the Hid experiment (sparse ablation of LNs) and in the SmoRNAi experiment (patches completely devoid of LNs). This suggests that around P38 the developmental program of extending photoreceptors changes from a LN-independent phase to a dependent phase. Both the assessment of the R4s wiring phenotype in the SmoRNAi and Hid experiment, as well as the evaluation of (adult) cartridges in both experiments, show that the presence of LNs is important for final wiring. The percentage of correctly extending R4s in the late extension phase is considerably higher for photoreceptors growing in the environment with less LNs compared to the environment without LNs. In the total absence of LNs, instances are observed where six photoreceptors are collected in an area completely devoid of LNs. It is unclear why certain cartridges can form and look normal, while others fuse and look abnormal. In any case, it is remarkable that photoreceptors are at all able to form cartridges in target areas without post-synaptic LNs. Immunohistochemistry shows that these areas are not devoid of Ncad. This means that adhesion amongst Ncad-expressing photoreceptors is sufficient to have them adhere to one another. While no functional visual circuit would sprout from areas without post-synaptic partners, it is interesting to observe the robustness of photoreceptor wiring.

The seeming discrepancy between the 80% correct targeting of R4s observed in the live-imaging data vs. the 50% correct cartridges in the adult may have two non-exclusive explanations. 1) In the live-imaging data set the extension of only one photoreceptor sub type was assessed, and therefore 5/6 of the photoreceptors that are sorting were not observed. Wiring mistakes made by these other sub types are not included in the data set. 2) Wiring mistakes continue after P46. While it is always assumed that sorting happens between P25-P50, there may be instances of destabilization after the imaging session, that ran until P46. The live-imaging data-set shows that defects only start to arise from P38 onward and continue until P46; the end of the imaging session. It is likely that wiring mistakes continue after this time, which increases the percentage of wiring mistakes.

The late stabilization defect in the Hid experiment is presumably caused by the same mechanism as observed in the SmoRNAi experiment. Because the SmoRNAi and the NcadRNAi in LNs show the same phenotype of retraction after P38, adhesion by Ncad is likely the adhesive force that photoreceptors require in the late extension phase. This suggestion is backed by the fact that the Hid experiment, where there are more LNs than in SmoRNAi, has a smaller retraction phenotype after P38. Even though there is an increase in mis-organization compared

to control, it seems that the presence of more LNs–and therefore more Ncad–results in less final adhesion defects than in the SmoRNAi experiments. The targeting mistakes in SmoRNAi and NcadRNAi are distributed 50/50, while in Hid this approaches a 30/70 distribution between retraction and extension towards a wrong target, respectively. I hypothesize that the ablation of few LNs by Hid over-expression made some clusters/cartridges more attractable to photoreceptors than others, likely contributing to the preference of photoreceptors to adhere to alternative targets. Thus, in an environment where some LN target regions express Ncad, and some do not (or very low expression), photoreceptors more often mis-wire because they tend to adhere to the target with the higher Ncad content. This was also suggested by Prakash et al. (2005), who reported that R-cell axons typically choose to adhere to the target with more adhesive activity, even if such a target is incorrect. If all LNs, and thereby all high levels of Ncad are absent, photoreceptors can adhere to other photoreceptors because they all express low levels of Ncad. This leads to the 50% normal R4 extension stabilization. For the other 50%, growth cones either retract back, or try to adhere at a different cluster of photoreceptors in their vicinity.

Thus, it is concluded that photoreceptor extension acts independent of the presence of LNs and Ncad up to a certain point in development. After this independent phase, the targeting choices are dependent on permissive, N-cadherin–mediated interactions whereby the source of Ncad is less important than the levels of Ncad present. If levels of Ncad are too low, or a higher Ncad source is available, then photoreceptors retract or adhere to the alternative target leading to mis-wiring of the lamina.

During the extension phase of neural superposition sorting, small differences in bundle rotation are resolved in the R4 outgrowth direction. In fact, it seems that bundle rotation is variable in the uneven scaffold created in the Hid OE experiment, yet R4s are capable of correcting their extension angle. While a correlation does not mean that the relationship between two variables is causative of an event, one can draw certain conclusions from it. It seems that the R4 extensions are rather stable and not directed by bundle rotation/scaffold organization. A correlation that accounts for correction of variability in the scaffold is also found in WT, albeit a narrower data distribution. This suggests that variability is a naturally occurring event that can be corrected for during development, before defects arise. It might be another mechanisms by which photoreceptors ensure that developmental noise that occurs is reduced.

These conclusions lead to the question how photoreceptor can regulate their extension angle during neural superposition sorting. I hypothesize that there may be a correction or feedback mechanism in place that corrects the R4 outgrowth direction for any disturbance in the early

lamina organization. Both the removal of all LNs and the ablation of some LNs introduced changes to the scaffold. Yet, (leaving the adult outcome aside) the initial extension of photoreceptors during the sorting phase was only mildly affected. If, indeed, there is a correction mechanism, the question is how this is organized and by which cells and by which means. In the next chapter, the independent photoreceptor dynamics are assessed and the possibility of a feedback mechanism that could ensure correct extensions is evaluated.

Chapter 6

Target-independent growth cone extension during sorting

Throughout the 19th century, numerous hypotheses regarding brain wiring mechanisms have developed. Most models that describe axon extension, and brain wiring in general, rely on guidance cues (Tessier-Lavigne and Goodman, 1996). These theories tie back to a classic theory in neurobiology: Sperry's chemo-affinity theory (Sperry, 1963). In short, it states that some target tissue or environmental tissue expresses ligands that are perceived by the receptors on an axon growth cone to which it responds either by growing away from the signal or being attracted to it. As the name implies, this hypothesis postulates that correct brain wiring is directed by chemo-affinity; the attraction of axons by chemicals that are either soluble or substrate-bound.

Despite the discovery of numerous membrane-associated molecules with indicated functions in axon guidance–such as Dscam (Neves et al., 2004), a true "Sperry molecule" that could account for identification-coding of neurons has not been discovered. In fact, the question remains if such molecules exists at all (Petrovic and Schmucker, 2015). Moreover, it is questioned if mechanisms based on chemo-affinity are able to build neural circuits in a robust manner. Robustness of an organism is the ability of resilience of a phenotype to perturbation. The robustness of a phenotype appears at various levels of biological organization including gene expression, protein folding, physiological homeostasis, and development (de Visser et al., 2003). Labeling neurons with a unique marker and directing them to find a cell with another unique marker to connect to, may sound like an ideal way to wire a brain. It does, however, not account for developmental noise or disturbance of developmental processes. A slight

change in temperature, light intensity, radiation, chemical components present in the environment, or other environmental factors, could influence gene expression, protein expression levels, or protein folding and make the whole system fall apart. Even the use of gradients; directional information provided by concentration gradients (either attractive or repulsive) would not be sufficiently reliable, by itself, to robustly direct precise brain wiring (Goodhill, 2016). In order to reliably wire a brain, it needs a different approach, or at least, additional mechanisms.

In recent years, there have been discoveries of target-independent mechanisms that can reliably wire axons. Harada et al. (2020) describe, for instance, emerging evidence for target-independent retinotopic map formation. Extracellular phosphorylation generates a self-guiding mechanism that affects axon growth independent of signals from the surrounding target tissue. Target-independent wiring mechanisms are more robust to developmental noise because they do not depend on precise instructions from the surroundings (Petrovic and Schmucker, 2015). There are many mechanisms that could contribute to robust brain wiring that do not depend on pure molecular guidance (Agi et al., 2020). Partners do not need molecular specification in such cases, but partnerships are restricted by who sees whom at the right time during development. Timing could be regulated through birth-order, time-controlled neuron differentiation, axon descent, or cell migration (Agi et al., 2020; Holguera and Desplan, 2018; Kulkarni et al., 2016). Spacing could be specified through formation of columns, cell tiling, self-avoidance, or through regulation of localization in a sorting field (Agi et al., 2020; Langen et al., 2015; Millard and Zipursky, 2008). This last suggestion relates to the lamina scaffold. Developmental rules could form patterned cell formations that enable neurons to form synapses only between partners that occupy the same place at the right time.

Langen et al. (2015) propose that neural superposition sorting follows a developmental program (or algorithm) with distinct developmental steps and rules. Following an algorithm in a step-wise manner may be key to understanding circuit wiring (Hassan and Hiesinger, 2015). The underlying mechanisms of this specific algorithm are not yet resolved and part of a larger question in neurobiology, namely; how does a brain wire itself?

In previous chapters I showed that photoreceptors can create a patterned scaffold without the need of LNs (see Section 4.3). Moreover, while the organization of the scaffold may be variable, i.e. variability in the bundle orientation, R4 photoreceptors have a robust growth cone extension angle independent of this developmental noise (see Section 4.4 and Section 5.3). Lastly, I found that photoreceptors are able to cluster together in cartridges, even in the total absence of LNs (see Figure 5.5). A combination of these results suggests a photoreceptor

wiring mechanism that is highly robust and highly immune to developmental noise. The next question is where this robustness comes from and what the underlying mechanism is.

In this Chapter I consider the question: Are photoreceptors capable of target-independent wiring? First, I show independent LN and PR dynamics observed during live-imaging. Second, I show that photoreceptors act independently of other cell types present and that glia nor Ncad expression by glial cells are involved in photoreceptor sorting. Next, I investigate the possibility of a feedback mechanism amongst photoreceptors that could account for stable extension angles. Finally, I discuss the possibility that filopodia are involved in a target-independent phase of growth cone extension and subsequent stabilization at the lamina plexus.

6.1 Independent cellular behaviors of LNs and PRs

During development, photoreceptors and LNs extensively overlap during neural superposition sorting (Langen et al., 2015). This observation was the initial motivation to investigate the wiring mechanisms underlying photoreceptor sorting. While photoreceptors extensively touch multiple LN clusters, they do not directly connect to them, only to their correct target cartridge. Meanwhile, results from the SmoRNAi experiments (see Chapter 4) show that PRs can create a scaffold and extend their growth cones in an environment without LNs, suggesting that the overlap with LN clusters is not necessary for these processes. It could imply that there is a target-independent wiring mechanism that aids scaffold formation and axon extension. The *Drosophila* visual map is currently not considered amongst systems that have wiring mechanisms independent of target cues or target cells.

To properly test for independence, one needs to affect dynamics of a single cell type only, without affecting the dynamics of the other. If, during this experiment, the affected cell type does not disturb the development of the other then one can assume independent dynamics. This is what was accomplished in the Hid OE experiment. With the sparse ablation of LNs in the Hid over-expression experiment (UAS-Hid expressed under 9B08-Gal4 LN driver; described in Section 5.1), a phenomenon not seen in WT was observed; the fusion of cartridges. LNs express GFP under the same 9B08-Gal4 driver that drives Hid OE in this experiment. Figure 6.1 A shows fixed images of the lamina at P50 that displays this fusion phenotype (white arrow). It shows an unevenly organized lamina. Normal cartridges are mixed with big fused cartridge-clusters counting two- to three times the normal number of photoreceptor axons in a cartridge. These fused cartridges are increased in size. The normal star shape of a

cartridge (LN neurites in the middle surrounded by six photoreceptor axons) has changed into a "blob" where axons could sometimes be encountered on the inside of the cartridge, instead of around the edge. Images of adult lamina with DCSP-2 staining to label the photoreceptors are not shown, but show the same phenotype.

With the live-imaging data set obtained for the Hid OE experiment, the dynamics of photoreceptors and LNs are visualized in time, and cellular dynamics can be analysed with 3D visualization software (Amira 5.6; FEI Visualization Sciences Group). In this way, information is obtained on when LN clusters fuse. Results, presented in Figure 6.1 B (R4 channel only) show that PRs display completely WT behavior between P25 and P35 and extend the growth cone in the correct R4 direction in the Hid OE experiment, LNs often leave their position in the scaffold and fuse with neighboring LNs (see Figure 6.1 B-C (LNs in green). This analysis[1] includes fusions on any depth of the LN cluster in the lamina plexus. Fusion is considered as the extensive touching of neurites and the collision of the main bulk of LN neurites as indicated with arrows and arrowheads in Figure 6.1 C. The graph in Figure 6.1 D illustrates that almost all LN clusters fuse with at least one other cluster at any time between P28 and P44 in the Hid OE experiment. Fusion can be reversible when LNs move away from each other and neurites separate. This is observed in approximately 10% of LNs that fuse, and is often followed by repeated fusion of the same LNs. In WT, the touching of LN neurites during the developmental phase of neural superposition sorting is rarely observed. Moreover, they never move away from their position in the scaffold, and never move towards each other or collide. Over a time span of 16 hours (P28-P44), the progressive fusion to up to approximately 92% of LN clusters at the lamina plexus is observed in the experimental condition ($N = 57$). In the control condition, few LN clusters touch, but do not collide or totally fuse ($N = 32$; see Figure 6.1 D). Fusions of LN clusters result in a uneven spacing of LNs at the lamina plexus. In WT, spacing between LNs is stable and space between LN clusters increases towards the final stage of neural superposition sorting when LNs shrink back and obtain a star shape in the center of the cartridge where they are encircled with six photoreceptors. Glia move in between cartridges, which also provides spacing (discussed in Section 6.2). In the experimental condition, the spacing between cartridges remains uneven.

6.2 Glia are not required for photoreceptor extension

As the neurites of lamina monopolar cells are not the only candidates that could play a role in guidance or aid in photoreceptor wiring, another cell type; glia, is investigated. Glia

[1] Analysis of fusions in the Hid OE experiment was performed jointly with Monika Kauer.

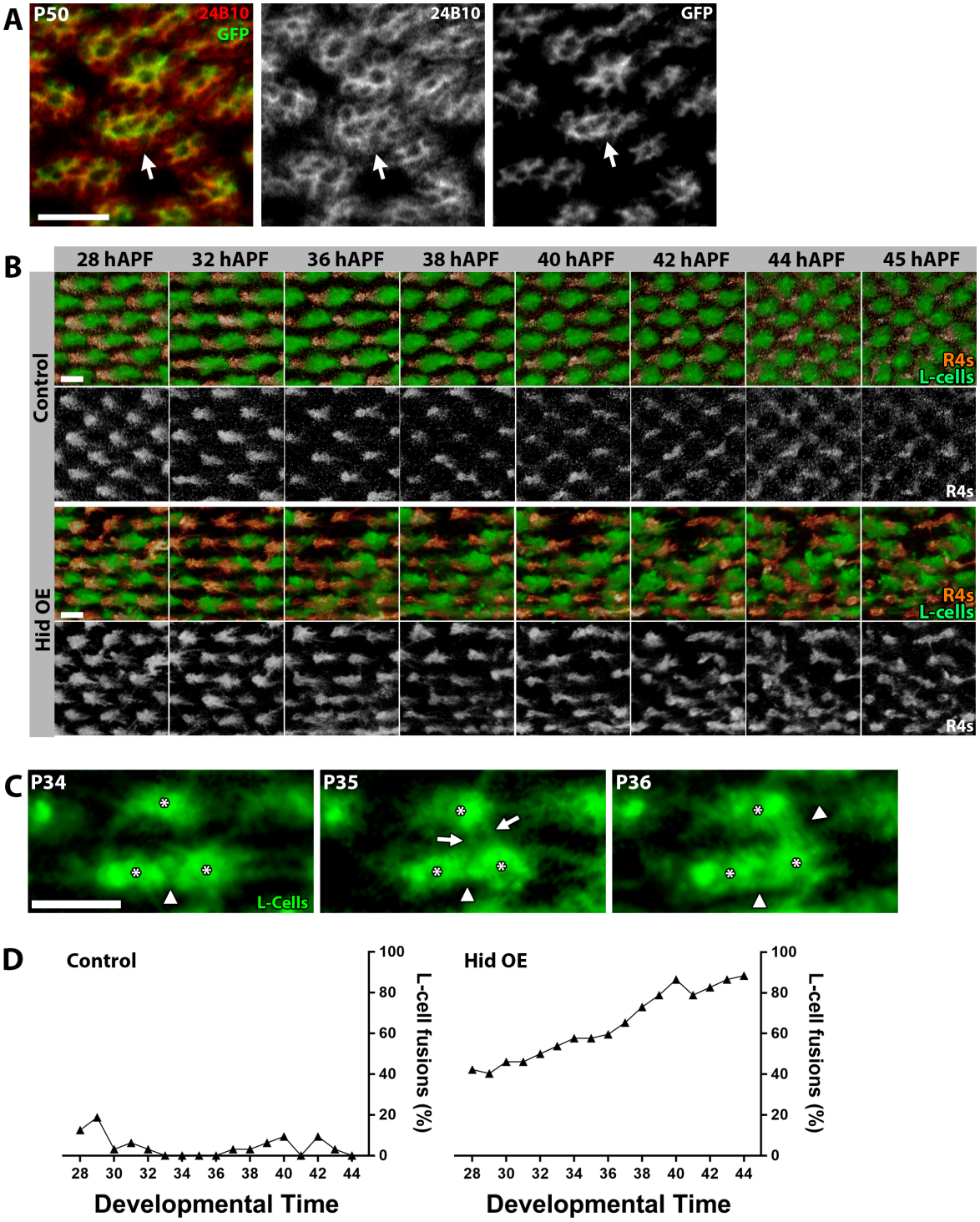

FIGURE 6.1: LNs fuse at the LP during Hid OE experiment

A) Fixed confocal image of the lamina at P50. LNs in green, photoreceptors stained with 24B10 in red. White arrow indicates a fused cartridge. **B**) Snapshots from live-imaging data during the Hid over-expression experiment between P25-P45. R4 photoreceptors in glow, LNs in green. Data obtained by Egemen Agi. **C**) Three LN clusters fuse over time. LN channel (GFP) only at P34, P35 and P36. Asterisk indicate LN clusters, arrowhead indicates collision/fusion, arrow indicates extensive neurite overlap preceding full fusion of LNs. Both extensive overlap and collision are quantified as fusion in panel D. **D**) Quantification of LN fusion over time as a percentage of all investigated LN clusters ($N = 52$ for experiment and $N = 32$ for control). Images for panel B and data analysis for panel C by Monika Kauer. All scale bars 5μm

are non-neuronal cells in the nervous system that hold a variety of functions. There are different types of glia in the optic lobe; including wrapping glia around photoreceptor bundles (Fernandes et al., 2017; Poeck et al., 2001) and epithelial and marginal glia above and below the lamina plexus, respectively (Chang et al., 2018; Poeck et al., 2001). During axon descent from the eye to the lamina, glia are essential for targeting to the lamina (Poeck et al., 2001). Furthermore, wrapping glia are involved in a signaling cascade that induces differentiation of LPCs into LNs (Fernandes et al., 2017). Hence, glia have important roles during the development of the lamina.

To exclude the possibility that glia have a role during the extension phase, the presence of glia at the lamina plexus during development is investigates. In this experiment, GFP is expressed under the Repo-Gal4 driver, active in glia cells, in an otherwise WT *Drosophila* brain. During different developmental time points, the *Drosophila* brain is dissected and stained with the 24B10 antibody to visualize photoreceptors. Figure 6.2 shows that a layer of glia is present above, and beneath the lamina plexus throughout development, but only invade the lamina plexus after sorting is done. Around P40 glia invade the lamina plexus and position in between forming cartridges. Glia position suggests that they provide spacing in between cartridges.

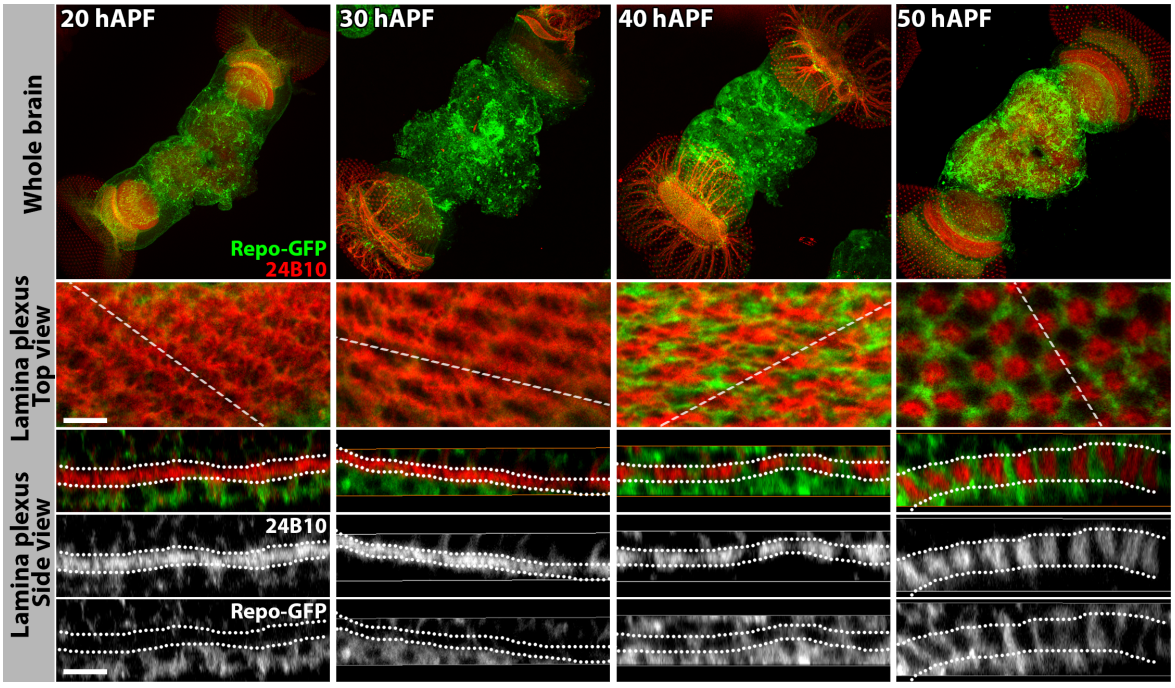

FIGURE 6.2: Glia localization during development of the LP

Overview of glia localization from P20-P50. From fixed data. Photoreceptors (24B10 staining) in red, glia (Repo-Gal4 x UAS-CD4::tdGFP) in green. **Top section**, overview of the complete brain. **Middle section**, top view of the lamina plexus. Dotted line represents the location of the oblique slicer to produce images for the side view section (below). **Bottom section**, side view of the lamina plexus. Scale bar 5 μm.

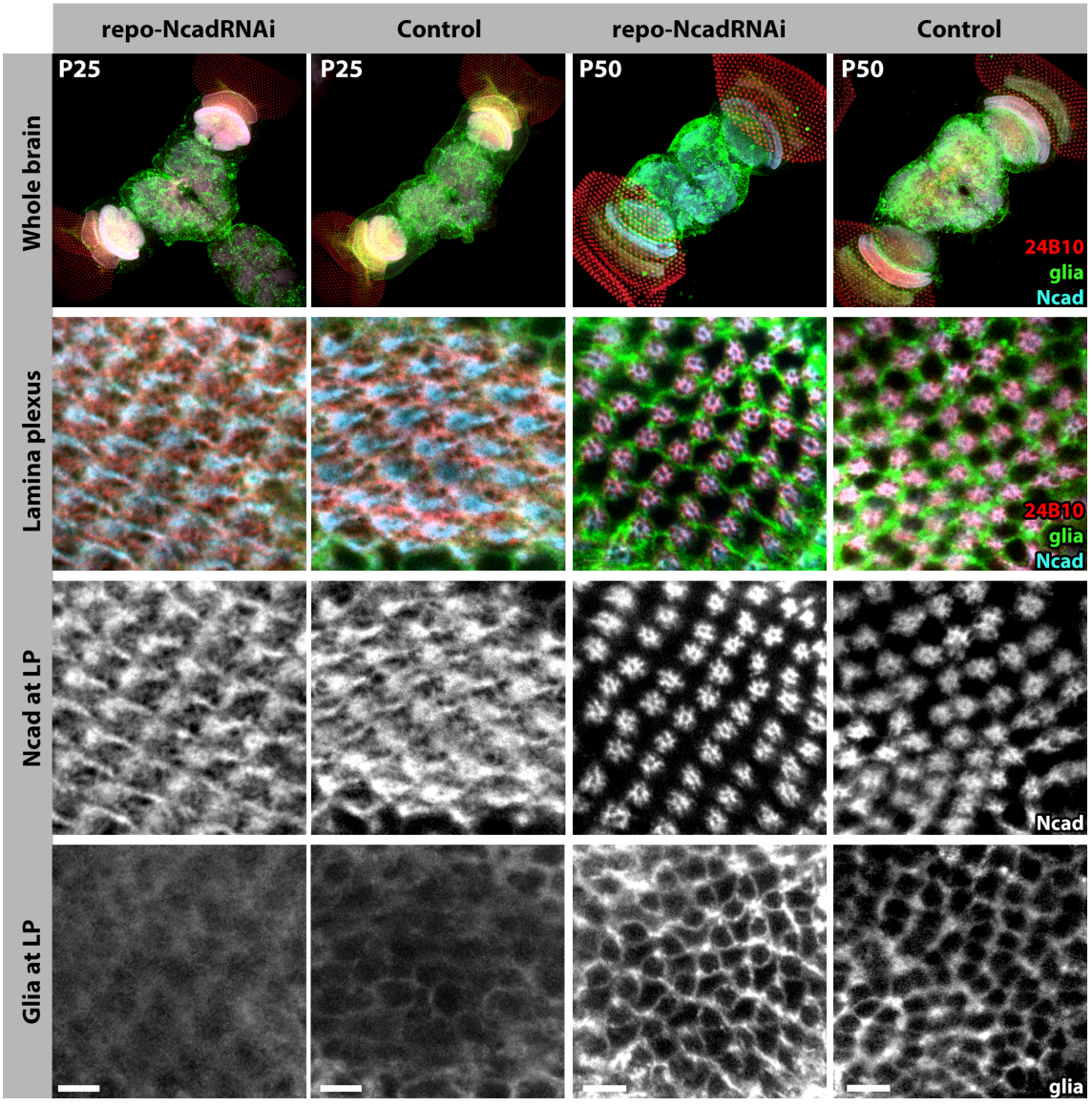

FIGURE 6.3: NcadRNAi expression in glia does not change lamina organization

Comparison of development of the lamina with WT glia, and glia expressing NcadRNAi (Repo-Gal4 driver) during development. Pupal stages P25 and P50 side by side. **Top row**: Overview of the *Drosophila* brain. Photoreceptors (24B10 staining) in red, glia (expression of GFP under Repo-Gal4 driver) in green, anti-Ncad antibody staining in magenta. **Second row**: Section of the lamina. Top view of the lamina plexus at P25, and section through lamina cartridges at P50. Overlay of all three channels. **Third row**: Ncad channel. **Bottom row**: glia channel. Scale bar 5 μm.

Given that glia are not present in the lamina plexus during photoreceptor extension, this suggests that glia could not aid the regulation of photoreceptor extension angles. However, marginal and epithelial glia are present below and on top of the lamina plexus around that time. To exclude the possibility that adhesion molecule Ncad is expressed by glia and influences photoreceptor stabilization in the correct outgrowth direction in that way, the following experiment is conducted. NcadRNAi is expressed in glia under the Repo-Gal4 driver and the scaffold at the lamina at P25 and at P50 is assessed, before and after sorting, respectively. Figure 6.3 Shows fixed confocal microscopy images of the lamina where no difference between experiment and control in the organization of the lamina plexus or the formed cartridges can be observed. The normal lay-out of the lamina plexus at P25 and the normal spacing and axon number in cartridges at P50 indicate that Ncad in glia does not influence stable PR extension, nor stabilization at the target.

6.3 A network of photoreceptor filopodia guide and stabilize the growth cone

Filopodia, thin and highly dynamic membrane protrusions on the growth cone of the axon tip, display random extensions and retractions during development. Their roles during neural development are not fully understood, but there is much evidence that suggests that filopodia are involved in almost all developmental stages; from neuron differentiation, to migration, and from axon and dendrite extension, to the final step of synapse formation (Gallo, 2013; Wit and Hiesinger, 2022). Filopodia can sense the environmental stiffness (mechanosensing) (Koser et al., 2016) and are believed to make out the chemical composition of the environment (Tessier-Lavigne and Goodman, 1996), as filopodial tips are loaded with receptors. Directional movement of the growth cone based on sensing environmental cues is one of the best characterized roles for filopodial dynamics (Davenport et al., 1993; Heckman et al., 2013). The role of filopodia in growth cone movements has been investigated in detail and implicates a role for filopodia in directional choices during axon outgrowth.

Filopodia have other functions as well, and are involved in stabilization of the growth cone (Özel et al., 2015; Sahasrabudhe et al., 2016). From experiments described in Chapter 4 and Chapter 5, it is hypothesized that photoreceptors are able to extend their growth cone in a target-oriented direction despite changes in the environment. This seems to be a LN-independent mechanism that continues at least until P35 before the first defects in photoreceptor extension angles appear. Even though the SmoRNAi scaffold was different from WT, it might have functioned in a way to ensure proper extension angles due to its stereotypical

organization. Yet, in the Hid over-expression experiments–where the variability in the scaffold was increased–a robust outgrowth direction of R4 photoreceptors was also observed (see Section 5.3). Moreover, a negative correlation between bundle rotation and R4 outgrowth direction was found. This observation, that rotation of the bundle is not indicative of the R4 extension angle, but seems corrected for this developmental noise, raises the question if there is a feedback system in place that ensures that the extension of photoreceptors is in the right direction. Bases on previous experiments, one can already exclude certain cell types that do not have the possibility to provide such feedback. The Shibire^{ts} experiment blocked membrane dynamics of LNs (see Section 4.2), thereby ruling out LN membrane dynamics as a guiding factor. Results from the SmoRNAi experiment, where the differentiation of LNs was blocked, suggest that feedback cannot be provided from LNs. The absence of glial cells at the lamina plexus during sorting (see Figure 6.2) excludes this cell type from consideration. Hence, the only other cell type in the lamina plexus around this time, and the most likely candidate for the feedback; interactions among PRs themselves. In particular, interactions between their growth cones.

To investigate the possibility that photoreceptors guide each other to obtain correct extension angles, WT R4 photoreceptors expressing GFP were imaged with high-resolution fast-imaging microscopy[2] (see Figure 6.4 A). With this technique, one can observe the fast dynamics of filopodia *in vivo*. The live-imaging data set of fast dynamics of all R4s shows that PRs are in contact with almost all their neighboring R4s via filopodial contacts. Figure 6.4 A indicates single filopodial contacts that are stable throughout the imaging period of two hours with red arrowheads. Other filopodia are more dynamic and have shorter life times. A remarkable feature is that most of the filopodial interactions are from growth cone fronts to heels of adjacent R4s (see Figure 6.4 B). Based on these findings of filopodial contacts amongst R4 photoreceptors, it is hypothesized that contacts between other photoreceptor sub types are equally prevalent.

6.4 Conclusions and Discussion

Although target-dependent neuronal wiring mechanisms have been described, for instance for the mouse olfactory map (Takeuchi and Sakano, 2014), it is clear that PR growth cones can not be involved in a sorting mechanism that is dependent on the target. First of all, growth cones of photoreceptors have been found to touch multiple LN clusters during extension Langen et al. (2015), which makes it a dubious target. Secondly, the removal of LNs from the

[2]Live-imaging data of filopodia on WT R4 growth cones was obtained by Egemen Agi.

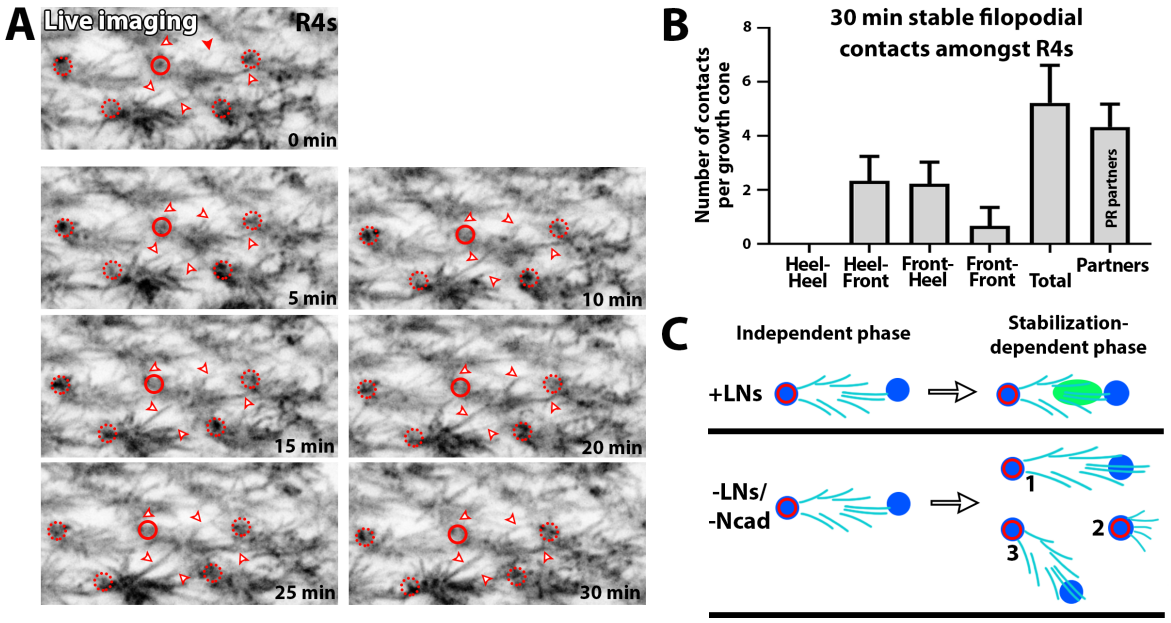

FIGURE 6.4: Filopodial contacts could aid extension and stabilization

A) Snapshots from 30 min live-imaging data around P25 show stable filopodia over long periods of time. Dotted red circles represent the location of R4 heels. Arrowheads point at extending filopodia from the middle R4 (solid circle represents the heel position of this R4). **B**) Quantification of filopodia that remain stable over 30 minutes. Scale bar 5 μm. Data obtained by Egemen Agi. **C**) Model of an independent extension phase followed by a stabilization-dependent phase. Top: Example of growth cone extensions in case LNs are present. In the LN independent phase growth cones extend by filopodial extensions that sense the next PR heel. Upon the shift to stabilization-dependent phase, PRs can sense the presence of Ncad at LNs and stabilize there. Bottom: Examples of growth cone behaviour when adhesion to the target is not possible due to absence of either LNs or Ncad from LNs. Independent phase similar to scenario described above. During the stabilization-dependent phase, PRs could 1) adhere to a (cluster of) photoreceptor heel(s), 2) retract back to their own heel structure and stabilize there, 3) change direction and stabilize at an alternative cluster of PR heels.

lamina plexus does not disturb growth cone polarization and extension. The finding that LNs start fusing and leaving the regular scaffold while PRs are stably extending only strengthens the conviction that growth cone extension during superposition sorting is a target-independent mechanism. Around P36, photoreceptors start retracting, or displaying other false movements (towards other targets, or at least in other directions) when their correct target is absent or displaced. In some cases, their extension in an alternative direction matches them with their correct LN target. In other cases, this leads to photoreceptor mis-wiring (discussed in Chapter 5). Nevertheless, the early independent photoreceptor dynamics are a novel finding.

In an algorithmic program, where steps follow each other up and the output of one step is the input for the next, early patterning defects and altered cell arrangements can ultimately result in chaos and misalignment of an entire structure. I found disorganization in early developmental processes and patterns that may have been caused by the chaos in bundle rotation and adhesion defects in bundles.

The photoreceptor scaffold in early development would be an ideal algorithmic step since it creates order and does not allow for much developmental noise to be carried over to subsequent developmental steps.

The target-independent mechanism is likely guided by filopodia on the growth cone itself that has interactions with other heels in the scaffold. The live-imaging data presented here shows a dense network of filopodia amongst photoreceptor growth cones. Axonal growth cone filopodia have been shown in many instances to be able to serve as a site of organization of motility for the elongating axon. Moreover, their dynamic extensions and retractions are able to sample their environment and provide feedback to the axon. PR heels provide stable anchoring points to the axon, and additionally may also function as a guide post for extending growth cones. I propose an axon sorting mechanism in which filopodia provide stabilization of the growth cone in a developing environment. Figure 6.4 C provides a schematic model. During the extension phase, growth cones extend in a target-independent way in a sub type specific direction, as described by (Langen et al., 2015). Their filopodia interact with other growth cones, mainly with stable heels, gives the growth cone feedback about its extension length and angle and allows for slight adjustments of the growth cone extension angle when this deviates. After a certain time, indicated by an unknown signal, photoreceptors are able to sense the presence of Ncad. A target-dependent phase of stabilization starts between P35-P38. The presence of LNs close to the heel position coincides with the presence of the main bulk of growth cone filopodia that provide stabilization at the target (see Figure 6.4 C top panel). In the absence of LNs (or the absence of Ncad in LNs), the growth cone will not adhere to LNs. There are three possible outcomes. 1) The main bulk of filopodia extend a little further so that the growth cone can adhere to a Ncad positive heel structure. 2) Filopodia are unable to stabilize the growth cone and it retracts back to its own heel structure and stabilizes there. 3) In the absence of the correct target, filopodia dynamically sense the presence of an alternative target, after which the growth cone turns and stabilizes at the incorrect target.

It has been shown that single filopodia that contact a target cell can redirect the entire growth cone and extend the axon in an alternative direction. In vivo, *Xenopus* retinal ganglion cells were shown to exhibit growth cone turning based on a single filopodium (Chien et al., 1993). Moreover, grasshopper Ti neurons extend filopodia in all directions at specific 'choice points' and one filopodium touching a guidepost neuron was shown sufficient to stabilize in this direction and dilate the filopodium to form the new growth cone. The original growth cone and filopodia along the shaft disappeared and growth continued in the newly chosen direction (O'Connor et al., 1990). Similarly, wild-type RP2 motor neurons in intact *Drosophila*

embryos were shown to extend single filopodia that underwent dilation upon touching an unknown target (Murray et al., 1998). These examples show that it is possible for growth cones to redirect their extension angles based on the sensing input of single filopodia.

Note that only one photoreceptor sub type is imaged in the R4 live-imaging experiment and that interactions between other photoreceptors cannot be observed. Schwabe et al. (2013) determined with sparse photoreceptor labeling that R4 growth cones contact both R3 and R5 growth cones from the same ommatidium, as well as R1, R2, and R6 growth cones from neighboring ommatidia. In addition, I determined that an R4 growth cone also contacts the heel of the next neigboring R4. Thus, there are many filopodial contact points that could influence photoreceptor outgrowth, correction, and stabilization. If indeed a feedback mechanism among axonal filopodia exist, this has the ability to make photoreceptor extension angles more robust. Correction of slight alterations in the outgrowth direction of photoreceptors would increase robustness of the system without a complicating targeting mechanism.

Prakash et al. (2005) raised the question why photoreceptors can leave their initial arrival point (which is next to a N-cad positive LN cluster), when PRs need Ncad to adhere to a target. One possibility is that N-cad adhesion is temporally regulated by post-translational modifications. In this case, Ncad in PRs, LNs, or both, could be inactive during a long period of time. After PR axons have extended, adhesion could increase, stabilizing the projections. Such temporal regulation could be at the level of post-translational changes in Ncad itself. This has been described to be the case for vertebrate Ncad (Tanaka et al., 2000). Another possibility is that temporal control of adhesion by Ncad is regulated by molecules that couple Ncad to the cell membrane. This mechanism has been described for E-cadherin (Hogan et al., 2004). Such temporal regulation would explain why PRs can leave their initial arrival points and additionally explains how PRs could make transient connections with LNs during extension without "choosing" them as a target. In summary: PR growth cone extend independently from LNs or Ncad presence until P38. At that point, when Ncad adhesion is activated, their main bulk is located at the heart of the correct target LN cluster. Thus, most overlap of growth cone with target after P38 determines the correct partner. This would mean that neural superposition sorting is not regulated by a very difficult developmental program; adhesion might just be regulated in time (adhesion is possible after P35) and space (main bulk of the growth cone is at that time located at the target location).

Chapter 7

Discussion

In the previous chapters, I have considered a number of scientific research questions related to bundle organization, scaffold formation, and the requirements for robust photoreceptor extensions during neural superposition sorting. Here, conclusions are combined and summarized to gain an overall overview of the current state. Furthermore, open questions are discussed in the light of recent and relevant literature.

7.1 The basic understanding of bundle organization

The organization of the fly visual system has been researched for a long time, but predominantly at the adult stage (Horridge and Meinertzhagen, 1970; Kirschfeld and Franceschini, 1968; Meinertzhagen and O'Neil, 1991). The 180 degree rotation of bundles between the retina and lamina was first described by Hardie (1983) in the house fly (*Musca* domestica). In this publication, bundles with axons from one ommatidium are referred to as "pseudo-cartridges" and are traced from the cell bodies in the eye to the adult cartridges in the lamina. Drawings of superimposed electron microscopy (EM) sections beautifully show that axons from one bundle spread out in the opposite direction and connect to six different cartridges (Hardie, 1983), thereby following the principle of neural superposition sorting that was published several years before (Braitenberg, 1967; Kirschfeld and Franceschini, 1968). Only recently, evidence was provided that shows the bundle organization between eye and retina during development (Chang et al., 2018). This publication supports my findings that neighboring ommatidia project as neighboring heel structures in the lamina, and that neighboring PRs in a bundle keep their relative position within the bundle, e.g. both inter-bundle

organization as well as intra-bundle organization are a representation of the inter- and intra-ommatidial position, respectively (see Chapter 2).

It is unknown how the 180 degree rotation of a photoreceptor bundle is orchestrated between the retina and lamina. I discovered that the bundle rotation is disturbed in the Sdk mutant. Hence, Sdk may be involved in the process of bundle rotation, yet the underlying mechanism remains unknown. Moreover, the heel positions in the scaffold are affected by this rotation defect, which is not caused by a orientation defect of ommatidia in the eye. Naturally, the analysis of orientation of bundles from fixed data does not tell how rotation happens during development, or where it originates from. Currently, there is no technique to observe bundle rotation with live-imaging due to technical constraints. Drivers are not active right after photoreceptor differentiation and live imaging during this early stage of development is made virtually impossible due to rotation of internal structures in the optic lobe (Langen et al., 2015).

To really understand the underlying principles of brain wiring, it is necessary to investigate what the requirements for bundle rotation during descent are, and how bundles obtain the correct orientation to form a perfect pattern of heel crescents at the lamina plexus. Solid knowledge on bundle rotation will contribute to discovering all underlying mechanisms of brain wiring. Furthermore, it is interesting to investigate how the orientation of crescents is managed in relation to the equator (mirror symmetry). It has been described that cartridges around the equator receive a higher number of axons (Horridge and Meinertzhagen, 1970; Meinertzhagen, 1972) because R3 and R4 axons extend in a mirror-symmetric manner towards the equator and innervation overlaps at equator cartridges (Langen et al., 2015), but what initiates the orientation of crescents in this way is unknown.

The analysis of heel crescent orientation at the lamina plexus in combination with the upwards following of photoreceptor bundles at P20, analysis as presented in Chapter 3, could provide a means of quantifying bundle rotation and identifying bundle orientation defects that occur earlier during development. Using this analysis, one can screen for mutants or protein knock-down experiments in PRs that result in bundle orientation defects. If bundle rotation is not a cell-autonomous process, other cell-types could also play a role. To a certain degree, it can be excluded that lamina neuron cell bodies play a role in this process. One reason is that LPCs only start differentiation and columns formation during the descent of photoreceptors (at least the pioneer axon) (Fernandes et al., 2017). Furthermore, the SmoRNAi experiment, in which LPCs do not differentiate and LNs do not form columns in between bundles, shows that bundle orientation is not affected and photoreceptors are capable to form a perfectly

organized scaffold in their absence. Other cell types, like wrapping glia, or internal forces during axon extension, or intra-bundle adhesion are interesting candidates to investigate.

Hein et al. (2013) describe a mutant that resembles the Sdk mutant investigated in this thesis and described by Astigarraga et al. (2018). There are multiple similarities between Sdk and Golden goal (Gogo) mutant phenotype. Gogo is reported to influence bundle spacing in the lamina and therefore influences scaffold formation, similar to Sdk (see Section 3.3). Moreover, the Gogo mutant affects extension angles only indirectly as a consequence of the disordered scaffold. Furthermore, single Gogo mutant photoreceptors do not mis-wire but arrive at the correct target location (Hein et al., 2013). The latter two phenotypes are reported for the Sdk mutant by Astigarraga et al. (2018), and normal extensions of single Sdk mutants in Section 3.6. Thus, it is worthwhile to investigate the similarities and differences between Sdk and Gogo. A comparative study at the lamina would increase our understanding of their (overlapping) function on intra-bundle and inter-bundle organization and subsequent scaffold formation.

Another Sdk mutant phenotype is defective bundle adhesion which affects adhesion of some, but not all photoreceptors in a bundle. This is very likely to affect the intra-bundle organization. Sdk likely plays a redundant role in bundle adhesion. Other proteins, like Armadillo and Flamingo, may be candidates for complementary roles. Double, or triple mutants, or the simultaneous expression of RNAi by a photoreceptor-specific driver (GMR-Gal4 or mδ05-Gal4 for R4 only) are suitable experiments to uncover their roles in bundle adhesion and rotation.

7.2 Scaffold formation models

My results support a model in which scaffold formation does not rely on the presence of lamina neurons in the lamina. In the absence of LNs, induced by the expression of SmoRNAi in LNs (see Chapter 4), photoreceptors target correctly to the lamina and set up a scaffold. This resembles results from Poeck et al. (2001), who show that only glia are responsible for initial photoreceptor targeting. Yet, how the scaffold is formed out of arriving PRs, and how they set up their regular pattern remains largely unknown.

It has been shown during *Drosophila* embryonic development that differential adhesion by Sdk, that localizes at cell-cell contact sites, can drive patterning during epithelial morphogenesis (Finegan et al., 2020). Furthermore, differential adhesion as a patterning principle has been shown for photoreceptor columns at both the lamina (Schwabe et al., 2013) and medulla (Trush et al., 2019), but this involves adult cartridges and not the scaffold at the

LP. Planar cell polarity would have been a possible explanation for the patterning of the scaffold. Cells can create a pattern in a polarized structure using PCP signaling in multiple tissues (Davey et al., 2016; Jenny, 2017). However, other than Flamingo and Sidekick, no interaction partners from the PCP pathway are localized at the lamina plexus during scaffolding (see Section 2.3). Thus, although PCP signaling pathway components are present at the LP during scaffold formation, their function is not related to the classical PCP pathway.

Based on my results that show that the organization of the scaffold can be build independent of LNs, PRs should have a self-organization mechanism that organizes heel structures in a patterned way. Currently, there is no model for how the lamina scaffold develops in a self-organizing way. Cell-adhesion molecules may contribute to building the scaffold and to the stability of the structure. Loss of Sdk influenced both these factors: orientation and organization of bundles in the scaffold is affected, thus the intra-bundle organization in the scaffold is affected, (see Sections 3.3 and 3.4) and LN cell bodies can fall through the lamina, thus inter-bundle adhesion is affected (Astigarraga et al., 2018). Similarly, Fmi is thought to aid scaffold organization. Especially because R2 and R5 are the first pair of outer photoreceptors to differentiate, and Fmi expression in the LP is primarily found at these two photoreceptors. If indeed photoreceptors descent to the LP in pairs, these are the first ones to stabilize at the LP and initiate the pattern. This could follow a similar gradient of morphogenesis as the patterning of the eye during differentiation. Figure 7.1 A shows this transition in the eye imaginal disc. It follows a wave initiated by the morphogenetic furrow that moves over the eye (Wolff and Ready, 1991). During this event, the sequential recruitment of ommatidial cells, controlled by the short-range ligands, alters the epithelial sheet into a perfectly patterned structure (Roignant and Treisman, 2009). Figure 7.1 B shows a hypothesized model of photoreceptor arrival at the LP and the progressive stabilization of heels at the LP during the formation of the scaffold. The progressive addition of more photoreceptors and the expansion of LN neurites in the LP makes that photoreceptor heels occupy more space over time until all six photoreceptors have stabilized their heels and LNs occupy their center. This transition shows resemblance with the morphological transition in the eye imaginal disc as presented by Wolff and Ready (1991). In the hypothesized scaffold formation model, the removal of LNs would decrease the space that heel structures occupy, but LNs are otherwise not required for scaffolding since the patterning of the scaffold is initiated and maintained by the stabilization of photoreceptor heels.

Moreover, the schematic representation of the epithelial organization of the developing eye (see Figure 7.1 A, top panel) from Wolff and Ready (1991) could reveal where the curvature of the lamina plexus originates from. The LP is broader at the anterior side and curves to the

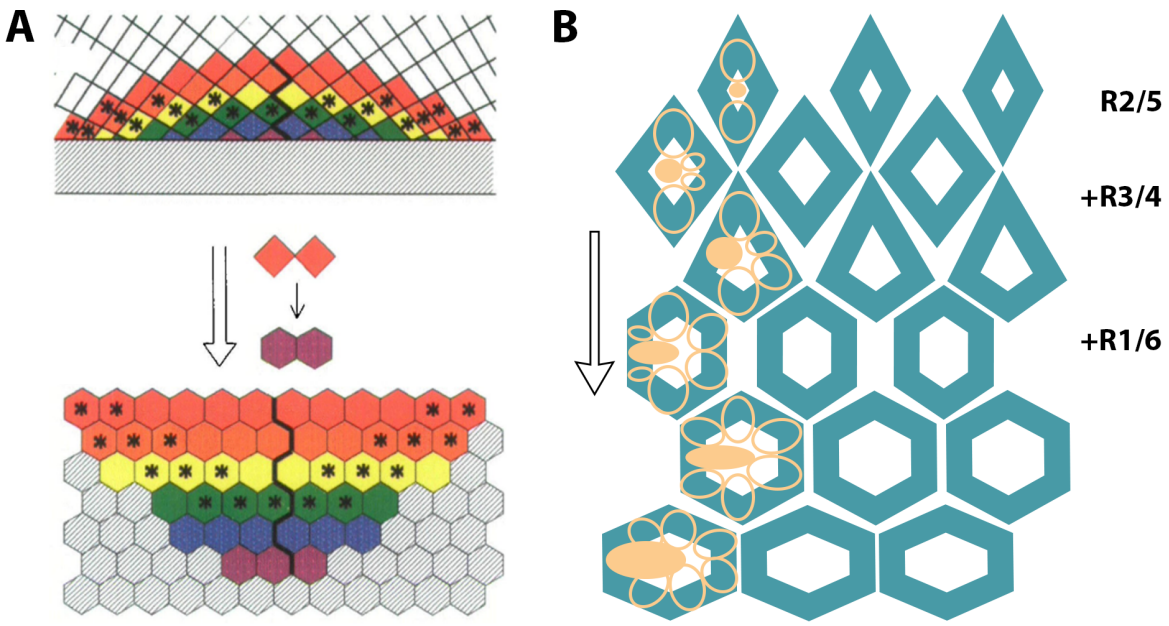

FIGURE 7.1: Models for pattern transitions in the eye and lamina

A) Pattern transition in the eye follows the morphogenetic furrow (grey bar). This schematic summary of lead sulfide observations in the furrow and mitotic labeling results shows six rows immediately behind the furrow (top). Each row is a different color. Purple is the first developing row, red the sixth. Bottom represents ommatidial arrangement in the adult eye. Asterisks indicate mitotically active cells (top) or labeled with lead sulfide (bottom). Bold line is the equator. Panel adapted from Wolff and Ready (1991). **B**) Graphical representation of progressive heel stabilization during scaffold formation. The arrival of photoreceptor axons in to the lamina plexus in pairs. Blue shapes represent a schematic representation of the transition of space occupation from 2 to 6 photoreceptors and LNs in a regular scaffold. This schematic representation of lamina development shows a resemblance to the pattern transition in the eye during development.

posterior side (Langen et al., 2015). This might seem counter-intuitive since the incoming bundles and LN neurites occupy less space at the anterior side. The oval shape of the eye would actually explain how fewer axons descent to the lamina at the posterior side and increasingly more towards the middle of the eye, after which it again decreases towards the most anterior side of the eye. If neighboring bundles actually stabilize as indicated in Figure 7.1 (top panel), this may explain the curvature of the lamina plexus during development.

7.3 Patterns and patterned proteins to aid development

Scaffold formation at the lamina plexus is a crucial step in the formation of a functional visual system (Clandinin and Zipursky, 2000; Langen et al., 2015). It is a pre-patterning step that ensures a capable environment for subsequent photoreceptor extension in the developmental program of neural superposition sorting. In this sense, patterning can be viewed as a strategy to aid developmental processes.

There are many patterns described that aid developmental processes in a multitude of ways. For instance, the striped expression pattern of Even-skipped (Eve) at the *Drosophila* embryo that prepares the segmentation of the body. The expression of two opposing gradients of transcription repressors lead to differential repressing of two enhancers of the pair-rule gene Eve in the *Drosophila* embryo. The alternating expression pattern of these two enhances leads to the precise positioning of eight stripe borders (four stripes) without specifying their precise position (Clyde et al., 2003). Thus, expression gradients can create a seemingly complex pattern in the embryo through the simple expression of two proteins. This was predicted in a theory of pattern formation (Gierer and Meinhardt, 1972), and illustrates that the use of patterns in biology can create the means of developing more complex structures by using simple construction rules.

There have been multiple mechanisms described that aid neuronal wiring that are target-independent (Agi et al., 2020), which would qualify as "simple rules". They share a principle that pre-specifies the location of axons and dendrites in a non-deterministic way so that subsequent synapse formation can be a permissive mechanism. Among them, birth-order dependent axon extension (Kulkarni et al., 2016), where timing ensures synaptic connectivity; self-avoidance, which enforces spreading of neurites without specific rules on the morphological outcome (Hattori et al., 2007; Matthews et al., 2007); and axonal and dendritic tiling, which prevent overlap between neighboring axonal branches or dentritic trees, respectively (Millard and Zipursky, 2008; Millard et al., 2007). Neuronal tiling can be viewed as a patterning mechanism that creates spacing between neurons. Both self-avoidance and neuron tiling are developmental mechanisms that work without the need for guidance cues to direct neurites to their correct location or for complex genetic programs to create correct neuron morphology. In this way, self-avoidance and tiling are examples of "simple rules to wire a brain", as advocated by Hassan and Hiesinger (2015) and Petrovic and Schmucker (2015).

It is likely that similar developmental rules apply to pattern formation in the lamina plexus, although the underlying principles remain to be elucidated. Bundle spacing, is an example of a "simple" rule that fulfills an important role in scaffold patterning. Hein et al. (2013) show that bundle spacing in the Golden goal (Gogo) mutant can be rescued with the expression of Gogo in R8 specifically. Furthermore, results from the Sdk mutant analysis show that correct orientation of a bundle upon arrival is an essential input for a stereotypic patterning of heel crescents in the lamina (see Section 3.3). Thus Sdk and Gogo seem to be important players in the creation of the scaffold without precise guidance instructions for the lay-out of the structure. The presence of adhesion molecules Skd, Arm, and Ecad, may aid intra-bundle organization in the heel crescents at the LP and stabilize the scaffold. Ablation of all LNs

leaves the distinct pattern of dots between R1-R6 heels intact, revealing that, Ecad, Arm, and Sdk are localized in between photoreceptor growth cone heels and act independently from LN presence. The heterophilic interaction between Ecad and Ncad at adherens junctions was described by (Straub et al., 2011). Moreover, photoreceptors express low levels of Ncad at certain stages of development (Prakash et al., 2005). Thus, it is not unlikely that the PCP components and adhesion molecules detected at the lamina plexus, interact with Ncad to form a special kind of adherens junctions, similar to the ones described by Zou (2020) for growth cones. Additionally, Flamingo may regulate the stability of the scaffold via adhesion between heel crescents. Its localization, primarily on the surface of R2 and R5, would make it a perfect candidate for adhesiveness between heel structures, e.g. inter-bundle or inter-crescent adhesion. In these ways, patterned proteins in the lamina can aid stability of the scaffold, thereby providing a canvas for subsequent neural network assembly.

7.4 The requirement of LNs during development

Post-synaptic cells are often considered indispensable for the attraction of the pre-synaptic cells and for target recognition in developing neuronal structures. They are either believed to express certain guidance molecules, or exhibit membrane dynamics that should be recognized by the pre-synaptic cell to extend in the axon in a correct direction and adhere to the correct partner (Melnattur and Lee, 2011; Tessier-Lavigne and Goodman, 1996). However, in an environment where many identical post-synaptic targets are tightly packed together, it is unlikely that guidance by post-synaptic cells is a wiring mechanism that can direct axons to the correct target.

The findings presented in this thesis suggest a circuit-assembly process in which pre- and post-synaptic neurons engage in separate developmental programs (up to a certain point in development). PRs exhibit target-independent properties for correct extension angles and provide feedback to correct for variability in the sorting environment (see Chapter 5). This independent sorting program ensures robustness: independent of the behavior or state of the post-synaptic partner, neurites of pre-synaptic partners are sorted together to the correct location, thereby preventing mis-guidance by intermediate targets. Only very late in the developmental program PRs need stabilization at the post-synaptic partners to make appropriate synapses. Adhesion to the target is likely managed through the adhesion molecule Ncad (see Section 5.6).

The findings presented in Chapter 6, suggest a feedback mechanism among photoreceptor filopodia to steady the outgrowth direction of photoreceptors. Upon extension of the growth cone, filopodia may sense the environment and therefore the presence of other growth cones, which could aid the stable extension of growth cones and correction for slight deviations. This would enable a robust wiring mechanism. Filopodial interactions between photoreceptors were also described by Schwabe et al. (2013), who show that growth cones extensively touch one another with filopodia during the extension phase. They express both Ncad and Flamingo on the growth cone, which both contribute to wiring precision in a redundant way.

Following the conclusion that photoreceptors and LNs display independent behaviors during the extension phase of neural superposition sorting, this should naturally extend to the independence of any molecule presented by LNs. Ncad is one of these molecules present on LNs during the extension phase. Ncad was previously described to be necessary for R8 axon targeting to the medulla (Yonekura et al., 2007). However, verification of these results through live-imaging revealed that adhesion to the correct layer was affected, but not initial targeting (Özel et al., 2015). This is similar to the results presented in this thesis. While Ncad was previously described to be necessary for correct targeting to lamina cartridges by Prakash et al. (2005); Schwabe et al. (2013, 2014), results now show that not targeting, but stabilization at the target location is affected (see Section 5.6).

At the end of the sorting phase, LNs improve correct adherence through probabilistic stabilization of PR growth cones but are not necessary for PRs to stop extending. This finding is in line with predictions from the computational model of Langen et al. (2015). Based on the described localization of Ncad at LNs (Lee et al., 2001; Nern et al., 2008), it was hypothesized that Ncad would be absent from cartridges without LNs. Surprisingly, this is not the case, as the combined low expression of Ncad on PR axons creates a "pool" of Ncad at the target location in the absence of LNs (see Figure 5.6). This shows to be sufficient for photoreceptor adhesion in approximately 50% of cases. Hence, this stabilization function of Ncad does not require active LNs, but simply N-cadherin-mediated adhesion. At this late stage, when LNs are (sparsely) ablated from the lamina, photoreceptors that cannot stabilize at their correct target either retract back or mis-target. The stochastic adhesion events of photoreceptors that cannot adhere to their appropriate target illustrate the dynamics that underlie the robustness of neural superposition sorting. The fact that not all photoreceptors retract underlines that photoreceptor wiring is based on adhesion possibility, instead of on target recognition.

7.5 Neural superposition sorting models

The majority of current models of axon extension within the central nervous system (CNS) is based on a principle of axon guidance and chemo-affinity as described in the chemo-affinity hypothesis by Sperry (Sperry, 1963). In short, a surrounding tissue or target tissue presents a set of guidance molecules or environmental cues that either restrict or promote axon growth, thereby providing guidance instructions to developing axons. Tessier-Lavigne and Goodman (1996) propose four axon guidance mechanisms that are related to the Sperry chemo-affinity hypothesis; chemo-repulsion, chemo-attraction, contact-repulsion, and contact-attraction, for either long- or short-range guidance. These all imply that the environment guides extending axons in the correct direction.

For neural superposition sorting, results described in this thesis suggest an axon extension model that is independent of target cells. It resembles predictions based on the computer simulation of Langen et al. (2015). They consider neural superposition sorting as a developmental algorithm, where the output of one step is the input for the next. They suggest that if photoreceptors move through a stereotypical environment, synaptic partners can be sorted together independent of target cell recognition. The developmental algorithm as proposed by Langen et al. (2015) relies on distinct phases; scaffolding, extension, and stop phase.

In accordance with the model presented by Langen et al. (2015), I propose a model (see Figure 7.2) in which axon sorting follows distinct developmental phases. Scaffolding, extension, and stabilization. Both the scaffolding and the extension phase are completely independent from input from the post-synaptic target. Moreover, the axon extension period lasts only until P35, after which target-dependent stabilization sets in. After LN-dependent stabilization of the growth cone, extension of the axon proceeds in the Z-axis where LNs and PRs form elongated cartridges and synaptogenesis finalizes circuit wiring. While mistakes in early developmental steps can introduce developmental noise that can carry over to subsequent developmental steps, pattern-encoded steps (like the formation of the scaffold) and a regulatory feedback mechanism (like feedback among photoreceptors) ensure reduction of developmental noise, thereby contributing to robust neuronal wiring.

Although my results show that the photoreceptor growth cones can extend independent of post-synaptic cells and the signals derived from them, it remains to be established how photoreceptors determine their extension angle and where this directional information comes from. It has been suggested that multiple proteins influence synaptic partner choice in the lamina. Flamingo expression has been linked to mis-wiring phenotypes in knock-down experiments in both the lamina and the medulla (Chen and Clandinin, 2008; Lee et al., 2003). Its

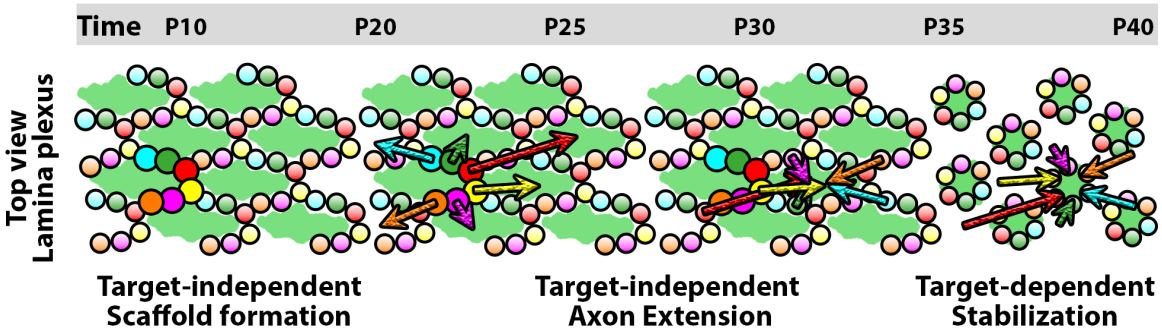

FIGURE 7.2: Proposed model for neural superposition sorting

Neural superposition sorting as a developmental program that progresses over time. Based on the algorithm-like model of Langen et al. (2015). Scaffold formation is followed by target-independent axon extension, axon arrival, and target-dependent growth cone stabilization. Brightly colored circles represent axon heels in one crescent (from one ommatidium/bundle). Colored arrows represent individual growth cones of photoreceptor sub types. Different colors indicate photoreceptor sub type (blue R1; green R2; red R3; yellow R4; purple R5; orange R6).

localization at photoreceptors in the lamina has been suggested to be involved in the spread of PRs during photoreceptor sorting (Schwabe et al., 2013). This role of projecting in an angle to avoid other photoreceptor heels resembles a role of self-avoidance that was found for Fmi in dendrites (Matsubara et al., 2011). However, photoreceptors do not obtain maximal-projection angles, so that self-avoidance does not explain polarization completely. Recently, a study based on R3 and R4 projections in the lamina plexus has suggested that cell identity is instrumental in determining extension speed and therefor correct targeting (Ji et al., 2021). Irrespective of the source of these initial instructions, the conclusions drawn from all experiments in this thesis point towards an axon path-finding mechanism with cell-intrinsic guidance that takes place without the involvement of other environmental cues. Eventually, it all comes down to what makes seemingly identical photoreceptors different from each other, and how these differences integrate their function in a certain position in the scaffold.

7.6 Target-independent wiring and robustness of development

In a hard-wired system, such as the *Drosohila* visual map, an obvious assumption is that pre- and post-synaptic partners are pre-specified as in a key-and-lock system. However, being hard-wired (little variability between individuals) is different from being created through a deterministic process. Noisy developmental processes can coincide with robust wiring (Hiesinger and Hassan, 2018). This thesis provides evidence that the formation of the visual map is not a deterministic process, but rather relies on a target-independent mechanisms in a developmental program.

Investigating if pre-synaptic cells are able to organize themselves can only be done in an environment without post-synaptic cells. Through live-imaging it is discovered that initial photoreceptor extension is independent of the presence of LNs (see Figure 4.4), and independent of abnormalities in the scaffold (see Figure 5.4). The sparse ablation of LNs results in fusions of remaining LNs in the scaffold. Fusion of LNs results in a disrupted structure of the adult lamina; something that is often regarded as proof of the necessity of molecules or cells during development. However, fusions start early and do not disrupt the structure of the scaffold at that point in development. Moreover, it does not coincide with PR wiring defects (see Figures 4.4, 5.4, and 6.1). Fusions are observed at P28, while defects in photoreceptor extension are detected earliest at P36. Thus, these late-arising PR wiring defects seem unrelated to LN behavior and are not correlated to areas of LN disruption, suggesting independent developmental networks of LNs and PRs.

Independent from LNs, photoreceptors can adjust their extension angle to correct for any disturbance in the scaffold (bundle orientation). A surprising finding is the correlation between R4 extension angle and bundle orientation in the control experiments for both Hid OE and SmoRNAi (see Figure 5.3. This implies that variability in the scaffold is a naturally occurring event and abnormalities can be corrected before defects arise. These target-independent mechanisms make neural superposition sorting more robust against developmental noise. From the results presented in this thesis, it is suggested that growth cone filopodia interact with other axons to establish stability of extension angles (see Figure 6.4) and can create feedback for alterations in initial polarization (see Section 5.3). A great focus for future research are filopodial dynamics during neural superposition sorting. The small protrusions on the photoreceptor growth cone may play a big role in photoreceptor extension and stabilization.

The realization that alternative wiring principles exist became more prevalent in recent years. An example is the formation of synapses on motorneurons in the *Xenopus* spinal cord. It was shown that the number of synaptic connections received from pre-motor inter-neurons is conditioned by the positioning of motor neuron dendrites (Sternberg and Wyart, 2015). Another example is presented by Kiral et al. (2020), who show that synaptic partner choice can be regulated by membrane dynamics and relative partner availability during development, instead of through a wiring code. Hence, the synapse formation program seems a more permissive mechanism that allows neurons to form synapses with the partner with whom they make most membrane contact. This resembles the situation of photoreceptor growth cone stabilization at the LP where PRs seem to terminate at the target with which they overlap most. When axon sorting has happened properly, this is automatically the correct partner. This suggests a more basic wiring mechanism of "most overlap", than a deterministic approach.

If, for any reason, axons and dendrites of "wrong" partners overlap, neurons make synapses with these wrong partners (Edwards and Meinertzhagen, 2009; Hiesinger et al., 2006). This resembles Peter's Rule, which predicts synapse formation among neuron types (or individual neurons) that anatomically overlap their axonal and dendritic arbors (Rees et al., 2017).

Photoreceptor wiring defects (wrong number of PR terminals in cartridges) are observed in experiments where LNs are completely, or partially, removed from the LP. Defects arise late (after correct targeting) and 20-50 percent of cartridges is affected, depending on the experiment (see Figure 4.4 and 5.4). At the final stage of wiring, even though PRs can stabilize in target areas with varying numbers of LNs, there seems to be a trend of LNs improving correct PR adherence through stabilization. It would be very interesting to investigate if photoreceptors in cartridges without LNs form synapses, and with whom. An anti-Brp staining (visualizes synaptic protein Bruchpilot at active zones) could provide an easy answer to the question if there are synapses or not. To determine who are the partners is more elaborate. A methods for the labeling of synapses called GFP Reconstitution Across Synaptic Partners (GRASP)(Feinberg et al., 2008), would not suffice to provide solid information on synaptic partners since it cannot detect synapses between photoreceptors and unknown partners, nor can it detect autapses (synapses with itself). The technique called Trans-Tango (Taley et al., 2017), does allow for the identification of unknown synaptic partners. Yet, it labels partners sparsely, which could hide possible partners from view. Hence, the most reliable method to investigate synapse formation in LN-deprived cartridges would be serial EM.

7.7 Concluding remarks and directions for future research

The general aim of this thesis was to describe the molecular and cellular mechanisms underlying neural superposition sorting in *Drosohila*. This was divided into two sub-goals. The first was to uncover the role of pattern formation, and proteins that enable pattern formation, during scaffold formation. The investigation of the bundle organization in WT and in the Sdk mutant reveal that both the intra- and inter-bundle organization are important during the formation of the scaffold at the LP. The current understanding is that disruption of the scaffold during early developmental steps causes defects in axon extension and incorrect wiring. The second goal was to uncover the developmental contribution of post-synaptic target cells (LNs) during neural superposition sorting. Their organization in the early steps of scaffold formation and filopodial dynamics during the photoreceptor extension phase raised questions about their role during brain wiring. Results show that PRs and LNs run their developmental programs independently from each other. R4 extension angles, taken as exemplary for all PR

axons, are fairly stable in the first half of the extension phase. In contrast to the cell-intrinsic alteration in Sdk levels that alters bundle orientations and R4 outgrowth angles, the presence or absence of LNs has remarkably little effect on the polarization angle of the growth cone. In late stages of the extension phase, LNs are required for growth cone stabilization through expression of the adhesion molecule Ncad.

In summary, as suggested by Langen et al. (2015) and Hassan and Hiesinger (2015), the formation of the *Drosophila* visual map is likely regulated by a developmental program containing "simple rules". Subsequent rules may look like this: 1) The intra-bundle and inter-bundle organization are maintained between the retina and the lamina. Correct bundle organization ensures the correct input for the next developmental step. 2) Bundles stabilize photoreceptor heels in a pattern oriented towards the equator. Adhesion molecules stabilize the axonal heels within a crescent, and stabilize the scaffold with adhesion between crescents. The correct pattern of heels in the scaffold may be a relying heavily on the correct placement (bundle rotation and neighbor-to-neighbor localization, e.g. inter-bundle organization) and order (R1-R6 as neighbors within a bundle, e.g. intra-bundle organization) of incoming PR bundles and LN neurites. The formed scaffold creates a stereotypical environment, and the context for subsequent developmental steps. 3) Extension of photoreceptor growth cones while maintaining correct angles and controlling extension length via a feedback mechanism among photoreceptor growth cones. Correction of extension angles from a slightly variable scaffold ensures robust developmental outcomes. 4) Ncad-mediated adhesion of the growth cone to the target. This step can be a permissive mechanism to match axons and dendrites that overlap most. 5) Synapse formation between synaptic partners. This can be a permissive mechanism to connect axons and dendrites that overlap most. The developmental steps described above would function with instructive mechanisms (rotate bundle to particular orientation) combined with permissive mechanisms (stabilization and synapse formation between partners that overlap most) in a combined program of instructions. Although neuronal circuits often appear complex, the genetic program and developmental algorithms to build them do not have to be complex by themselves. Pattern-formation steps and feedback mechanism during development underlie robustness in neural wiring. This is why pattern formation makes an excellent neuronal wiring strategy during development of the *Drosophila* visual system. While the underlying molecular mechanisms in these developmental steps are not elucidated, progress has been made in understanding which proteins and processes are involved during distinct steps. Further research is needed to investigate the requirement and necessity of adhesion proteins, filopodial dynamics and other underlying mechanisms of target-independent processes during neural superposition sorting.

Chapter 8

Materials and Methods

8.1 Fly Genetics

Chapter 2:

MultiColor FlpOut labeling: MCFO-1 (Nern et al., 2015). pBPhsFlp2::PEST in attP3;; HA_V5_FLAG/ longGMR-Gal4.

Planar cell polarity components screen (gifts from Gary Struhl; Columbia University): +; UAS-CD4::tdGFP; Fz::GFP , +; UAS-CD4::tdGFP/Cyo; Fz-2::GFP , w; Pk::GFP/UAS-CD4::tdGFP; .

WT analysis: yw^{122}; ; .

To label all photoreceptors: +; GMR-Gal; UAS-CD4::tdGFP; .

Chapter 3:

Sidekick mutant analysis (gifts from Jessica Treisman; NYU School of Medicine): FRT19A, $Sdk^{\Delta 15}$; ; .

Sdk single clones: FRT19A, Tub-Gal80, HsFlp/FRT19A, $Sdk^{\Delta 15}$; ; longGMR-Gal4/UAS-CD4::tdGFP.

R1 and R6 clones: FRT19A, Tub-Gal80, HsFlp/FRT19A, GMRFlp, $Sdk^{\Delta 15}$; ; longGMR-Gal4/UAS-CD4::tdGFP.

Chapter 4:

$Shibire^{ts}$ experiments: eyGal80/+ or Y; UAS-CD4::tdGFP/+; 9B08-Gal4/UAS-$Shibire^{ts}$,

+; +/Cyo; UAS-Shibire^{ts} , ; mδ05::tdTomato/Cyo; 9B08-Gal4/UAS-Shibire^{ts} , and ; mδ05-Gal4/+; UAS-Shibire^{ts} .

Block LN differentiation: NP6099-Gal4/+; UAS-SmoRNAi/UAS-CD4::tdTom; and NP6099-Gal4/+; UAS-SmoRNAi/UAS-CD4::tdTom; mδ05::GFP, UAS-CD4::tdTom/+

Chapter 5:
LN ablation experiments: UAS-Hid/Y; UAS-CD4::tdGFP/+; 9B08-Gal4 and UAS-Hid/Y; mδ05-CD4::tdGFP/+; 9B08-Gal4

LN visualization ; UAS-CD4tdGFP/+; 9B08-GAL4/+

Chapter 6:
Glia visualization: +; UAS-CD4::tdGFP; Repo-Gal4/TM3.

Ncad knock-down experiment in LNs: +; GCM-Gal4/UAS-NcadRNAi; UAS-CD4::tdTom, mδ05::GFP/mδ05::GFP

Ncad knock-down in glia: +; UAS-NcadRNAi/+; Repo-Gal4/+

Filopodia visualization: ; mδ05-Gal4/+; UAS-CD4::tdGFP/ UAS-CD4::tdGFP

8.2 Experimental Conditions

Flies were cultured on standard food and raised at 25°C. Parental flies were kept at 22°C. Experiments were conducted at 25°C except for the following experiments: Hid over-expression, and their respective control experiments were performed at 29°C. Parental flies were kept at room temperature (22°C), but crosses were kept at 29°C at all times. P0 pupae were collected from these crosses and again placed back in 29°C to age them to the correct developmental stage when they were dissected. For experiments in which pupae were heat shocked, P0 pupae were first collected in Eppendorf tubes, lined with moist tissue paper and ventilation holes and placed in heat blocks during heat shock protocols. For the HsFlp and GMRFlp clone experiments pupae were kept at RT before heat shock and at 37°C. After heat shock, tubes were kept on ice for 5 minutes and afterwards transferred to RT again until dissection. For the Shibire^{ts} experiments, Pupae were staged at 25°C and membrane dynamics were blocked at 31°C. Afterwards, pupae were dissected immediately, or kept at RT until adulthood and dissection.

8.3 Dissection and Immunohistochemistry

For larval dissection, L3 larvae were collected from the wall of their experimental vials and transferred to a dissection dish. Pupal dissections were always performed on staged ages and dissected at the appropriate developmental time. Therefore, white pupae (accounting for P0) were collected from the experimental vials and placed in little Eppendorf tubes. An air hole and a little piece of wet tissue paper ensured ventilation and moist. Tubes were either kept at 25°C or 29°C until dissection, depending on the experiment. For adult dissection, experimental vials were kept on ice to anaesthetise the flies, after which they were taken from the vial by the wing and placed in a dissection dish. All dissections were performed with sharp forceps under a stereo microscope in ice cold PBS. Dissected brains were transferred to an Eppendorf tube containing 4% Paraformaldehyde (PFA) and fixated for 30-45 minutes after which they were washed with 0.4% PBST (PBS with 0.4% Triton X-100) at room temperature. After three short washes, tubes were placed on a shaker and gently rocked during 3 consecutive 30-minute wash steps. Two rounds of antibody staining followed. In the first round, brains were incubated with cocktails of primary antibodies and 0.2% NGS at 4°C overnight (antibody cocktails specified at the respective experiment). Afterwards, brains were washed with 0.4% PBST in three short washes, and 3 consecutive 30-minute wash steps. Then, brains were incubated with cocktails of secondary antibodies and 0.2% NGS at 4°C overnight or for 3 hours at room temperature. For the MCFO experiments specifically, a third antibody round was performed to stain V5 labels with a V5-549-conjugated antibody. Washing followed as described above. Finally, brains were washed in one last round of 3 consecutive 30-minute wash steps.

8.4 Antibodies

All primary antibodies are used in a total of 500 μl PBST solution with either 1:20 NGS (normal goat serum) or NDS (normal donkey serum) and 1 μl NaAz to prevent fungal infection. All secondary antibodies are used in PBST solution with 1:20 (5%) NGS or NDS.

Primary antibody	Source	Host	Concentration
anti-Armadillo (N2 7A1)	DSHB	Mouse	1:200
anti-Chaoptin (24B10)	DSHB	Mouse	1:50
anti-DCSP-2 (6D6)	DSHB	Mouse	1:10
anti-dsRed	Abcam	Rabbit	1:200
anti-Ecad	DSHB	Rat	1:100
anti-Ebony	from P.Robin Hiesinger	Rabbit	1:200
anti-Elav (7E8A10)	DSHB	Rat	1:50
anti-Elav (9F8A9)	DSHB	Mouse	1:50
anti-FLAG	NovusBio	Rat	1:200
anti-Flamingo (#74)	DSHB	Mouse	1:50
anti-Frizzled (1C11)	DSHB	Mouse	1:10
anti-Frizzled-2 (1A3G4)	DSHB	Mouse	1:10
anti-GFP	Abcam	Chicken	1:500
anti-HA	BioLegend	Rabbit	1:300
anti-HRP	DSHB	Rabbit	1:100
anti-N-cadherin (DNEx8)	DSHB	Rat	1:50
anti-RFP	Rockland	Rabbit	1:500
anti-Sdk	gift from J.Treisman	Guinea pig	1:200
anti-V5 Epitope Tag Dylight 549 conjugated antibody	Rockland	Rabbit	1:500

Secondary antibody	Source	Host	Concentration
anti-chicken Alexa Fluor 488	Thermo Fisher Scientific	Goat	3:500
anti-guinea pig Cy3	Jackson ImmunoResearch Laboratories	Goat	1:500
anti-mouse 405	Thermo Fisher Scientific	Goat	3:500
anti-mouse Cy3	Jackson ImmunoResearch Laboratories	Goat	1:500
anti-mouse Cy3 (minimal cross-reacting antibody)	Jackson ImmunoResearch Laboratories	Donkey	1:250
anti-mouse Cy5	Jackson ImmunoResearch Laboratories	Goat	1:500
anti-mouse 568	Jackson ImmunoResearch Laboratories	Goat	3:500
anti-mouse 647 (minimal cross-reacting antibody)	Jackson ImmunoResearch Laboratories	Donkey	1:250
anti-rat Cy3 (minimal cross-reacting antibody)	Jackson ImmunoResearch Laboratories	Donkey	1:250
anti-rat Cy5	Jackson ImmunoResearch Laboratories	Goat	1:500
anti-rat 647 (minimal cross-reacting antibody)	Jackson ImmunoResearch Laboratories	Donkey	1:250
anti-rabbit Cy5	Jackson ImmunoResearch Laboratories	Goat	1:500
anti-rabbit Alexa Fluor 488	Thermo Fisher Scientific	Goat	3:500

8.5 Mounting and Microscopy

Fixed specimens were mounted on glass microscopy slides. On a slide, I created two walls of 3-layered sticky tape that created a slot for the *Drosophila* brains. After transferring the brains to the slide with a widened pipette tip excessive PBST was removed with a pipette. Brains were mounted so that the lamina would lay on top of the optic lobe, or as much tilted in that direction as possible. For pupal brains, forceps pushing gently on the side of the optic lobe could manage this. For adult brains, the optic lobes were severed from the brain and mounted with the lamina upwards. A droplet of Vectashield Antifade Mounting Medium was added in which the brains were emerged and they were covered with a cover slip, which was sealed with nail polish. Microscopy slides were imaged right away, or stored at 4°C until imaging. Images were obtained on a Leica SP8 White Laser Confocal Microscope with 20x or 63x objective for high magnification, and HyD detectors for increased resolution and reduced background noise. Typically, data was acquired in frames of 1024x1024 or 1024x512 pixels of a 100x100 or 100x50 μm area and Z-stacks had a step size of 0.5 μm between optical sections.

Live imaging in living and developing pupae (intra-vital imaging) was performed for Hid over-expression experiments, Smoothened-RNAi experiments, and Shibire^{ts} experiments, and their respective controls. Pupae with the correct genotype were collected at P0 and staged at 25°C (or 31°C in case of Shibire^{ts}). In preparation for imaging, the pupal case surrounding the head was removed, exposing both eyes. The pupae was placed sideways on supporting filter paper with its right eye facing up. Pupae were stabilized with more wet strips of filter paper and 4% low melting point agarose (Ultra Pure Low Melting Point Agarose, Invitrogen, Cat. No. 15517-022) to a slightly tilted position. Once the agarose had set, high vacuum grease (Dow Corning Corporation) was applied by a syringe around the sample. A droplet of HL3 was placed between the eye and cover slip that was placed on top (VWR micro cover glass, 22x22 mm, No.1.5, Cat.No. 48366-227). Samples were immediately imaged. For live Shibire^{ts} experiments, a temperature controller (Cube) with a closed chamber (Life Imaging Service) was used to keep the sample at a constant 31°C temperature. All live imaging data was collected with Leica SP8 upright multi-photon microscope which is equipped with HyD detectors.

8.6 Image Analyses

Most of the live and fixed image analyses were performed in Amira 5.6 (FEI Visualization Sciences Group). For the live experiments, the same set of cells in the Region Of Interest

(ROI) were isolated for all time points and a cross section picture was taken by using the oblique slicer tool. Afterwards, all the images were aligned, and all the figures were assembled in Adobe Photoshop CS6. Figures were saves at .tif and .png files. Images for R4 growth cone extensions were visually aligned so that R4 extensions in the ROI were horizontal and extended to the right side of the image (equator right). Armadillo and Sidekick dots were used to draw vertical lines to represent bundle orientation/rotation. Lines were drawn through the center of dots. Spacing between LNs was measured from the center of an Armadillo/Sidekick line. All distances and R4 extension angles were measured with ImageJ (Fiji Is Just ImageJ) from images taken with the oblique slicer tool in Amira. Tracing of R4 heel and front position in time were performed with IMARIS (Oxford Instruments) to obtain position information (coordinates). Surface reconstruction and analysis of the MCFO experimental data was analysed with IMARIS (Oxford Instruments). All numerical data was exported to Microsoft Excel for further processing.

8.7 Statistical Analyses

All numerical data was ordered and summarized in Microsoft Excel. When needed, data was normalized to the mean value of a ROI to obtain values that would be comparable between samples. Subsequently, statistical analyses were preformed using GraphPad (Prism). All data sets were checked for their data distribution (QQ plot for normality and log-normality and Shapiro-Wilk normality test) before subsequent statistical tests. For normally distributed data I used unpaired T-tests to compare means between groups and F-test for testing equal variance between groups. For non-normally distributed data I used Mann-Withney test to compare medians between groups and get an estimated p-value. Exact p-values are given in the results sections. For all statistical tests the significance level α was set to 0.05. In figures, significant differences between groups is indicated by stars in the graph. p-value <0.05 is represented by one star (*), p-value <0.01 by two stars (**) and p-value <0.001 by three stars (***). Non-significant differences are either represented by "ns." or with a lack of stars. Linear regression analysis was performed to discover correlation between data sets. Best fit slope is represented in graphs as a red line. All output graphs were designed in Graphpad Prism and exported as TIF files. All bar graphs and boxplots represent the mean value +/- standard deviation (SD). In some cases individual data points are plotted as circles on top of the bar graph or boxplot to illustrate the data distribution. In other cases, SD is plotted as a horizontal line and outliers are plotted as dots (outliers identified by Tukey test). Which one is the case is always stated in the caption below the figure.

8.8 Text processing

This thesis was written in LaTeX, using the online collaborative cloud-based LaTeX editor Overleaf (WriteLatex Limited). LaTeX script was written by Steve R. Gunn and modified by Sunil Patel.

Contributions by Others

The work presented in this thesis is supported by work preformed by others. In footnotes and figure legends, it is stated clearly when the research was supported with data or analyses that were obtained or performed by others, or in collaboration with other people.

In summary:

- All live-imaging data was obtained by Egemen Agi
- Analysis of live-imaging data was performed in collaboration with Egemen Agi
- Analysis of Hid perturbation experiments was performed in collaboration with Monika Kauer
- Data collection on Flamingo localization and other PCP components was performed in collaboration with Melinda Kehribar
- Summary was translated to German by Juliane Uhlhorn

Acknowledgements

What an achievement. It is with great pride that I hand in this thesis and present my work. I would like to thank everyone that was there for me over the years because I could not have done this alone. The people around me, with whom I worked, my friends, my family, people who helped and supported me; you all deserve credit.

Robin. If life is an algorithm in itself, you provided a pivotal step in it. I want to thank you for all the opportunities that I was offered during my time in your lab. Thank you for taking me in, for your support, attention, suggestions and chances. You always tried to push for the biggest and best possible. I've grown in confidence in your lab, hit rock bottom, and stood up again.

Mathias, it all started with you. Thank you for introducing me to Robin, for the cookies, and for showing me the beauty in neurobiology.

And then there is Egemen (not Amen), who is just always there. You, my friend, are what Tina Turner sang about: "Simply the best". From day one, you helped me in the lab, came with suggestions, helped me out when I didn't know, supported my data with yours. Thank you for your friendship. And also thanks to Monika, who grew from student assistant to an important part of our team and stayed with us for years. Little Monkey, I'm very proud of you for paving your own path to success.

Over the years I've worked in an energizing, tiring, stressful and inspiring environment with so many loving colleagues that became really good friends. The starting crew in Berlin; Jen, Neşet, and Egemen. Thank you for taking me in and being my friends. I'm so happy to have worked with you, learned from you, and had fun with you guys. And then, of course, more colleagues joined and the three labs of Robin, Mathias, and Bassem fused into one big pile of great people. Heike, Doreen, Ridvan, Gizem, Amr, Friederike, Marco, Abhi, Maheva, Suchetana, Juliane, Emil, Jana B., Thomas, Gerit, Isa, Monika, Christopher, Joy, Melinda, Heidi, Büşra, Jana M. and the many bachelor and master students who always come and go. You made work a happier place, and could cheer me up. I will remember hidden ice cream, bbq's in the garden, and drawers full of goodness.

In particular, I want to thank the following people: Egemen, Monika, Christopher, Melinda, and Büşra, thanks for working together on scientific projects. Maheva, thanks for being my bench-buddy. Ridvan, thank you for making me happy with just little nice remarks in the

morning. Marco, Juliane and Monika, for fun outside of the lab either on a beach volleyball field, or during one of our board game evenings.

Of course, one cannot go without support from home. My friends are so important to me. I want to thank Christiaan for pushing me to go to Berlin. I want to thank "de Bioloogjes" (Amanda, Noortje, Emke, Geerke, Maaike, Esther and Rianne) for our continuous friendship over the years. Hamideh, thank you for your friendship, advise, and listening ear when needed. Jana W., thank you for second breakfasts, volleyball evenings and mental support.

I want to say special thanks to my family, from whom I can always count on love and support. Lieve zusjes, Jennifer en Karina, bedankt voor jullie liefde en aandacht en gewoon omdat jullie er zijn. Inge, je bent bijna een derde zusje. Je bent zo goed in luisteren zonder oordeel te vellen. Oma, dankjewel dat ik je mee naar Berlijn mocht nemen om je "mijn" microscopen te laten zien. Papa en mama, bedankt voor jullie eindeloze steun en voor de talloze reizen naar Berlijn voor mij, en voor ons.

And, of course, the most love and support comes from the ones closest to me. Jacob, I wouldn't be who I am without you. You help me be who I want to be, and help me do what I want to do. You are my balance, my guide, my true love. Arthur and Sophie, you continue to wonder and inspire me every day. All I do is for you. You are the greatest achievements of my life and nothing can ever beat that.

Bibliography

E. Agi, A. Kulkarni, and P. R. Hiesinger. Neuronal strategies for meeting the right partner during brain wiring. *Current Opinion in Neurobiology*, 63:1–8, 2020. doi: 10.1016/j.conb.2020.01.002.

Y. Ahmed, S. Hayashi, A. Levine, and E. Wieschaus. Regulation of Armadillo by a Drosophila APC Inhibits Neuronal Apoptosis during Retinal Development. *Cell*, 93:1171–1182, 1998. doi: doi.org/10.1016/S0092-8674(00)81461-0.

S. Astigarraga, J. Douthit, D. Tarnogorska, M. S. Creamer, O. Mano, D. A. Clark, I. A. Meinertzhagen, and J. E. Treisman. Drosophila sidekick is required in developing photoreceptors to enable visual motion detection. *Development*, 145(3):2–11, 2018. doi: 10.1242/dev.158246.

C. B. Brachmann and R. L. Cagan. Patterning the fly eye: The role of apoptosis. *Trends in Genetics*, 19(2):91–96, 2003. doi: 10.1016/S0168-9525(02)00041-0.

V. Braitenberg. Patterns of Projection in the Visual System of the Fly. I. Retina-Lamina Projections. *Experimental Brain Research*, 3:271–298, 1967. doi: doi.org/10.1007/BF00235589.

A. H. Brand and N. Perrimon. Targeted gene expression as a means of altering cell fates and generating dominant phenotypes. *Development*, 118:401–415, 1993. doi: doi.org/10.1242/dev.118.2.401.

J. Briscoe and S. Small. Morphogen rules : design principles of gradient-mediated embryo patterning. *Development*, 142:3996–4009, 2015. doi: 10.1242/dev.129452.

Y.-c. Chang, C.-k. Tsao, and Y. H. Sun. Temporal and spatial order of photoreceptor and glia projections into optic lobe in Drosophila. *Nature*, 8(12669):1–14, 2018. doi: 10.1038/s41598-018-30415-8.

P.-l. L. Chen and T. R. Clandinin. The Cadherin Flamingo Mediates Level-Dependent Interactions that Guide Photoreceptor Target Choice in Drosophila. *Neuron*, 58(1):26–33, 2008. doi: 10.1016/j.neuron.2008.01.007.

Y. Chen and X. Zhao. Shaping Limbs by Apoptosis. *The Journal of Experimental Zoology*, 282:691–702, 1998. doi: doi.org/10.1002/(SICI)1097-010X(19981215)282:6<691::AID-JEZ5>3.0.CO;2-S.

D. Chetverikov. Pattern regularity as a visual key. *Image and Vision Computing*, 18(12): 975–985, 2000. doi: 10.1016/S0262-8856(00)00041-X.

C. B. Chien, D. E. Rosenthal, W. A. Harris, and C. E. Holt. Navigational errors made by growth cones without filopodia in the embryonic Xenopus brain. *Neuron*, 11(2):237–251, 1993. doi: 10.1016/0896-6273(93)90181-P.

T. R. Clandinin and S. L. Zipursky. Afferent growth cone interactions control synaptic specificity in the Drosophila visual system. *Neuron*, 28(2):427–436, 2000. doi: 10.1016/S0896-6273(00)00122-7.

D. E. Clyde, M. S. G. Corado, X. Wu, A. Pare, D. Papatsenko, and S. Small. A self-organizing system of repressor gradients establishes segmental complexity in Drosophila. *Letters to Nature*, 426:849–853, 2003. doi: 10.1371/journal.pbio.0000060.

M. Cohen, M. Georgiou, N. L. Stevenson, M. Miodownik, and B. Baum. Dynamic Filopodia Transmit Intermittent Delta-Notch Signaling to Drive Pattern Refinement during Lateral Inhibition. *Developmental Cell*, 19(1):78–89, 2010. doi: 10.1016/j.devcel.2010.06.006.

M. T. D. Cooper and S. J. Bray. Frizzled regulation of Notch signalling polarizes cell fate in the Drosophila eye. *Letters to Nature*, 397(February):526–530, 1999. doi: doi.org/10.1038/17395.

M. M. Cox. The FLP protein of the yeast 2-eum plasmid : Expression of a eukaryotic genetic recombination system in Escherichia coli Biochemistry :. *Proceedings of the National Academy of Sciences*, 80(July):4223–4227, 1983. doi: doi.org/10.1073/pnas.80.14.4223.

R. T. Cox, C. Kirkpatrick, and M. Peifer. Armadillo Is Required for Adherens Junction Assembly, Cell Polarity, and Morphogenesis during. *Journal of Cell Biology*, 134(1):133–148, 1996. doi: doi.org/10.1083/jcb.134.1.133.

G. Das, J. Reynolds-kenneally, M. Mlodzik, O. Gustave, L. L. Place, N. York, and N. York. The Atypical Cadherin Flamingo Links Frizzled and Notch Signaling in Planar Polarity Establishment in the Drosophila Eye. *Developmental Cell*, 2:655–666, 2002. doi: doi.org/10.1016/S1534-5807(02)00147-8.

R. W. Davenport, P. Dou, V. Rehder, and S. B. Kater. A sensory role for neuronal growth cone filopodia. *Letters to Nature*, 361:721–724, 1993. doi: doi.org/10.1038/361721a0.

C. F. Davey, A. W. Mathewson, and C. B. Moens. PCP Signaling between Migrating Neurons and their Planar-Polarized Neuroepithelial Environment Controls Filopodial Dynamics and Directional Migration. *PLoS Genetics*, 12(3):1–30, 2016. doi: 10.1371/journal.pgen.1005934.

J. A. G. M. de Visser, J. Hermisson, G. P. Wagner, L. A. Meyers, H. Bagheri-Chaichian, J. L. Blanchard, L. Chao, J. M. Cheverud, S. F. Elena, W. Fontana, G. Gibson, T. F. Hansen, D. Krakauer, R. C. Lewontin, C. Ofria, S. H. Rice, G. von Dassow, A. Wagner, and M. C. Withlock. Perspective: evolution and detection of genetic robustness ¨. *Evolution*, 57(9): 1959–1972, 2003.

J. B. Duffy. GAL4 system in Drosophila: a fly geneticist's Swiss army knife. *Genesis (New York, N.Y. : 2000)*, 34(1-2):1–15, 2002. doi: 10.1002/gene.10150.

T. N. Edwards and I. A. Meinertzhagen. Photoreceptor neurons find new synaptic targets when misdirected by overexpressing runt in Drosophila. *Journal of Neuroscience*, 29(3): 828–841, 2009. doi: 10.1523/JNEUROSCI.1022-08.2009.

E. H. Feinberg, M. K. VanHoven, A. Bendesky, G. Wang, R. D. Fetter, K. Shen, and C. I. Bargmann. GFP Reconstitution Across Synaptic Partners (GRASP) Defines Cell Contacts and Synapses in Living Nervous Systems. *Neuron*, 57(3):353–363, 2008. doi: 10.1016/j.neuron.2007.11.030.

V. M. Fernandes, Z. Chen, A. M. Rossi, J. Zipfel, and C. Desplan. Glia relay differentiation cues to coordinate neuronal development in Drosophila. *Science*, 357(6354):886–891, 2017. doi: 10.1126/science.aan3174.

T. M. Finegan, N. Hervieux, A. Nestor-Bergmann, A. G. Fletcher, G. B. Blanchard, and B. Sanson. The tricellular vertex-specific adhesion molecule Sidekick facilitates polarised cell intercalation during Drosophila axis extension. *PLoS Biology*, 17(12):1–32, 2019. doi: 10.1371/journal.pbio.3000522.

T. M. Finegan, D. T. Bergstralh, and D. T. Bergstralh. Neuronal immunoglobulin superfamily cell adhesion molecules in epithelial morphogenesis : insights from Drosophila. *Philosophical Transactions B*, 375:1–12, 2020. doi: dx.doi.org/10.1098/rstb.2019.0553.

S. Fung, F. Wang, S. R. Spindler, and V. Hartenstein. Drosophila E-cadherin and its binding partner Armadillo / β -catenin are required for axonal pathway choices in the developing larval brain. *Developmental Biology*, 332(2):371–382, 2009. doi: 10.1016/j.ydbio.2009.06.005.

G. Gallo. Mechanisms Underlying the Initiation and Dynamics of Neuronal Filopodia. From Neurite Formation to Synaptogenesis. *International Review of Cell and Molecular Biology*, 301:95–156, 2013. doi: 10.1016/B978-0-12-407704-1.00003-8.

A. Gierer and H. Meinhardt. A Theory of Biological Pattern Formation. *Kybernetik*, 12: 30–39, 1972. doi: doi.org/10.1007/BF00289234.

P. T. Gonzalez-Bellido, T. J. Wardill, R. Kostyleva, I. A. Meinertzhagen, and M. Juusola. Overexpressing Temperature-Sensitive Dynamin Decelerates Phototransduction and Bundles Microtubules in Drosophila Photoreceptors. *The Journal of Neuroscience*, 29(45): 14199–14210, 2009. doi: 10.1523/JNEUROSCI.2873-09.2009.

G. J. Goodhill. Can Molecular Gradients Wire the Brain? *Trends in Neurosciences*, 39(4): 202–211, 2016. doi: 10.1016/j.tins.2016.01.009.

K. M. Goodman, M. Yamagata, X. Jin, S. Mannepalli, P. S. Katsamba, G. Ahlsén, A. P. Sergeeva, B. Honig, J. R. Sanes, and L. Shapiro. Molecular basis of sidekick-mediated cell-cell adhesion and specificity. *eLife*, 5(September2016):1–21, 2016. doi: 10.7554/eLife.19058.

H. Hamada, M. Watanabe, H. E. Lau, T. Nishida, T. Hasegawa, and D. M. Parichy. Involvement of Delta / Notch signaling in zebrafish adult pigment stripe patterning. *Development*, 141:318–324, 2014. doi: 10.1242/dev.108894.

H. Harada, J. Charish, and P. P. Monnier. Emerging evidence for cell-autonomous axon guidance. *Development Growth and Differentiation*, 62(6):391–397, 2020. doi: 10.1111/dgd.12666.

R. C. Hardie. Projection and connectivity of sex-specific photoreceptors in the compound eye of the male housefly (Musca domestica). *Cell and Tissue Research*, 233:1–21, 1983. doi: doi.org/10.1007/BF00222228.

B. A. Hassan and P. R. Hiesinger. Beyond Molecular Codes: Simple Rules to Wire Complex Brains. *Cell*, 163(2):285–291, 2015. doi: 10.1016/j.cell.2015.09.031.

D. Hattori, E. Demir, H. W. Kim, E. Viragh, S. L. Zipursky, and B. J. Dickson. Dscam diversity is essential for neuronal wiring and self-recognition. *Nature*, 449(7159):223–227, 2007. doi: 10.1038/nature06099.

C. A. Heckman, H. K. P. Iii, and H. K. Plummer. Filopodia as sensors. *Cellular Signalling*, 25(11):2298–2311, nov 2013. doi: 10.1016/j.cellsig.2013.07.006.

I. Hein, T. Suzuki, and I. C. G. Kadow. Gogo Receptor Contributes to Retinotopic Map Formation and Prevents R1-6 Photoreceptor Axon Bundling. *PLoS ONE*, 8(6):1–11, 2013. doi: 10.1371/journal.pone.0066868.

P. R. Hiesinger and B. A. Hassan. The Evolution of Variability and Robustness in Neural Development. *Trends in Neurosciences*, 41(9):577–586, 2018. doi: 10.1016/j.tins.2018.05.007.

P. R. Hiesinger, R. G. Zhai, Y. Zhou, T. W. Koh, S. Q. Mehta, K. L. Schulze, Y. Cao, P. Verstreken, T. R. Clandinin, K. F. Fischbach, I. a. Meinertzhagen, and H. J. Bellen. Activity-Independent Prespecification of Synaptic Partners in the Visual Map of Drosophila. *Current Biology*, 16(18):1835–1843, sep 2006. doi: 10.1016/j.cub.2006.07.047.

M. R. Higgins, N. J. Gibson, P. A. Eckholdt, A. Nighorn, P. F. Copenhaver, J. Nardi, and L. P. Tolbert. Different Isoforms of Fasciclin II Are Expressed by a Subset of Developing Olfactory Receptor Neurons and by Olfactory-Nerve Glial Cells during Formation of Glomeruli in the Moth Manduca sexta. *Developmental Biology*, 244:134–154, 2002. doi: 10.1006/dbio.2002.0583.

C. Hogan, N. Serpente, P. Cogram, C. R. Hosking, C. U. Bialucha, S. M. Feller, V. M. M. Braga, W. Birchmeier, Y. Fujita, and M. Delbru. Rap1 Regulates the Formation of E-Cadherin-Based Cell-Cell Contacts. *Molecular and Cellular Biology*, 24(15):6690–6700, 2004. doi: 10.1128/MCB.24.15.6690.

I. Holguera and C. Desplan. Neuronal specification in space and time. *Science*, 1(October): 176–180, 2018. doi: 10.1126/science.aas9435.

G. A. Horridge and I. A. Meinertzhagen. The accuracy of the patterns of connexions of the first- and second-order neurons of the visual system of Calliphora. *Proceedings of the Royal Society of London. Series B, Biological Sciences*, 175(1038):69–82, 1970. doi: doi.org/10.1098/rspb.1970.0012.

J. Huang, L. Huang, Y.-j. Chen, E. Austin, C. E. Devor, F. Roegiers, and Y. Hong. Differential regulation of adherens junction dynamics during apical-basal polarization. *Journal of Cell Science*, 124:4001–4013, 2011. doi: 10.1242/jcs.086694.

Z. Huang and S. Kunes. Hedgehog, transmitted along retinal axons, triggers neurogenesis in the developing visual centers of the Drosophila brain. *Cell*, 86(3):411–422, 1996. doi: 10.1016/S0092-8674(00)80114-2.

Z. Huang and S. Kunes. Signals transmitted along retinal axons in Drosophila: Hedgehog signal reception and the cell circuitry of lamina cartridge assembly. *Development*, 125: 3753–3764, 1998. doi: doi.org/10.1242/dev.125.19.3753.

Z. Huang, B. Z. Shilo, and S. Kunes. A retinal axon fascicle uses spitz, an EGF receptor ligand, to construct a synaptic cartridge in the brain of Drosophila. *Cell*, 95:693–703, 1998. doi: 10.1016/S0092-8674(00)81639-6.

B. Y. D. H. Hubel and A. D. T. N. Wiesel. Receptive Fields, Binocular Interaction and Functional Architecture in the Cat's Visual Cortex. *Journal of Physiology*, 160:106–154, 1962. doi: 10.1113/jphysiol.1962.sp006837.

A. Jenny. Planar Cell Polarity Signaling in the Drosophila Eye. *HHS Public Acces*, 2017. doi: 10.1016/B978-0-12-385044-7.00007-2.Planar.

W. Ji, L. F. Wu, and S. J. A. Id. Analysis of growth cone extension in standardized coordinates highlights self- organization rules during wiring of the Drosophila visual system. *PLoS Genetics*, pages 1–16, 2021. doi: 10.1371/journal.pgen.1009857.

T. Kidd, K. S. Bland, and C. S. Goodman. Slit Is the Midline Repellent for the Robo Receptor in Drosophila. *Cell*, 96:785–794, 1999. doi: doi.org/10.1016/S0092-8674(00)80589-9.

F. R. Kiral, G. A. Linneweber, T. Mathejczyk, S. V. Georgiev, M. F. Wernet, B. A. Hassan, M. von Kleist, and P. R. Hiesinger. Autophagy-dependent filopodial kinetics restrict synaptic partner choice during Drosophila brain wiring. *Nature communications*, 11, 2020. doi: 10.1038/s41467-020-14781-4.

K. Kirschfeld and N. Franceschini. 0ptische Eigenschaften der 0mmatidien im Komplexauge yon. *Kybernetik*, BandV(2):48–52, 1968. doi: doi.org/10.1007/BF00272694.

D. E. Koser, A. J. Thompson, S. K. Foster, A. Dwivedy, E. K. Pillai, G. K. Sheridan, H. Svoboda, M. Viana, L. D. F. Costa, J. Guck, C. E. Holt, and K. Franze. Mechanosensing is critical for axon growth in the developing brain. *Nature Neuroscience*, 19(12):1592–1598, 2016. doi: 10.1038/nn.4394.

R. Kraut and M. Levine. Mutually repressive interactions between the gap genes giant and Kruppel define middle body regions of the Drosophila embryo. *Development*, 111:611–621, 1991. doi: doi.org/10.1242/dev.111.2.611.

J. R. Kroll, K. G. Wong, F. M. Siddiqui, and M. A. Tanouye. Disruption of Endocytosis with the Dynamin Mutant. *Genetics*, 201(November):1087–1102, 2015. doi: 10.1534/genetics.115.177600.

A. Kulkarni, D. Ertekin, C. H. Lee, and T. Hummel. Birth order dependent growth cone segregation determines synaptic layer identity in the Drosophila visual system. *eLife*, 5 (MARCH2016):1–22, 2016. doi: 10.7554/eLife.13715.

T. Labhart. Polarization-opponent interneurons in the insect visual system. *Nature*, 331:4–6, 1988. doi: doi.org/10.1038/331435a0.

M. Langen, E. Agi, D. J. Altschuler, L. F. Wu, S. J. Altschuler, and P. R. Hiesinger. The Developmental Rules of Neural Superposition in Drosophila. *Cell*, 162(1):120–133, 2015. doi: 10.1016/j.cell.2015.05.055.

C. H. Lee, T. Herman, T. R. Clandinin, R. Lee, and S. L. Zipursky. N-cadherin regulates target specificity in the Drosophila visual system. *Neuron*, 30(2):437–450, 2001. doi: 10.1016/S0896-6273(01)00291-4.

R. C. Lee, T. R. Clandinin, C.-h. Lee, P.-L. Chen, I. A. Meinertzhagen, and S. L. Zipursky. The protocadherin Flamingo is required for axon target selection in the Drosophila visual system. *Nature neuroscience*, 6(6):557–563, 2003. doi: 10.1038/nn1063.

T. Lee and L. Luo. Mosaic analysis with a repressible cell marker (MARCM) for Drosophila neural development. *Trends in Neurosciences*, 24(5):251–254, 2001. doi: 10.1016/S0030-6657(08)70226-9.

A. Letizia, D. Q. He, S. Astigarraga, J. Colombelli, V. Hatini, M. Llimargas, and J. E. Treisman. Sidekick Is a Key Component of Tricellular Adherens Junctions that Acts to Resolve Cell Rearrangements. *Developmental Cell*, 50(3):313–326.e5, 2019. doi: 10.1016/j.devcel.2019.07.007.

D. M. Lin, V. J. Auld, and C. S. Goodman. Targeting Neuronal Cell Ablation in the Drosophila Embryo: Pathfinding by Follower Growth Cones in the Absence of Pioneers. *Neuron*, 14:707–715, 1995. doi: doi.org/10.1016/0896-6273(95)90215-5.

L. Luo, E. M. Callaway, and K. Svoboda. Genetic Dissection of Neural Circuits. *Neuron*, 57: 634–660, 2008. doi: 10.1016/j.neuron.2008.01.002.

C. Ma, Y. Zhou, P. A. Beachy, and K. Moses. The Segment Polarity Gene hedgehog Is Required for Progression of the Morphogenetic Furrow in the Developing Drosophila Eye. *Cell*, 75:927–938, 1993. doi: doi.org/10.1016/0092-8674(93)90536-Y.

D. Matsubara, S. Y. Horiuchi, K. Shimono, T. Usui, and T. Uemura. The seven-pass transmembrane cadherin Flamingo controls dendritic self-avoidance via its binding to a LIM

domain protein, Espinas, in Drosophila sensory neurons. *Genes and Development*, 25(18): 1982–1996, 2011. doi: 10.1101/gad.16531611.

B. J. Matthews, M. E. Kim, J. J. Flanagan, D. Hattori, J. C. Clemens, S. L. Zipursky, and W. B. Grueber. Dendrite Self-Avoidance Is Controlled by Dscam. *Cell*, 128:593–604, 2007. doi: 10.1016/j.cell.2007.04.013.

I. A. Meinertzhagen. Errorneous projection of retinula axons beneath a deslocation in the retinal equator of calliphora. *Brain Research*, 41:39–49, 1972. doi: doi.org/10.1016/0006-8993(72)90615-4.

I. A. Meinertzhagen and S. D. O'Neil. Synaptic Organization of Columnar Elements in the Lamina of the Wild Type in Drosophila melanogaster. *The Journal of Comparative Neurology*, 305:232–263, 1991. doi: doi.org/10.1002/cne.903050206.

K. V. Melnattur and C.-H. Lee. Visual Circuit Assembly in Drosophila. *Developmental Neurobiology*, 71(12):1286–1296, 2011. doi: 10.1002/dneu.20894.Visual.

C. Mencarelli and F. Pichaud. Orthodenticle Is Required for the Expression of Principal Recognition Molecules That Control Axon Targeting in the Drosophila Retina. *PLoS Genetics*, pages 1–19, 2015. doi: 10.1371/journal.pgen.1005303.

S. S. Millard and S. L. Zipursky. Dscam-mediated repulsion controls tiling and self-avoidance. *Current Opinion in Microbiology*, 18:84–89, 2008. doi: 10.1016/j.conb.2008.05.005.

S. S. Millard, J. J. Flanagan, K. S. Pappu, W. Wu, and S. L. Zipursky. Dscam2 mediates axonal tiling in the Drosophila visual system. *Nature*, 447(June):720–725, 2007. doi: 10.1038/nature05855.

M. J. Murray, D. J. Merritt, A. H. Brand, and P. M. Whitington. In vivo dynamics of axon pathfinding in the Drosophila CNS: A time- lapse study of an identified motorneuron. *Journal of Neurobiology*, 37(4):607–621, 1998. doi: 10.1002/(SICI)1097-4695(199812)37:4<607::AID-NEU9>3.0.CO;2-Q.

S. Myat, T. W. Maung, and A. Jenny. Planar cell polarity in Drosophila. *Organogenesis*, 7 (3):165–179, 2011. doi: doi.org/10.4161/org.7.3.18143.

A. Nagafuchi and M. Takeichi. Transmembrane control of cadherin-mediated cell adhesion : a 94 kDa protein functionally associated with a specific region of the cytoplasmic domain of E-cadherin. *Cell Regulation*, 1(November):37–44, 1989. doi: doi.org/10.1091/mbc.1.1.37.

A. Nern, Y. Zhu, and S. L. Zipursky. Local N-Cadherin Interactions Mediate Distinct Steps in the Targeting of Lamina Neurons. *Neuron*, 58(1):34–41, 2008. doi: 10.1016/j.neuron.2008.03.022.

A. Nern, B. D. Pfeiffer, and G. M. Rubin. Optimized tools for multicolor stochastic labeling reveal diverse stereotyped cell arrangements in the fly visual system. *Proceedings of the National Academy of Sciences of the United States of America*, 112(22):E2967–E2976, 2015. doi: 10.1073/pnas.1506763112.

G. Neves, J. Zucker, M. Daly, and A. Chess. Stochastic yet biased expression of multiple Dscam splice variants by individual cells. *Nature Genetics*, 36(3):240–246, 2004. doi: 10.1038/ng1299.

T. P. Newsome, B. Åsling, and B. J. Dickson. Analysis of Drosophila photoreceptor axon guidance in eye-specific mosaics. *Development*, 127:851–860, 2000. doi: doi.org/10.1242/dev.127.4.851.

D. N. Nguyen, Y. Liu, M. L. Litsky, and R. Reinke. The sidekick gene, a member of the immunoglobulin superfamily, is required for pattern formation in the Drosophila eye. *Development*, 124(17):3303–3312, 1997. doi: doi.org/10.1242/dev.124.17.3303.

J. Noordermeer, J. Klingensmith, N. Perrimont, and R. Nusse. dishevelled and armadillo act in the Wingless signalling pathway in Drosophila. *Letters to Nature*, 367(January):80–83, 1994. doi: doi.org/10.1038/367083a0.

T. P. O'Connor, J. S. Duerr, and D. Bentley. Pioneer growth cone steering decisions mediated by single filopodial contacts in situ. *Journal of Neuroscience*, 10(12):3935–3946, 1990. doi: 10.1523/jneurosci.10-12-03935.1990.

M. N. Özel, M. Langen, B. A. Hassan, and P. R. Hiesinger. Filopodial dynamics and growth cone stabilization in Drosophila visual circuit development. *eLife*, 4(OCTOBER2015):1–21, 2015. doi: 10.7554/eLife.10721.

Y. Peng and J. D. Axelrod. Asymmetric protein localization in planar cell polarity: Mechanisms, puzzles and challenges. *Current Topics in Developmental Biology*, pages 1–19, 2012. doi: 10.1016/B978-0-12-394592-1.00002-8.Asymmetric.

M. Petrovic and D. Schmucker. Axonal wiring in neural development: Target-independent mechanisms help to establish precision and complexity. *BioEssays*, 37(9):996–1004, 2015. doi: 10.1002/bies.201400222.

B. Poeck, S. Fischer, D. Gunning, S. L. Zipursky, and I. Salecker. Glial cells mediate target layer selection of retinal axons in the developing visual system of Drosophila. *Neuron*, 29: 99–113, 2001. ISSN 08966273. doi: 10.1016/S0896-6273(01)00183-0.

C. J. Potter and L. Luo. Using the Q system in Drosophila melanogaster. *Nature Protocols*, 6(8):1105–1120, 2011. doi: 10.1038/nprot.2011.347.

C. J. Potter, B. Tasic, E. V. Russler, L. Liang, and L. Luo. The Q system: A repressible binary system for transgene expression, lineage tracing, and mosaic analysis. *Cell*, 141(3): 536–548, 2010. doi: 10.1016/j.cell.2010.02.025.

S. Prakash, J. C. Caldwell, D. F. Eberl, and T. R. Clandinin. Drosophila N-cadherin mediates an attractive interaction between photoreceptor axons and their targets. *Nature Neuroscience*, 8(4):443–450, 2005. doi: 10.1038/nn1415.

C. L. Rees, K. Moradi, and G. A. Ascoli. Weighing the Evidence in Peters' Rule: Does Neuronal Morphology Predict Connectivity? *Trends in Neurosciences*, 40(2):63–71, 2017. doi: 10.1016/j.tins.2016.11.007.

C. D. Rogers, L. K. Sorrells, and M. E. Bronner. Mechanisms of Development A catenin-dependent balance between N-cadherin and E-cadherin controls neuroectodermal cell fate choices. *Mechanisms of Development*, 152(June):44–56, 2018. doi: 10.1016/j.mod.2018.07.003.

J.-y. Roignant and J. E. Treisman. Pattern formation in the Drosophila eye disc. *The International Journal of Developmental Biology*, 53:795–804, 2009. doi: 10.1387/ijdb.072483jr.

G. Roman and R. L. Davis. Conditional Expression of UAS-Transgenes in the Adult Eye With a New Gene-Switch Vector System. *Genesis*, 34(September):127–131, 2002. doi: 10.1002/gene.10133.

A. Sahasrabudhe, K. Ghate, S. Mutalik, A. Jacob, and A. Ghose. Formin 2 regulates the stabilization of filopodial tip adhesions in growth cones and affects neuronal outgrowth and pathfinding in vivo. *Development*, 143:449–460, 2016. doi: 10.1242/dev.130104.

G. Sancer, E. Kind, J. Uhlhorn, J. Volkmann, J. Hammacher, and T. Pham. Cellular and synaptic adaptations of neural circuits processing skylight polarization in the fly. *Journal of Comparative Physiology A*, 206(2):233–246, 2020. doi: 10.1007/s00359-019-01389-3.

M. Sato, D. Umetsu, S. Murakami, T. Yasugi, and T. Tabata. DWnt4 regulates the dorsoventral specificity of retinal projections in the Drosophila melanogaster visual system. *Nature Neuroscience*, 9(1):67–76, 2006. doi: 10.1038/nn1604.

L. K. Scheffer, C. S. Xu, M. Januszewski, Z. Lu, S.-y. Takemura, K. J. Hayworth, G. B. Huang, K. Shinomiya, J. Maitlin-shepard, S. Berg, J. Clements, P. M. Hubbard, W. T. Katz, L. Umayam, T. Zhao, D. Ackerman, T. Blakely, J. Bogovic, T. Dolafi, D. Kainmueller, T. Kawase, K. A. Khairy, L. Leavitt, P. H. Li, L. Lindsey, N. Neubarth, D. J. Olbris, H. Otsuna, E. T. Trautman, M. Ito, A. S. Bates, J. Goldammer, T. Wolff, R. Svirskas, P. Schlegel, E. Neace, C. J. Knecht, C. X. Alvarado, D. A. Bailey, S. Ballinger, J. A. Borycz, B. S. Canino, N. Cheatham, M. Cook, M. Dreher, O. Duclos, B. Eubanks, K. Fairbanks, S. Finley, N. Forknall, A. Francis, G. P. Hopkins, E. M. Joyce, S. Kim, N. A. Kirk, J. Kovalyak, S. A. Lauchie, A. Lohff, C. Maldonado, E. A. Manley, S. Mclin, C. Mooney, M. Ndama, O. Ogundeyi, N. Okeoma, C. Ordish, N. Padilla, C. M. Patrick, T. Paterson, E. E. Phillips, E. M. Phillips, N. Rampally, C. Ribeiro, M. K. Robertson, J. T. Rymer, S. M. Ryan, M. Sammons, A. K. Scott, A. L. Scott, A. Shinomiya, C. Smith, K. Smith, N. L. Smith, M. A. Sobeski, A. Suleiman, J. Swift, S. Takemura, I. Talebi, D. Tarnogorska, E. Tenshaw, T. Tokhi, J. J. Walsh, T. Yang, J. A. Horne, F. Li, R. Parekh, P. K. Rivlin, V. Jayaraman, M. Costa, G. S. X. E. Jefferis, K. Ito, S. Saalfeld, R. George, and S. M. Plaza. A connectome and analysis of the adult Drosophila central brain. *eLife*, 9(e57443): 1–83, 2020. doi: doi.org/10.7554/eLife.57443.

T. Schwabe, H. Neuert, and T. R. Clandinin. XA network of cadherin-mediated interactions polarizes growth cones to determine targeting specificity. *Cell*, 154(2):351–364, 2013. doi: 10.1016/j.cell.2013.06.011.

T. Schwabe, J. A. Borycz, I. a. Meinertzhagen, and T. R. Clandinin. Differential adhesion determines the organization of synaptic fascicles in the drosophila visual system. *Current Biology*, 24(12):1304–1313, 2014. doi: 10.1016/j.cub.2014.04.047.

F. Schweisguth and F. Corson. Self-Organization in Pattern Formation. *Developmental Cell*, 49:659–677, 2019. doi: 10.1016/j.devcel.2019.05.019.

R. W. Sperry. Chemoaffinity in the Orderly Growth of Nerve Fiber Patterns and. *Proceedings of the National Academy of Sciences of the United States of*, 50:703–710, 1963. doi: 10.1073/pnas.50.4.703.

D. G. Stavenga. The Neural Superposition Eye and Its Optical Demands. *Journal of Comparative Physiology*, 304(102):297–304, 1975. doi: doi.org/10.1007/BF01464342.

A. Steimel, L. Wong, E. H. Najarro, B. D. Ackley, and G. Garriga. The Flamingo ortholog FMI-1 controls pioneer-dependent navigation of follower axons in C . elegans. *Development*, 137:3663–3673, 2010. doi: 10.1242/dev.054320.

M. S. Steinberg. Adhesion-guided Multicellular Assembly: a Commentary upon the Postulates, Real and Imagined, of the Differential Adhesion Hypothesis, with Special Attention to Computer Simulations of Cell Sorting. *Journal of Theoretical Biology*, 55:431–443, 1975. doi: doi.org/10.1016/S0022-5193(75)80091-9.

M. S. Steinberg. Differential adhesion in morphogenesis : a modern view. *Current Opinion in Genetics and Development*, 17:281–286, 2007. doi: 10.1016/j.gde.2007.05.002.

J. R. Sternberg and C. Wyart. Neuronal Wiring : Linking Dendrite Placement to Synapse Formation. *Current Biology*, 25(5):R190–R191, 2015. doi: 10.1016/j.cub.2015.01.006. URL `http://dx.doi.org/10.1016/j.cub.2015.01.006`.

B. K. Straub, S. Rickelt, R. Zimbelmann, C. Grund, C. Kuhn, M. Iken, M. Ott, P. Schirmacher, and W. W. Franke. E–N-cadherin heterodimers define novel adherens junctions connecting endoderm-derived cells. *Journal of Cell Biology*, 195(5):873–887, 2011. doi: 10.1083/jcb.201106023.

G. Struhl, J. Casal, and P. A. Lawrence. Dissecting the molecular bridges that mediate the function of Frizzled in planar cell polarity. *Development*, 139:3665–3674, 2012. doi: 10.1242/dev.083550.

H. Takeuchi and H. Sakano. Neural map formation in the mouse olfactory system. *Cellular and Molecular Life Sciences*, 71:3049–3057, 2014. doi: 10.1007/s00018-014-1597-0.

M. Taley, E. B. Richman, N. J. Snell, G. G. Hartmann, J. D. Fischer, A. Sorkac, J. F. Santoyo, C. Chou-Freed, N. Nair, M. Johnson, J. R. Szymanski, and G. Barnea. Transsynaptic mapping of second-order taste neurons in flies by trans-Tango. *Neuron*, 96:1–13, 2017. doi: doi.org/10.1016/j.neuron.2017.10.011.

H. Tanaka, W. Shan, G. R. Phillips, K. Arndt, O. Bozdagi, L. Shapiro, G. W. Huntley, D. L. Benson, and D. R. Colman. Molecular Modification of N-Cadherin in Response to Synaptic Activity. *Neuron*, 25:93–107, 2000. doi: doi.org/10.1016/S0896-6273(00)80874-0.

M. Tessier-Lavigne and C. S. Goodman. The Molecular Biology of Axon Guidance. *Science*, 274:1123–1134, 1996. doi: 10.1126/science.274.5290.1123.

N. A. Theodosiou and T. Xu. Use of FLP / FRT System to Study Drosophila Development. *Methods*, 14:355–365, 1998. doi: doi.org/10.1006/meth.1998.0591.

S. Toda, L. R. Blauch, S. K. Y. Tang, L. Morsut, and W. A. Lim. Programming self-organizing multicellular structures with synthetic cell-cell signaling. *Science*, 361:156–162, 2018. doi: 10.1126/science.aat0271.

O. Trush, C. Liu, X. Han, Y. Nakai, R. Takayama, H. Murakawa, J. A. Carrillo, H. Takechi, X. S. Hakeda-suzuki, T. Suzuki, and X. M. Sato. N-Cadherin Orchestrates Self-Organization of Neurons within a Columnar Unit in the Drosophila Medulla. *Journal of Neuroscience*, 39(30):5861–5880, 2019. doi: doi.org/10.1523/JNEUROSCI.3107-18.2019.

H. Uechi and E. Kuranaga. The Tricellular Junction Protein Sidekick Regulates Vertex Dynamics to Promote Bicellular Junction Extension. *Developmental Cell*, 50(3):327–338.e5, 2019. doi: 10.1016/j.devcel.2019.06.017.

D. Umetsu, S. Murakami, M. Sato, and T. Tabata. The highly ordered assembly of retinal axons and their synaptic partners is regulated by Hedgehog/single-minded in the Drosophila visual system. *Development*, 133(5):791–800, 2006. doi: 10.1242/dev.02253.

K. White, E. Tahaoglu, and H. Steller. Cell Killing by the Drosophila Gene reaper. *Science*, 271(February):805–808, 1996. doi: 10.1126/science.271.5250.805.

C. B. Wit and P. R. Hiesinger. Neuronal Filopodia: Dynamics in Brain Morphogenesis. *Seminars in Cell and Developmental Biology*, *, 2022. doi: underreview.

T. Wolff and D. F. Ready. The beginning of pattern formation in the Drosophila compound eye : the morphogenetic furrow and the second mitotic wave. *Development*, 113:841–850, 1991. doi: doi.org/10.1242/dev.113.3.841.

D. F. Woods, C. Hough, D. Peel, G. Callaini, and P. J. Bryant. Dlg Protein Is Required for Junction Structure, Cell Polarity, and Proliferation Control in Drosophila Epithelia. *The Journal of Cell Biology*, 134(6):1469–1482, 1996. doi: doi.org/10.1083/jcb.134.6.1469.

M. Yamagata, J. A. Weiner, and J. R. Sanes. Sidekicks: Synaptic adhesion molecules that promote lamina-specific connectivity in the retina. *Cell*, 110(5):649–660, 2002. doi: 10.1016/S0092-8674(02)00910-8.

S. Yonekura, L. Xu, C.-y. Ting, and C.-h. Lee. Adhesive but not signaling activity of Drosophila N-cadherin is essential for target selection of photoreceptor afferents. *Developmental Biology*, 304:759–770, 2007. doi: 10.1016/j.ydbio.2007.01.030.

Y. Zou. Breaking symmetry – cell polarity signaling pathways in growth cone guidance and synapse formation. *Current Opinion in Neurobiology*, 63:77–86, 2020. doi: 10.1016/j.conb.2020.03.010.

Appendix A

Appendix - Supplementary Figures

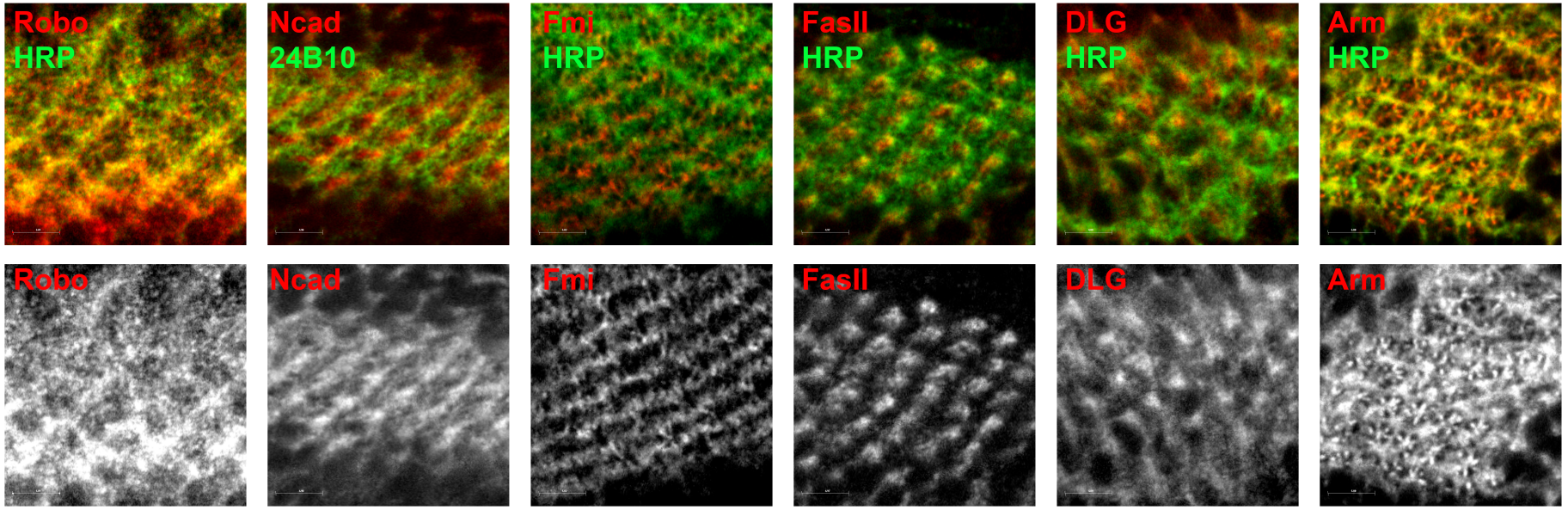

FIGURE A.1: An antibody screen reveals Armadillo as patterned protein at the LP

Panels showing a top view of the lamina plexus at P20 with a set of different antibodies (green) in combination with HRP to show photoreceptors (red).

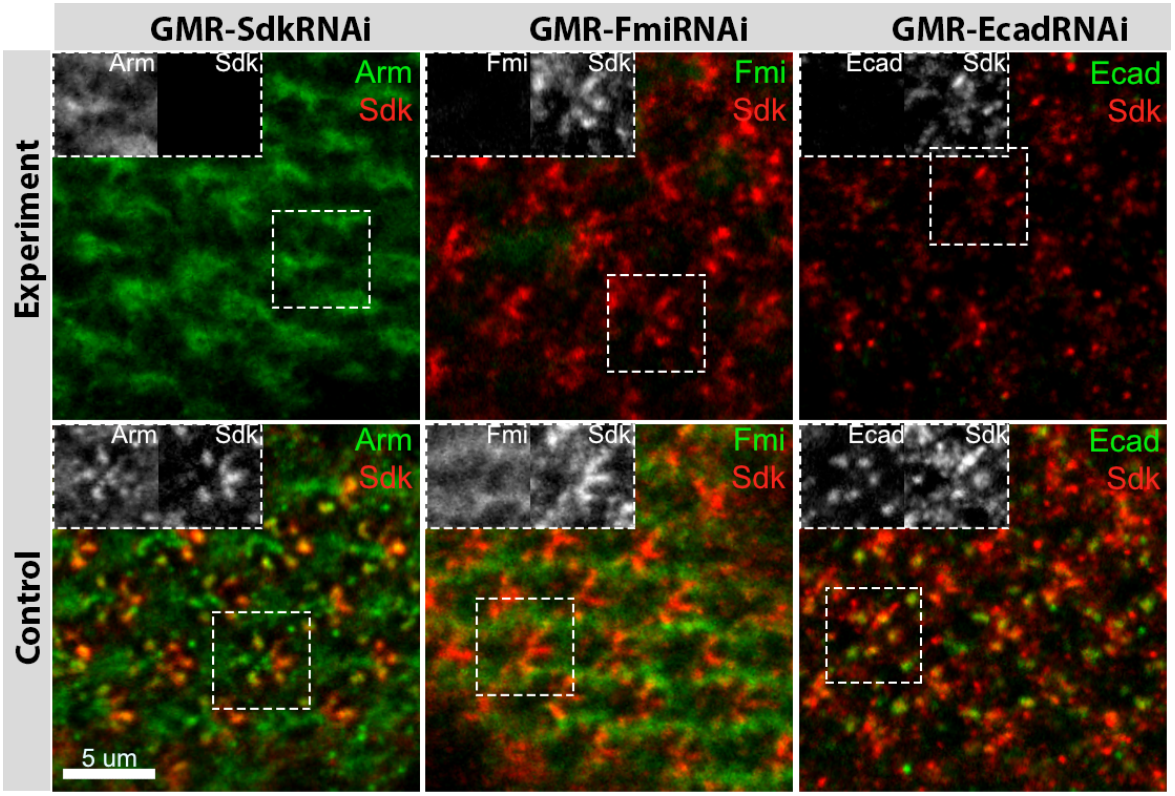

FIGURE A.2: Patterned proteins at the lamina plexus show dependent expressions

Expression of SdkRNAi (left), FmiRNAi (middle), and EcadRNAi under the GMR-Gal4 driver. Experimental condition at the top, control at the bottom. White framed areas are shown in detail at the corner of the panel. Scale bar 5 μm.

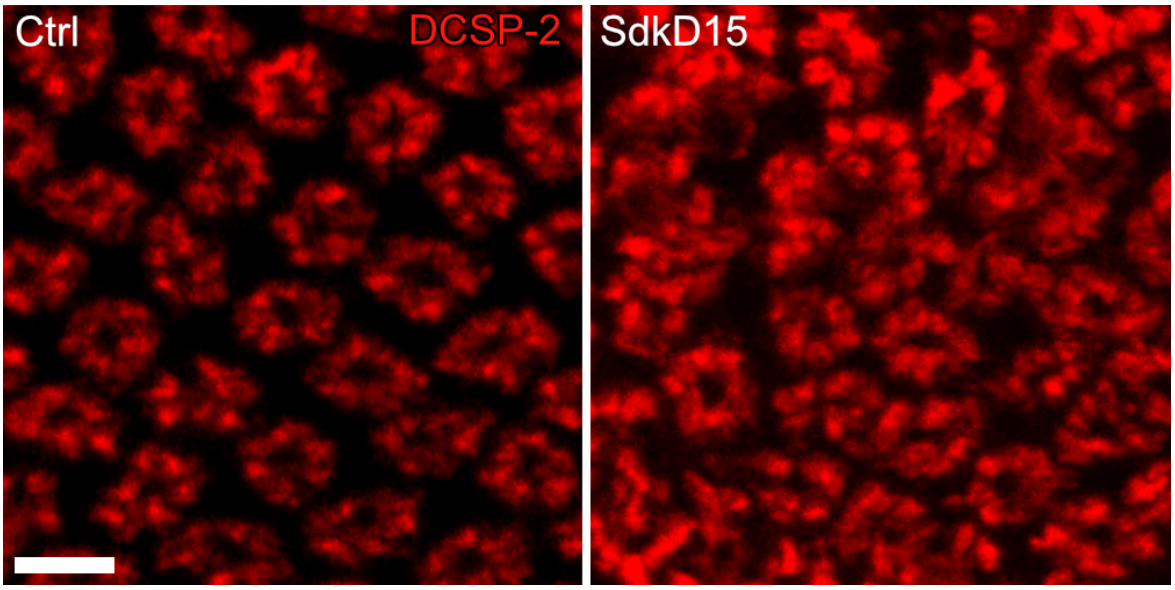

FIGURE A.3: The disturbed sorting outcome in the Sdk experiment

The adult sorting outcome in the full $Sdk^{\Delta 15}$ mutant is disturbed. Fixed images from P100 (adult) lamina. Photoreceptors (stained with DCSP-2 antibody) in red. Scalebar 5 μm.

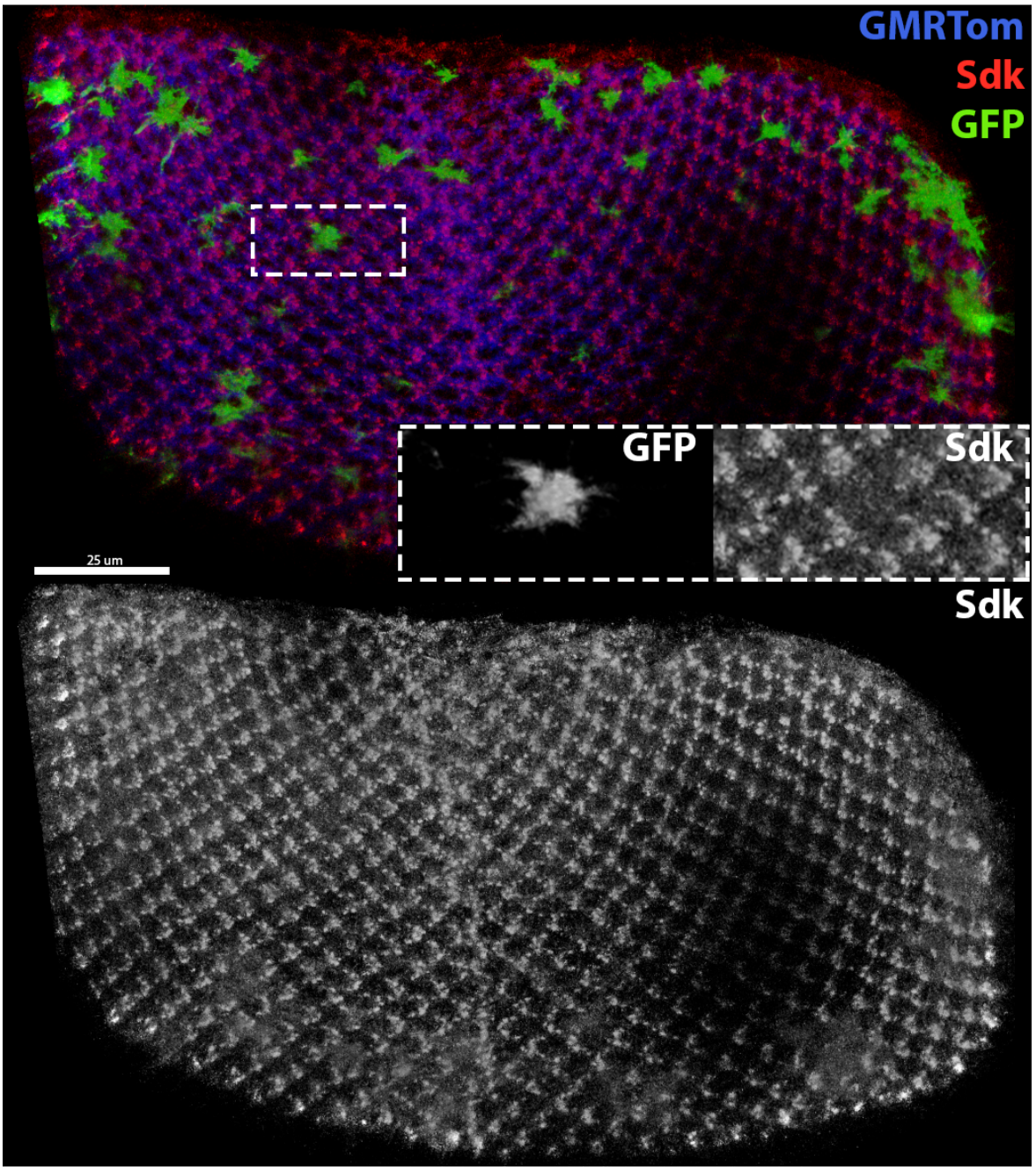

FIGURE A.4: Small Sdk mutant clones do not disturb lamina patterning

Top view of the complete lamina plexus where Sdk clones are created using MARCM. Sdk mutant photoreceptors are labeled with GFP (green). All photoreceptors are genetically labeled with the Tomato fluorophore (blue). Sdk antibody staining in red. Highlighted panel is enlarged and devided in a GFP (clone) panel, and a Sdk panel showing that the overall structure of the lamina is not affected. Lower large panel shows the Sdk staining over the complete lamina. Scalebar 25 μm.

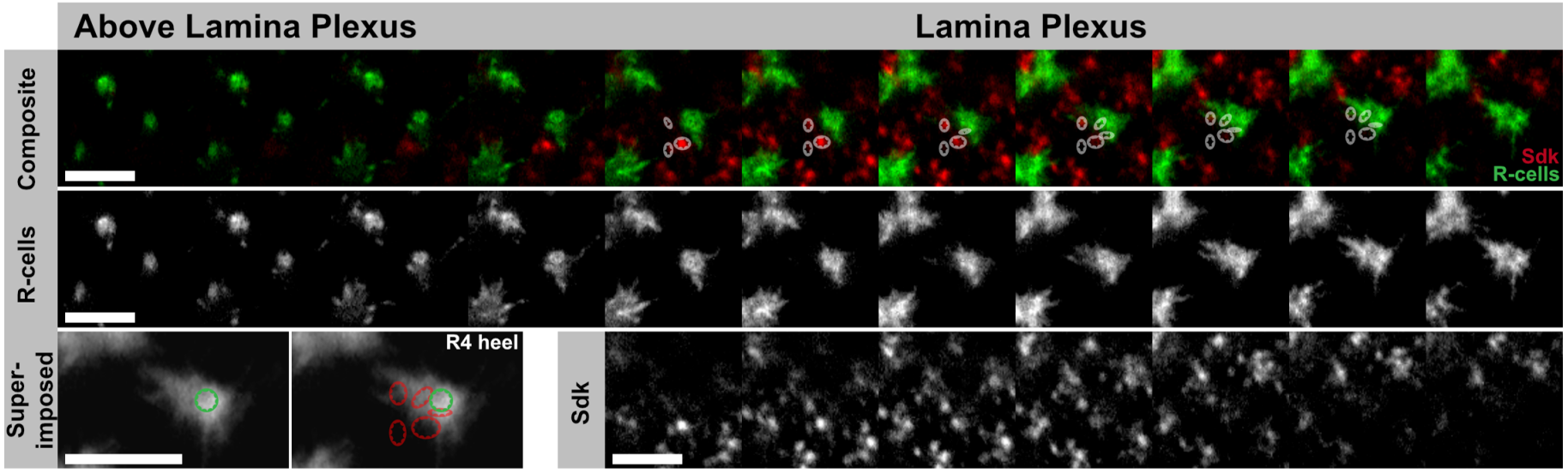

FIGURE A.5: Rare case of defective photoreceptor targeting in single Sdk mutant PRs

A single GFP labeled photoreceptor that is mutant for Sidekick has an anchoring point at the R4 heel location in the scaffold, but obtains a non-R4 outgrowth direction. Top panels show 0.5 μm steps down through the lamina plexus, showing the orientation of the photoreceptor growth cone. Most left images are above the lamina plexus, to the right at the lamina plexus.Green is GFP expressed by the Sdk clone. Red is Armadillo staining. White outlines the Sdk dots in between photoreceptor heels. Middle row of panels shows GFP channel only. Bottom panels left show the complete image stack and the Sdk outlines (red). Green circle represents the heel position in between the Sdk dots. Bottom panels right show the Sdk staining channel only (for the panels at the lamina plexus, not above). All scale bars 5 μm.

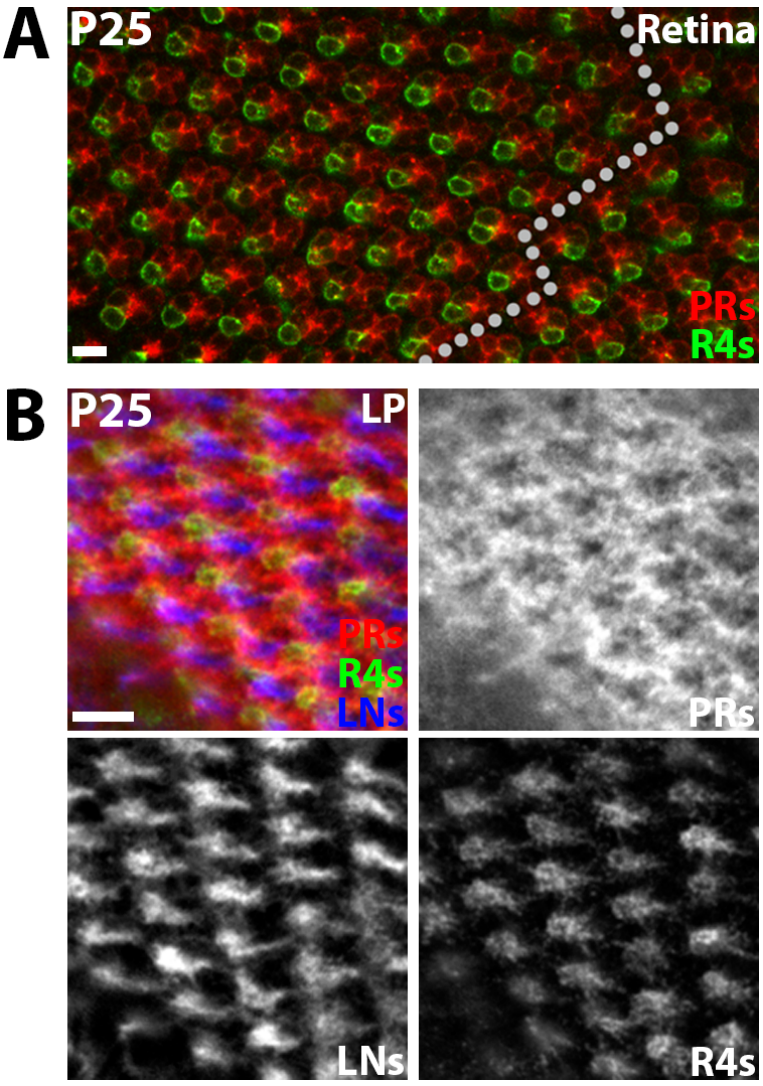

FIGURE A.6: GFP expression in R4 photoreceptors under mδ05-Gal4 driver

Expression of UAS-CD4::tdGFP with the mδ05-Gal4 driver in the eye and lamina at P25. A) Cut through the top of the retina where photoreceptor cell bodies reside. All photoreceptors in red. R4s in green. Dotted line represents the equator. R4s are oriented away from the equator in each ommatidium. B) Cut through the the lamina plexus. All photoreceptors in red. Lamina neurons in blue. R4 axonal growth cones in green. Equator is located on the right side of the image. R4s are oriented towards the equator. Scale bar 5μm.

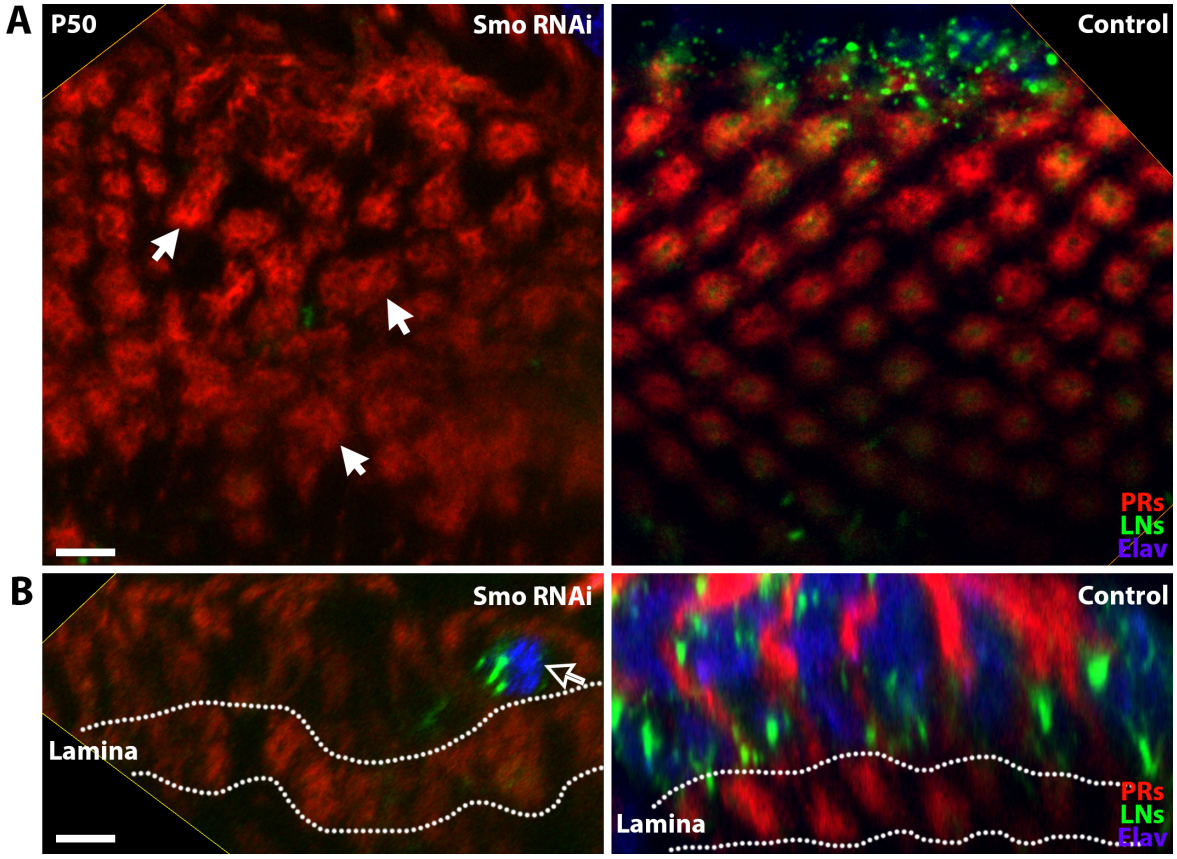

FIGURE A.7: The disturbed sorting outcome in the SmoRNAi experiment

A) Top view of the lamina plexus at P50. Cartridge organization is disturbed when SmoRNAi expression in LNs has prevented their differentiation. Examples of fused cartridges are indicated with white arrows. All photoreceptors in red (expression of GMR-Tomato), LNs in green, Elav staining in blue marks LN cell bodies. B) Side view of the lamina plexus (demarcated with dotted line) shows the lack of LNs in the lamina. Open arrow indicates a remaining LN cell body above the lamina plexus in the SmoRNAi experiment. Scalebar 5 μm.

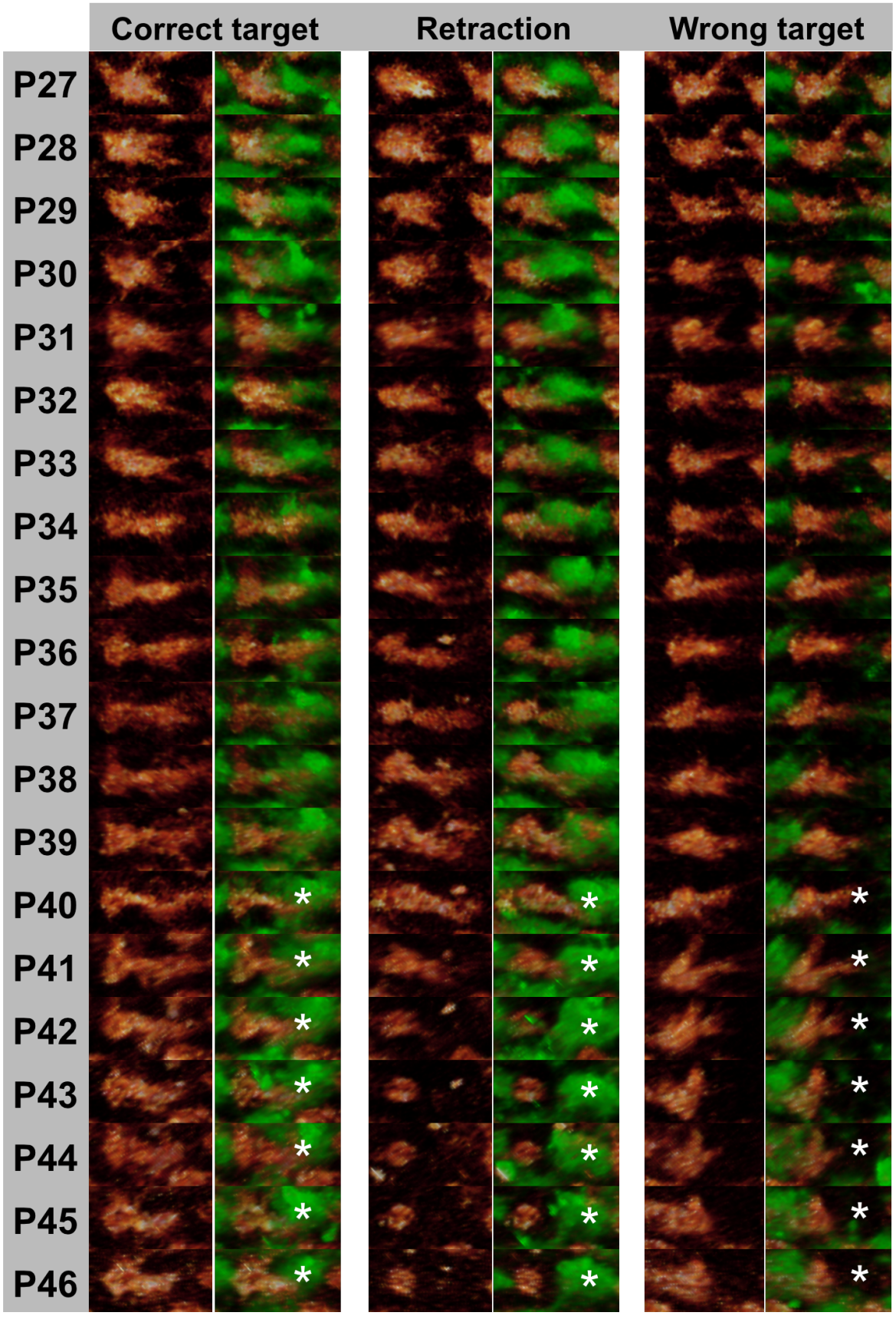

FIGURE A.8: Live imaging R4 extensions in lamina plexus with sparsely ablated LNs

Caption to Figure A.8: Live-imaging R4 extenstions in lamina plexus with sparsely ablated LNs

Snapshots from 20 hrs live-imaging data (obtained by Egemen Agi), ranging from P27 to P46. Initial extension of R4 growth cones is correct towards the equator (right of every image) where their correct target area (indicated with an asterisk) is located. Early R4 photoreceptors have correct extension angles, which can change into late defects. On the left: Correct extension and correct stabilization at the target LNs. In the middle: Correct extension but destabilization of the growth cone and subsequent retraction even though an LN cluster is present. On the right: Correct extension of the growth cone but incorrect stabilization. The growth cone turns and stabilizes at the home-cartridge. Phenotype is independent of LN availability.

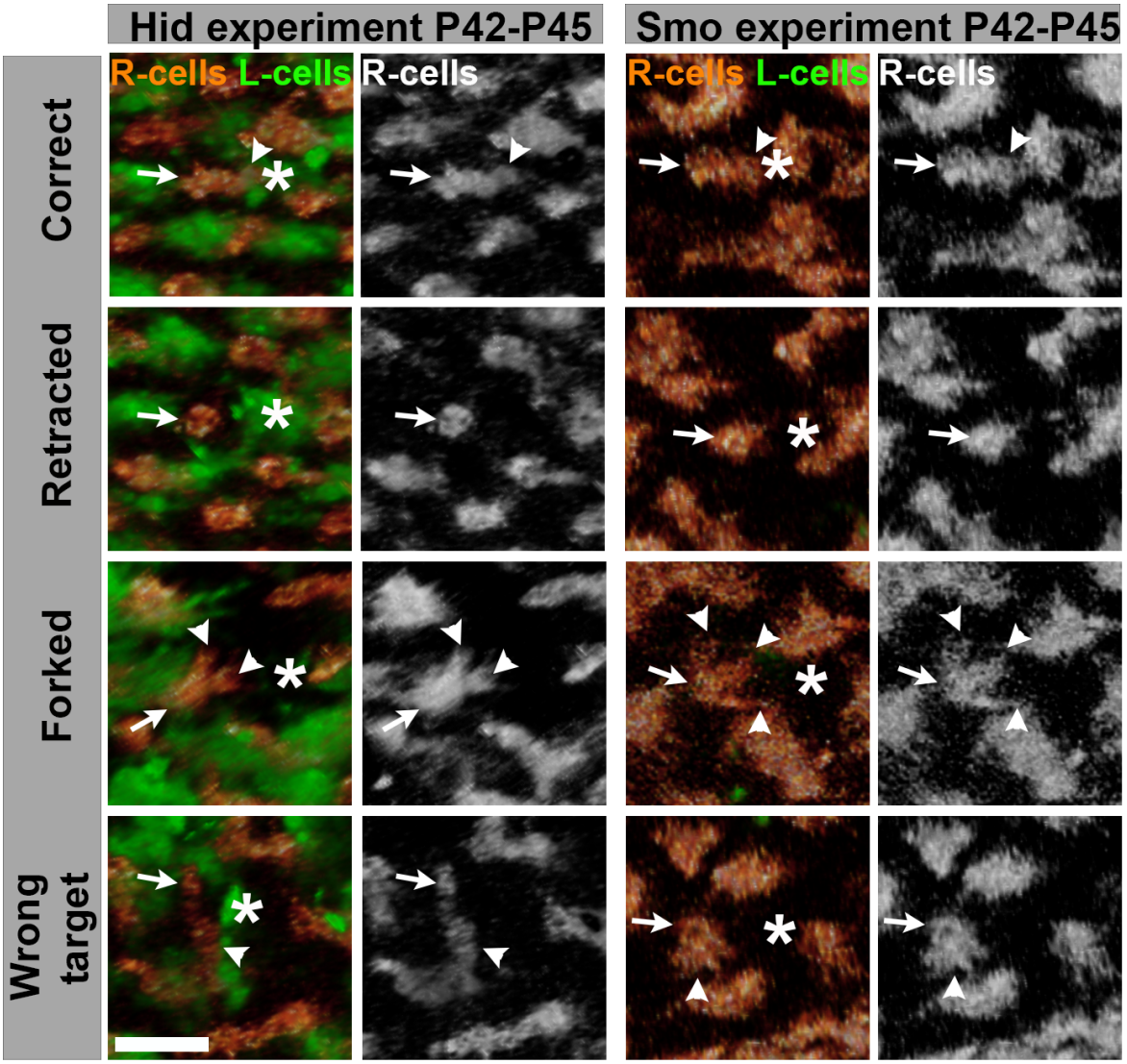

FIGURE A.9: R4 phenotypes in the Hid OE and SmoRNAi experiment

Comparison of R4 targeting phenotypes in the Hid OE experiment (left) and the SmoRNAi experiment (right). Photoreceptor growth cones can extend correctly towards a target area (asterisk), obtain a forked morphology, retract to the base of the heel structure, or miswire to wrong a target area in environments where LNs are missing. Photoreceptor heels marked with an arrow, photoreceptor fronts marked with an arrowhead. Scalebar 5 μm.